ENGINEERED MICROTISSUE PLATFORMS FOR MODELING HUMAN PATHOPHYSIOLOGY AND DRUG METABOLISM

by

CHERI YINGJIE LI

B.S. Chemical Engineering, Stanford University (2008)

Submitted to the Department of Chemical Engineering
in partial fulfillment of the requirements for the degree of

Doctor of Philosophy in Chemical Engineering

at the

MASSACHUSETTS INSTITUTE OF TECHNOLOGY

June 2013

Author_____
Department of Chemical Engineering
May 21, 2013

Certified by_____
Sangeeta N. Bhatia
John J. and Dorothy Wilson Professor of Health Sciences and Technology
& Electrical Engineering and Computer Science
Thesis Supervisor

Certified by _____
Robert S. Langer
David H. Koch Institute Professor of Chemical Engineering
Thesis Supervisor

Accepted by_____
Patrick S. Doyle
Chairman, Department Committee on Graduate Students

Engineered Microtissue Platforms for Modeling Human Pathophysiology and Drug Metabolism

by Cheri Y. Li

Submitted to the Department of Chemical Engineering on May 21, 2013 in partial fulfillment of the requirements for the degree of Doctor of Philosophy in Chemical Engineering

Abstract

Over 50% of all drug candidates entering clinical trials are abandoned due to insufficient efficacy or unexpected safety issues despite extensive pre-clinical testing. Liver metabolites that cause toxicity or other side effects cannot always be predicted in animals, in part because of human-specific drug metabolism. Furthermore, while the clinical need for cancer drugs is increasing, anti-tumor activity in animals often leads to a disappointing lack of efficacy in real patients. *In vitro* models that can better predict *human* responses to drugs would mitigate the overall costs of development and help bring new therapies to market. In order to improve the predictive power of *in vitro* tissue models, various features of the microenvironment that modulate cell behavior have been investigated, such as cell-cell interactions, cell-matrix interactions, soluble signals, 3-dimensional (3D) architecture, and mechanical stiffness. Synthetic hydrogels offer a versatile platform within which these cues can be precisely perturbed in a 3D context; however, the throughput of these methods is quite limited. In this thesis, we explore the potential of high-throughput manufacturing and monitoring of populations of miniaturized 3D tissues, termed 'microtissues,' for modeling healthy and diseased tissues in both static and perfused systems.

First, we developed a flow-based platform to test tumor proliferation in defined microenvironmental settings with large numbers of replicates ($n > 1000$). A microfluidic droplet generator was designed to encapsulate tumor cells with stromal cells and extracellular matrix in 100 μm-diameter poly(ethylene glycol) (PEG) microtissues (6000 microtissues/min). Upon screening a small panel of soluble stimuli, TGF-β and the TGF-βR1/2 inhibitor LY2157299 were found to have opposing effects on the proliferation of lung adenocarcinoma cells in microtissues vs. in 2-dimensional culture, affirming a potential role for 3D models in the investigation of cancer therapies.

Next, we extend these techniques to the analysis of drug-induced liver injury. Phenotypic maintenance of primary hepatocytes was achieved by controlled pre-aggregation (~50 μm units) with J2-3T3 fibroblasts to establish cell-cell contacts prior to encapsulation into microtissues. Retention of both constitutive and inducible Phase I drug metabolism activity allowed detection of prototypical hepatotoxins through generation of toxic metabolites and emergence of drug-drug interactions, thereby demonstrating the suitability of hepatic microtissues for 3D, high-throughput toxicity screening.

Finally, we describe efforts to bridge the gap between multi-organ models and human drug metabolism. Modular human hepatocyte microtissues were entrapped by semi-circular microsieves in a microfluidic perfusion chamber for over 3 weeks. In contrast to immortalized hepatic cell lines, primary hepatocytes stabilized in microtissues exhibited human-specific induction profiles, reflected donor hetereogeneity in CYP2D6 and CYP2C19 enzyme activity levels, and performed xenobiotic detoxification on circulating drugs, establishing the ability to incorporate hepatic functions in 'human-on-a-chip' devices.

Collectively, these three applications of cell-laden microtissues demonstrate their versatility and potential impact in both drug development and fundamental studies of the cellular microenvironment.

Thesis Supervisor: Sangeeta N. Bhatia — Title: John J. and Dorothy Wilson Professor of Health Sciences and Technology & Electrical Engineering and Computer Science

Thesis Supervisor: Robert S. Langer — Title: David H. Koch Institute Professor of Chemical Engineering

Acknowledgements

First and foremost, I want to express my deepest thanks to my advisor, Sangeeta Bhatia, who has been a steady beacon of guidance and scientific vitality. Throughout this journey, she gave me room to explore intellectually and fully supported my independence, but had this uncanny ability to step in and ask "How's it going?" exactly when I needed it. Sangeeta has also carefully created a lab environment that is warm and collaborative, for which I am very grateful. Thank you for being a wonderful role model and teaching me not just how to do science, but also how to approach life's challenges (and celebrate crazy ideas).

Next, I would like to thank my co-advisor Robert Langer, for offering his unequivocal support and encouraging me to trust my instincts. I am also grateful to my thesis committee members Chris Love and Darrell Irvine, who have been more than generous with their time and provided tremendous insights and constructive feedback during our meetings.

In the lab, I owe gratitude to the many incredible scientists and individuals whom I've had the honor of working with. In particular, to Neetu Singh and David Wood, who have respectively taught me all things chemistry and microfluidics, thank you for being mentors and close confidants. I will miss our conversations on all sorts of different topics. I thank Kelly Stevens for being the ultimate cheerleader and for helping me navigate the academic landscape. I also thank Rob Schwartz for letting me take advantage of his encyclopedic brain, and ensuring that the tissue culture room never went silent. To my friends in the lab, thank you for being fun, unique, and always there for me. Kevin Lin, for everyday snax, chats, and quiet companionship. Nathan Reticker-Flynn for never failing to notice new outfits, and for establishing an excellent custom to greet unsuspecting lab members. Meghan Shan, for being my sole source of peer estrogen with all the trappings, including shopping trips and girly talks. Kartik Trehan, for sending me trendy YouTube links. Justin Lo, for your cheery imagination and artistic talent – purr. Arnout Schepers, for offering unsolicited but gallingly effective suggestions. Gabe Kwong, for thoughtful advice and for being inhumanly brilliant. David Malta and Vyas Ramanan, for wearing clever t-shirts, Warren for taking up the baton, and the rest of the lab for being generally outstanding colleagues.

Thank you to my devoted undergraduates, Caroline Hsu, Joanne Huang, and Brian Alejandro, for being excited, engaged, and in Brian's case very well dressed. This work could not have happened without your contributions, and I hope it was a gainful learning experience for you. Thanks are also due to our lab staff: to Steve Katz and Lia Ingaharro for making the lab run smoothly and keeping us in check. To Heather Fleming, for being simultaneously an editor, advocate, therapist, and event planner. And last but not least, to the gatekeeper Sue Kangiser, for taking care of everything else behind the scenes. I would also like to acknowledge Elisa Vasile from the Microscopy Core, Alex Austin from Biopolymers & Proteomics, and Dennis Ward and Kurt Broderick from the Microsystems Technology Laboratories.

This thesis is dedicated to my family, who have pushed me and buoyed me for so many years. My mom, for her empathy and restless sense of adventure. My dad, for his insatiable curiosity and sage strategies for feeding a grad student's appetite with minimal effort. And to my brother Michael, whom I am so proud of, for always taking my side no matter what. I also thank the Seibert family for welcoming me with open arms, and Lychee for encouraging high fives and staying up with me at night.

Finally, I would like to express my love and endless gratitude to Jeff, who has stood by me through all the ups and downs of this experience, supporting me and inspiring me by the pursuit of his own passions. In addition to his many known qualifications, Jeff is a master mixologist, ready to provide liquid courage on a moment's notice, and an accomplished pirate, having commandeered the fastest ship in the Caribbean. Thank you for encouraging me to follow my dreams, both big and small, even when this meant craft supplies strewn everywhere from my latest whim. I can't wait to find out what the future holds for us.

Table of Contents

Abstract 3

Acknowledgements 4

Table of Contents 5

List of Figures 8

List of Tables 9

Chapter 1: Introduction 10

1.1 The Drug Development Pipeline 10

1.1.1 Pre-Clinical In Vivo Animal Models 12

1.1.2 Cell-Based In Vitro Models for Drug Development 13

1.1.3 Microenvironmental Cues for Cell Behavior 15

1.2 Three-Dimensional Tissue Engineering 17

1.2.1 Scaffold Materials in Hepatic Tissue Engineering 17

1.2.2 Miniaturized, 3D Microenvironments 19

1.2.3 Fabrication of Polymeric Microtissues 20

1.3 Scope of the Dissertation 24

Chapter 2: Microtissue Fabrication and Templated Assembly 26

2.1 Introduction 26

2.2 Materials and Methods 28

2.3 Results and Discussion 34

2.3.1 High-throughput microtissue fabrication 34

2.3.2. Microtissue functionalization with surface-encoding DNA 36

2.3.3 Binding efficiency and specificity of DNA-templated assembly 40

2.3.4 DNA-templated assembly of multicellular tissue constructs 42

2.4 Conclusion 48

2.5 Acknowledgements 48

Chapter 3: Flow Analysis of Microenvironmental Effects on Tumor Proliferation 50

3.1 Introduction 50

3.2 Materials and Methods 53
3.3 Results and Discussion 56
3.3.1 Platform design 56
3.3.2 Controlling tumor homotypic and heterotypic interactions 60
3.3.3 Modulating cell proliferation with microenvironmental factors 64
3.3.4 Microenvironmental modulation of tumor drug response 68
3.4 Conclusion 72
3.5 Acknowledgements 74

Chapter 4: Hepatocyte Microtissues for Toxicity Screening and Drug-drug interactions 75
4.1 Introduction 75
4.2 Materials and Methods 77
4.3 Results 84
4.3.1 Control and uniformity of hepatocyte patterning 84
4.3.2 Effect of homotypic contacts on 3D albumin secretion 86
4.3.3 Effect of other supporting factors in 3D albumin secretion 88
4.3.4 Microfluidic production of hepatic microtissues 90
4.3.5 Species-specific cytochrome P450 enzyme activity 94
4.3.6 Acetaminophen toxicity 94
4.3.7 Cytochrome P450-mediated drug-drug interactions 96
4.4 Discussion 98
4.5 Conclusion 103
4.6 Acknowledgements 104

Chapter 5: Modular Construction of a Primary Human Liver-on-a-Chip 106
5.1 Introduction 106
5.2 Materials and Methods 108
5.3 Results and Discussion 117
5.3.1 Primary hepatocyte microtissue fabrication 117
5.3.2 Species- and donor-specific drug metabolizing enzyme activity 119
5.3.3 Microtissue response to hepatotoxic drugs and drug interactions 123
5.3.4 Design and operation of microfluidic perfusion chamber 127

5.4 Conclusion 131
5.5 Acknowledgements 132

Chapter 6: Perspectives and Future Direction 133
6.1 Microfluidic Fabrication of 3D Microtissues 133
6.2 Systematic Control of Microenvironmental Stimuli 134
6.3 High-Throughput 3D Phenotypic Screening 135
6.4 Towards Modular Organ-on-a-Chip Devices 136

Bibliography 139

List of Figures

1.1 Attrition of drug candidates during the development and testing process....12
1.2 Schematic of microenvironmental inputs that modulate cellular behavior....17
1.3 Batch and microfluidic processes to fabricate polymeric microparticles....23
1.4 Controlling cellular microenvironment on several length scales....25

2.1 Schematic of microtissue encapsulation, functionalization, and DNA-templated self assembly....28
2.2 Microencapsulation device....36
2.3 Microtissue functionalization with streptavidin and DNA....38
2.4 Optimization of acrylate-PEG-streptavidin conjugation....39
2.5 Capture efficiency and specificity of DNA-directed microtissue assembly....41
2.6 Distribution of cell encapsulation numbers within microtissues....44
2.7 Cell encapsulation and microtissue culture....45
2.8 Multi-photon images of fibroblast spreading within RGDS microtissues....47
2.9 Fibroblast-laden, RGD-decorated microtissues cultured in close contact and in the presence of non-encapsulated fibroblasts....47

3.1 3D tumor microenvironment screening platform....59
3.2 Correlation of number of (A) ZsGreen expressing 393T5 cells of (B) CellTracker FarRed DDAO-stained J2-3T3 fibroblasts....61
3.3 Control over homotypic and heterotypic microtissue composition....63
3.4 Flow analysis and sorting of microtissues containing co-encapsulated tumor (393T5) and stromal (J2-3T3) cells....64
3.5 Modulation of tumor cell proliferation by cytokines and ECM....66
3.6 Epifluorescence microscopy of cell-free microtissues containing encapsulated proteins....68
3.7 Comparison of 393T5 (A-B) and 394T4 (C-D) lung cancer cell response to drugs when cultured in 3D microtissues (A,C) vs. in 2D monolayers (B,D)....70

4.1 Hepatocyte puck formation and detachment from patterned collagen microislands....85
4.2 Microisland seeding (A-C) and puck formation (D-F) by primary hepatocytes over large areas....86
4.3 Hepatocyte pucks express liver proteins....87
4.4 2D culture of hepatocytes on either (A) micropatterned islands, or (B) unpatterned, collagen-coated plastic....88
4.5 Hepatocyte pucks in 8.5mm-diameter bulk PEG hydrogels....89
4.6 Microfluidic encapsulation of hepatocyte pucks....92
4.7 Flow-focusing nozzle of microfluidic encapsulation device....93
4.8 Sequential seeding of hepatocytes and fibroblasts to form mixed pucks....93
4.9 Induction of cytochrome P450 activity in hepatocyte-fibroblast mixed-puck microtissues....94

4.10 Acetaminophen-induced microtissue hepatotoxicity.....96
4.11 Cytochrome P450 inducer interactions with acetaminophen toxicity.....97

5.1 Setup and operation of microtissue perfusion chamber.....114
5.2 Mixed hepatocyte-fibroblast spheroid formation in pyramidal microwells.....118
5.3 Albumin secretion by encapsulated primary human hepatocytes.....119
5.4 Induction of cytochrome P450 activity in primary human hepatocyte microtissues....121
5.5 Comparison of cytochrome P450 activity between donor individuals.....123
5.6 Microtissue hepatotoxicity as measured by large particle flow cytometry.....124
5.7 Acetaminophen-induced hepatotoxicity in human hepatic microtissues.....125
5.8 Mechanism-based drug interactions with acetaminophen toxicity.....126
5.9 Microtissue trapping and perfusion device.....128
5.10 Albumin detected in perfusate of Huh7.5 microtissue-loaded devices.....129
5.11 Characterization of hepatocyte functions in microtissue perfusion device.....130

List of Tables

5.1 Donors of cryopreserved human hepatocytes.....109

Chapter 1: Introduction

1.1 The Drug Development Pipeline

New drug candidates undergo a gauntlet of tests before they reach the market, starting with extensive pre-clinical characterization, *in vitro* assays, and *in vivo* animal studies. After this, if a compound is selected for further development, it is assessed for the first time in humans and undergoes three phases of clinical trials: Phase I, which tests for safety in a small population of healthy participants, Phase II, which tests for effectiveness in a larger population of diseased patients, and finally Phase III, which compares the drug to existing treatments in hundreds to thousands of participants and continues to monitor for side effects. Despite the fact that this process spans over a decade of time and costs on average more than $800 million dollars per drug,[1] many drugs are entered into clinical trials that will never be approved. Because of this attrition rate, the cost of drug development is ultimately reliant on the proportion of drugs that fail in the end – currently 8 out of 9 drugs entering clinical trials.[2] The ability to make swift, accurate decisions early in the process about which drugs are worth pursuing would significantly reduce overall costs: the sooner a drug candidate that would have failed can be eliminated from further development, the fewer resources are wasted.

Why are we so bad at identifying eventual losers? Accurately predicting the human body's response to various drugs or drug combinations is difficult. Although there are several factors that contribute to drug candidate failure, two major reasons for the attrition are 1) lack of efficacy or 2) toxic side effects.[3] The efficacy of a drug candidate is especially difficult to predict

for diseases with complex processes such as cancer. Phenotypic hetereogeneity of tumor cells within a patient (or even within a given tumor),[4-6] tumor cell interactions with stromal and immune cells,[7, 8] and acquired chemoresistance are only some of the issues hindering effective cancer treatment. Indeed, oncology drugs have higher rates of Phase III failure than in any other disease area, with only a 6% success rate from first-in-man tests to registration.[2] Given the desperate need for new antineoplastic agents, and assuming that drug candidates are not entered into clinical trials without reasonable pre-clinical evidence of efficacy,[6] this abysmal success rate suggests that current pre-clinical disease models must be faulty.

Drug toxicity is inextricably linked to efficacy, as drugs are often given in ineffective doses because safety concerns. The most common toxicity discovered in clinical trials is unforeseen or idiosyncratic liver injury (hepatotoxicity),[9, 10] followed by kidney (nephrotoxicity) and cardiac effects. The liver is often the first casualty because it is the primary organ responsible for xenobiotic detoxification in the body. Unanticipated metabolism of a drug candidate by the liver can affect its clearance time, alter the level of drug activity, or produce metabolites that cause toxicity to the liver or other organs.[11-13] Thus, for efficacy as well as safety, pre-clinical models that enable better prediction of human liver metabolism and toxicity would be indispensable in lead selection and early mitigation of potential problems.

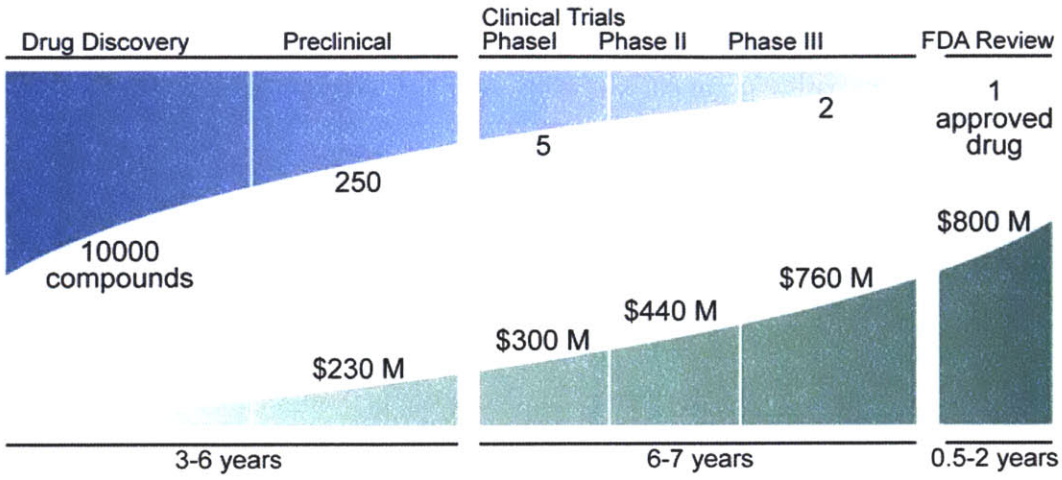

Figure 1.1. Attrition of drug candidates during the development and testing process. Adapted from http://www.ncats.nih.gov, and http://www.manhattan-institute.org/html/fda_05.htm, which based their findings on drugs first tested in humans between 1983-1994[1, 3] The approval rate of drugs entering clinical trials has continued to drop since then.[2]

1.1.1 Pre-Clinical In Vivo Animal Models

Currently, animals are widely used in pre-clinical studies as models to represent both healthy and diseased states. For oncology testing, xenograft models are common in which a tumor cell line is injected into an immune-compromised mouse.[6] *In vivo* models like these offer many advantages and allow examination of whole-organism effects such as bio-distribution, pharmacokinetics and pharmacodynamics, organ-organ interactions, and off-target effects. At the same time, animal models incur considerable costs, require lengthy experiments, can be difficult to manipulate, and raise ethical issues. There is also substantial evidence that in many cases animal models are not necessarily predictive of human behavior due to critical differences in disease etiology, drug metabolism, and other species-specific characteristics. Xenograft tumors for example are often in a location that does not correlate with the tumor origin (e.g.

lung cancer cells injected subcutaneously into the flank of the mouse), and the tumor develops over weeks instead of years in a human. More complex genetically engineered mouse models of specific cancers are becoming available[14-16] but are exorbitantly expensive. There have been similarly heroic efforts to resolve the significant discrepancy between human and rodent drug metabolism pathways, arising in part from different drug metabolizing cytochrome P450 enzymes or nuclear receptors that regulate levels of enzyme activity.[17-19] Due to these differences, animal models sometimes fail to distinguish drugs or drug combinations that may be toxic only to the human liver *via* metabolism by a human-specific enzyme.[11, 20] Attempts to "humanize" the mouse liver by injecting human hepatocytes are promising,[21, 22] but remain slow, finicky, and variable in the degree of humanization.

1.1.2 Cell-Based In Vitro Models for Drug Development

There is a clear need for pre-clinical models that can accurately and inexpensively assess the response of humans to drug candidates. To do so, they must accurately represent important facets of *human* tissue physiology before "first-in-human" trials are done. Experiments *in vitro* have the potential to meet these requirements, as well as generally increase throughput, provide early information for decision making, and reduce the need for animal studies. For example, human liver microsomes and isolated enzymes have helped identify pathways involved in drug metabolism.[23] However, these assays lack the dynamic gene expression and intact cellular machinery necessary for drug-interaction and toxicity testing, respectively. *In vitro* platforms

based on living cells are necessary to properly model the behavior of tissues with a multitude of biochemical functions such as the liver.

For this particular organ, human liver slices and primary hepatocytes and have been explored as cell-based models. Precision-cut liver slices retain structural tissue organization and have been shown to accurately reflect the metabolic capabilities of the liver *in vivo*,[23] but are viable for only ~1 day and are not amenable to high-throughput screening. Primary hepatocytes are thus ideal for studying ADME/TOX (absorption, distribution, metabolism, and excretion/toxicity),[24-26] but are similarly difficult to stabilize *in vitro* and lose their drug metabolism functions over the course of days.[27, 28] Instead, hepatocellular carcinoma cell lines are commonly used in place of primary hepatocytes,[29] but generally display abnormally low levels of cytochrome P450 enzymes,[25, 30] are less or non-responsive to known *in vivo* inducers of enzyme activity,[30, 31] and are more resistant to hepatotoxins known to cause clinical drug-induced liver injury. [32]

The relevance of an *in vitro* model is critically dependent on the type and *in vivo*-like phenotypic behavior of the cells used. Yet, proliferative cell lines cultured on 2D tissue culture plastic remain the industry standard today despite their distorted representation of *in vivo* cells. To improve the predictiveness of *in vitro* models, research efforts have turned towards learning to better culture more "authentic" cells such as primary hepatocytes or induced pluripotent stem cells that are more challenging to maintain,[33] but could better reflect *in vivo* organ behavior.

1.1.3 Microenvironmental Cues for Cell Behavior

Another factor that contributes to the limitations of conventional *in vitro* models is their inability to capture critical features of the cellular microenvironment. The cellular microenvironment, which includes extracellular matrix (ECM) interactions, cell-cell interactions, tissue architecture, and soluble signals (e.g. growth factors and hormones), provides cues that modulate cell behavior in both healthy and diseased tissues.[34-41] In the case of liver models, the *in vivo* structure of the liver is extraordinarily complex,[42] with hepatocytes arranged in cords lined by ECM and sinusoidal endothelial cells. Other non-parenchymal cell types in the liver include stellate cells and bile duct cells. When hepatocytes are isolated from this native environment, they rapidly lose their hepatocyte-specific functions, [27] undergoing what is often referred to as "de-differentiation".[33] Efforts to stabilize hepatocyte phenotype *in vitro* have thus focused optimizing culture conditions by recreating some of the appropriate microenvironmental cues, such as medium supplements,[43-45] culture on or within added ECM,[43, 45-55] and signals from non-parenchymal cells.[33, 45, 56-62] For instance, co-culture of hepatocytes with fibroblasts,[59, 61, 63-65] endothelial,[62] or epithelial cells,[66, 67] has been repeatedly shown to improve long-term phenotypic stability. Within this body of work, it has become clear that hepatocytes in 3-dimensional (3D) culture systems, for example in spheroids,[53, 68-70] sandwich culture,[49-52] porous scaffolds,[71-74] or gel encapsulation,[53-55, 75] show distinct phenotypic differences from hepatocytes in 2D monolayer cultures with, in many cases, increased levels and maintenance of albumin, urea, and cytochrome P450 metabolism. In general, 3D organization has been found to affect cell viability, morphology, differentiation, proliferation, gene and protein expression, and

response to stimuli for a range of cell types in addition to hepatocytes, including stem cells[76-80] and cancer cells.[81-85] Although the mechanisms have not been fully elucidated, these differences between 3D and 2D are thought to be mediated through changes in cell-ECM and cell-cell interactions. First, there is an increased surface area for both cell-ECM and cell-cell contacts in 3D, which more closely matches the *in vivo* situation where almost 100% of cell surface area is exposed to other cells or matrix. This geometry modulates the types and amount of cell interactions that occur; one example is the alteration of cell-cell contacts in 3D.[46, 86-89] Furthermore, cell-ECM focal adhesions in 3D have been found to be composed of a different distribution of integrins[83] and other cytoskeletal components[90] which interact with signaling pathways within the cell, for example pathways downstream to growth factor binding.[84, 91, 92] The presence of matrix surrounding cells rather than under them can alter the presentation of ligands[93] and the transport of nutrients or soluble signals.[94] Finally, changes in mechanical stimuli,[95-98] cell shape,[90, 99] and physical confinement[100] can also affect cell behavior. For all of these reasons, it is possible that 3D culture is necessary to truly approach more predictive *in vitro* models of cell behavior in response to therapies, especially as tissues in the body are 3-dimensional. Tumor cells in cultured in 3D, for instance, have been shown to be significantly more resistant to chemotherapeutics than in 2D.[82, 85-89, 101] In this thesis, we aim to design three-dimensional *in vitro* culture systems with sufficient microenvironmental complexity to maintain *in vivo* human cell phenotypes, focusing on hepatocytes in particular. Such alternative pre-clinical test platforms could form a crucial bridge between 2D experiments and developing clinically viable drugs to treat human disease, and additionally enable manipulation of specific environmental parameters to study underlying biological phenomena.

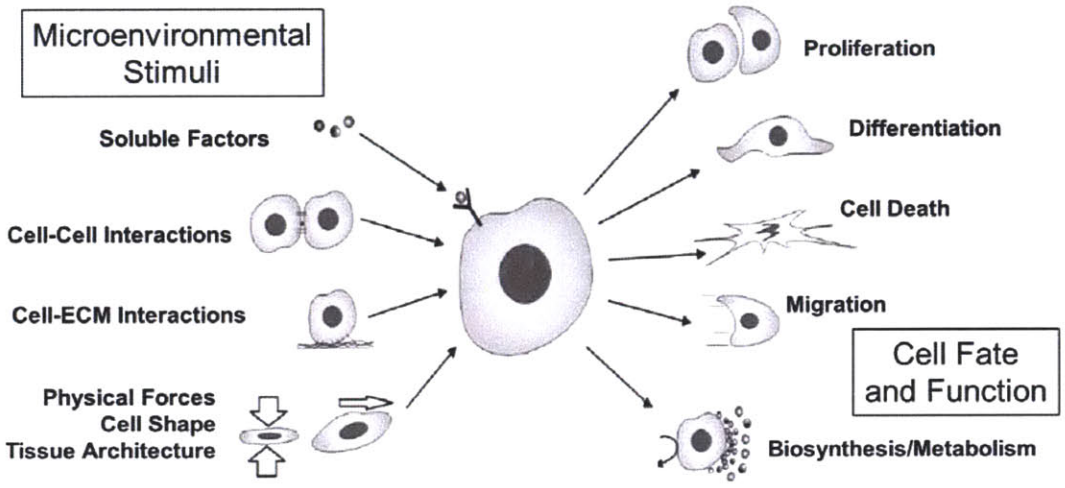

Figure 1.2. Schematic of microenvironmental inputs that modulate cellular behavior. Adapted from Alice Ann Chen.

1.2 Three-Dimensional Tissue Engineering

1.2.1 Scaffold Materials in Hepatic Tissue Engineering

As per the tissue engineering approach, hepatocytes have been cultured within various natural and synthetic scaffolds. Some of the natural hydrogels used are agarose,[102] alginate,[103] collagen,[54, 55] matrigel,[104] or fibrin.[105, 106] These hydrogel scaffolds not only provide structural support to encapsulated cells while remaining permeable to oxygen and nutrients, but can also interact with cellular process to modify cell behavior, for instance through integrin ligation,[92] growth factor binding,[107] or mechanical changes in response to secreted proteases.[97] However, the systematic examination of microenvironmental cues using such natural scaffolds is

challenged by lack of independent control over these biological interactions,[94, 108, 109] as well as by batch to batch material variability. Synthetic polymer scaffolds can offer improved control over scaffold features, mechanics, and the presentation of signals.[108, 110-112] In particular, poly (ethylene glycol)-based (PEG) hydrogels have been investigated for the 3D culture of a wide range of cell types including hepatocytes,[113-115] osteoblasts,[116, 117] chondrocytes,[118, 119] fibroblasts,[120-122] endothelial cells,[123] pancreatic β-cells,[124] and stem cells.[125-128] There are various polymerization techniques to form hydrogels from PEG,[121, 129-131] leading to different network structures, but a shared feature is that resulting hydrogels are non- interactive with encapsulated cells because of the neutral and hydrophilic PEG backbone. At the same time, advances in chemical modifications have enabled methodical incorporation of further functionality, such as adhesive peptides,[114, 116, 122, 123] tethered growth[132-134] or inflammatory factors,[135] enzyme mimetics[136], or degradable linkages.[117, 121, 129, 130]

While hydrogel encapsulation is an established approach for 3D cell culture, synthetic tissue constructs are typically slow to fabricate and require large amounts of cells and reagents, leading to experiments with generally low numbers of replicates (n~3-5). Moreover, the analysis of cell behavior within the hydrogels can be technologically challenging.[137] Current readouts can be broken down into three categories: cell release, pooled biochemical assays, and imaging. Cells can be released from confinement by enzymatic digestion of the scaffold,[129] reversal of ionic polymerization mechanisms (e.g. alginate[138]), or simply brute hydrolysis.[133] Depending on how gentle the method to degrade the gel is, released cellular components such as DNA can be quantified, or intact cells can be analyzed by conventional 2D and suspension methods such as flow cytometry.[139] This method is obviously destructive and can only be used for endpoint

studies. To probe the phenotype of cells still in a hydrogel, biochemical assays for properties such as mitochondrial activity[114, 116, 128] or protein secretion[114, 140] can be performed as long as any substrates or metabolites can permeate through the hydrogel network. However, these assays integrate over the entire cell population in the hydrogel, and thus cannot distinguish subtleties such as bimodal cell response outcomes. For imaging, the immobilization of cells in different focal planes necessitates confocal microscopy for accurate quantification. Thus, even something as simple as accurately measuring cell proliferation can require time-consuming image acquisition and processing procedures.[85, 125, 141] Sectioning of the hydrogels can be performed similar to tissue histology,[142] but is not compatible with all materials[114] and is also destructive. An ideal *in vitro* model would allow cell responses to treatment to be monitored over time.

1.2.2 Miniaturized, 3D Microenvironments

We propose that the miniaturization of cell-laden hydrogel scaffolds into small (<250 μm diameter) units of 3D engineered tissues, which we will call microtissues, could address some of these limitations and bring unique advantages to the table. Compared to conventional 3D hydrogels, which are often > 20 microliters in volume, each microtissue is on the order of 10 nanoliters, reducing the amount of cell and scaffold reagents needed, but most importantly reducing the amount of experimental drug compounds needed to treat the microtissues, which in early stages of development may only be produced in limited quantities. The length scale of microtissues is also highly relevant to the *in vivo* architecture of the body: because the diffusion distance of oxygen is approximately 150 μm in living tissues, cells in the body are located

within at most 150 μm from the nearest blood supply.[143-145] Similarly, cells in microtissues would remain less than this distance from the nearest medium supply, reducing concerns about insufficient diffusion of oxygen and nutrients into the cells at the core of the hydrogel, even if the local cell density of the microtissue is high and metabolically demanding. It has also been found through studies manipulating cell-cell interaction distances that critical short-range cell signaling occurs on the scale of hundreds of microns.[146] Indeed, the organization of multiple cell types in several organs is also seen to repeat on hundred-micron length scales (e.g. the liver , kidney, etc.[42]). Thus, microtissues are well poised to recapitulate tissue interactions at these distances, and could additionally be suitable for bottom-up assembly of complex patterned tissues.[147, 148] Recently, Chen *et al.* demonstrated the suitability of microbead-labeled microtissues for multiplexed *in vivo* experiments within an individual mouse, and illustrated "fluid-phase" handling of microtissue suspensions.[149] For *in vitro* experiments, the compatibility of microtissues with automated liquid handlers and microtiter plates is indispensable toward achieving high throughput screening of cellular responses to drugs in defined 3D microenvironments.

1.2.3 Fabrication of Polymeric Microtissues

Methods to fabricate microtissues fall under three categories, 1) physical molding, 2) photolithography, and 3) emulsification. Large-scale production of uniform polymeric particles has been achieved by a process called particle replication in non-wetting templates (PRINT).[150] In this elegantly straightforward method, a patterned fluoropolymer mold with nano- to

micron-scale indentations was used to make particles encapsulating proteins, DNA, and small molecules.[150] The PRINT process was integrated with roll-to-roll manufacturing techniques to produce sufficient nanoparticles for clinical trials [151], but is incompatible with cell encapsulation. Similar micromolding methods using elastomeric molds have been extended to template cell-encapsulating hydrogel particles,[152] but cytocompatible micromolding remains a batch process with unproven production capacity. For photolithographically defined microtissues, a hydrogel precursor is mixed with cells and a photoinitiator that triggers polymerization when selected spatial regions are exposed to light, typically in the UV range [149, 153, 154]. Dendukuri et al.[155] and Panda et al.[156] adapted hydrogel photolithography into a continuous microfluidic process, but the technique can be challenging to execute and cell-encapsulation *via* "stop flow lithography" has not become a widespread. Moreover, photolithography in general is wasteful: prepolymer in un-exposed regions is discarded, which is a considerable inefficiency especially when working with limited cell numbers or decorating the hydrogel with expensive bioactive ligands.

Emulsification techniques can be applied in either macroscale or microfluidic settings. A polymer precursor, usually in aqueous solution, is first broken up into droplets in a continuous phase, usually oil. Yet macroscopic emulsions formed by agitation are generally polydisperse[157]. Instead, microfluidic devices containing a T-junction[158-161] or flow-focusing junction[161, 162] can generate monodisperse droplets, and have been used without the polymerization aspect for applications like directed protein evolution[163], digital PCR[158, 164] and single-organism (e.g. yeast[165], C. elegans[159, 166]) droplet arrays. Alternatively, the droplets can then polymerized to

form spherical or modified spherical shapes,[160, 167, 168] which has been reported for both solid polymer microspheres[168, 169] and hydrogel particles.[170, 171] [160, 162]

Continued advances in polymer microparticle fabrication, and specifically cell-laden hydrogel microtissue fabrication as a small subset, will eventually lead to higher throughputs and expand the library of shapes and materials that can be used. The larger problem is that of the mammalian cell-laden microtissues thus far, encapsulated cells have been predominantly limited to more robust fibroblast [152, 156, 172] or cancer,[149, 154, 172, 173] or other immortalized cell lines.[171, 174] Moreover, cursory analysis of encapsulated cells entailed only staining for cell viability in the short term.[149, 152, 156, 171] Shear stresses, UV/free-radical damage, and chemical interactions with scaffold components can cause more subtle but undesirable changes in cell behavior, such as impaired growth rates or altered transcriptional profiles.[175-178] We reasoned that drug development applications would require both manufacturing throughput and robust maintenance of not just cell viability but also phenotype. Therefore, although the uniformity and production rate of microfluidic droplet-based encapsulation is promising, it remains unclear whether more sensitive but physiologically relevant cells such as hepatocytes can be successfully encapsulated with maintenance of important drug metabolizing functions.

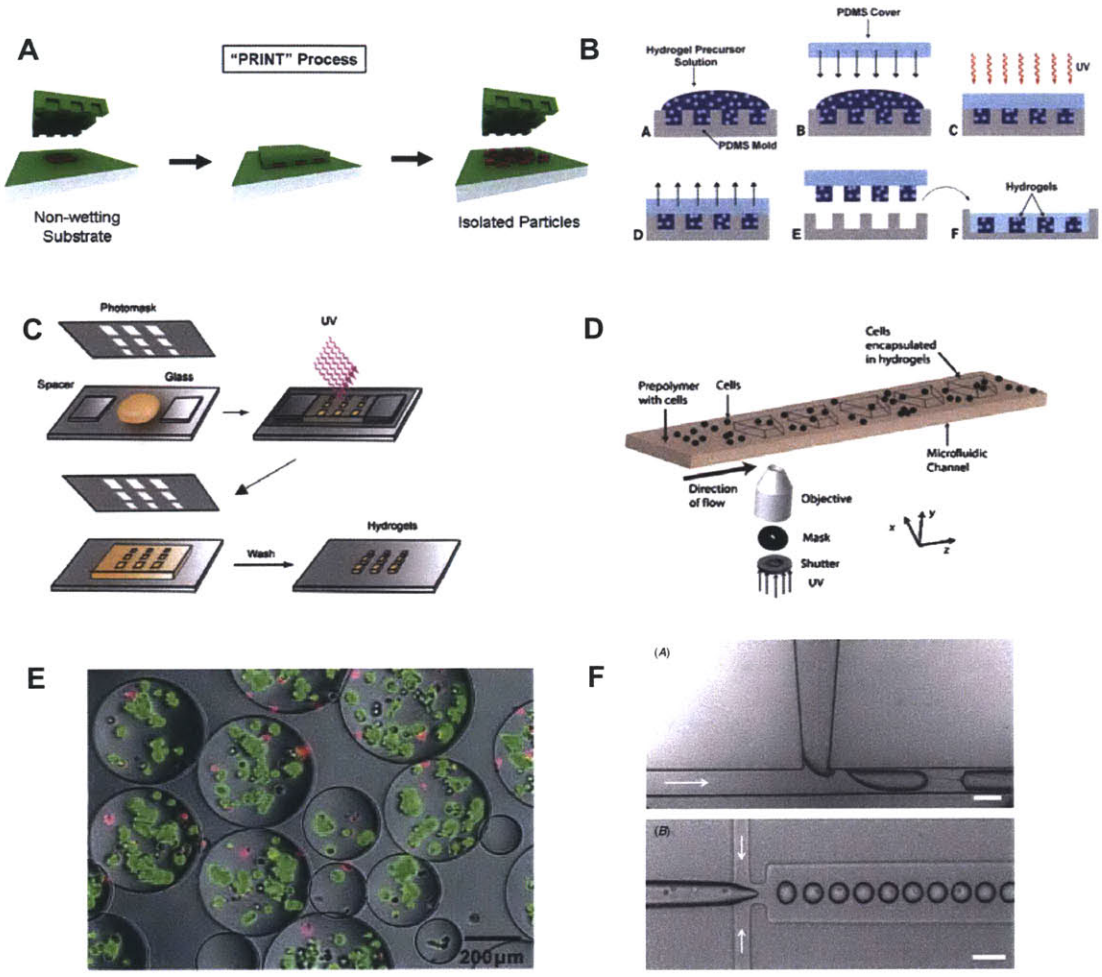

Figure 1.3. Batch and microfluidic processes to fabricate polymeric microparticles. (A) Molding of uniform particles in non-wetting perfluoropolyether (PFPE) molds.[150] (B) Cytocompatible "micromolding" of cell-laden hydrogels in PDMS molds.[179] (C) (D) Continuous photolithography through a mask using "stop-flow lithography."[155, 156] (E) Cell encapsulation using batch aqueous-in-oil emulsion and photopolymerization.[157] (F). Microfluidic T-junction and flow-focused formation of aqueous-in-oil droplets. [174]

1.3 Scope of the Dissertation

Our overall goal is to create improved *in vitro* models of liver and tumor tissue for drug development applications. Specifically, we hypothesize that 3D organization and encapsulation of cancer cells or hepatocytes within miniaturized polymer hydrogels ("microtissues") that provide appropriate cues will stabilize their tissue-specific phenotype *ex vivo*. In this thesis, we construct and systemically manipulate microtissue-based microenvironmental parameters on several length scales. Towards this end, we first aimed to develop a device that could continuously encapsulate relevant cell types (i.e. primary human hepatocytes) into customizable PEG microtissues. In **Chapter 2**, we establish methods to microfluidically generate droplets of cells with prepolymer in fluorocarbon oil, and photopolymerize the droplets on-chip to manufacture microtissues at a rate of ~10^5 gels/hr. We then chemically modified the hydrogel network to encode microtissues with specific biomolecular (DNA oligonucleotide) spatial "addresses." These addresses template the binding of microtissues containing two cell types into 2D and 3D heterostructures that enable secreted cell-cell interactions on the multiple-microtissue length scale. **Chapter 3** describes a high-throughput, high-powered (n > 1000) flow-based assay to examine 3D tumor proliferation within microtissues in the presence of growth-modulating cytokines or small molecule drug candidates, and demonstrates our ability to control cellular microenvironment on a single-microtissue scale (homotypic/heterotypic cell density, ECM proteins, soluble factors). Together, these chapters showcase unique advantages of microtissue-based platforms in scalability, modularity, and versatility. In **Chapter 4**, we focus on the long-term phenotypic maintenance of primary hepatocytes within microtissues (~weeks),

which is achieved by pre-stabilizing hepatocytes through micropatterned cell-cell interactions, and demonstrate the direct use of hepatocyte-laden microtissues for toxicity and drug interaction studies. We extend these findings to primary *human* hepatocytes in **Chapter 5**, which describes extensive characterization of microencapsulated human hepatocytes for organ-specific, species-specific, and donor-specific drug metabolism functions. Finally, we load and culture human hepatic microtissues in a perfused liver-on-a-chip device (Chapter 5), laying the groundwork for future microtissue applications in multi-organ human-on-a-chip systems.

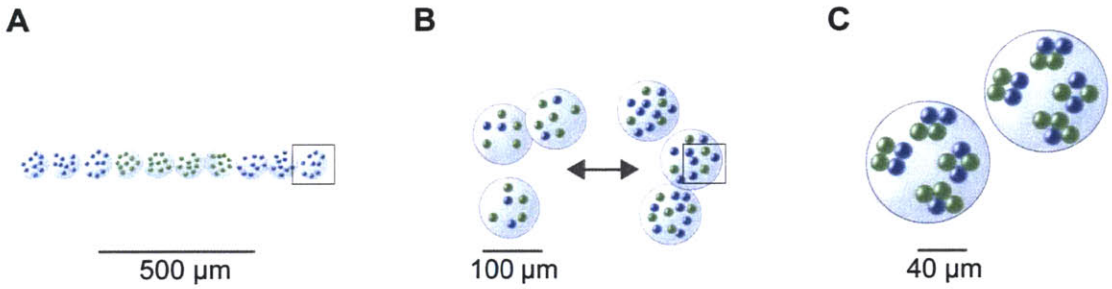

Figure 1.4. Controlling cellular microenvironment on several length scales. (A) Multiple microtissue scale (Chapter 2): templated distances for soluble-factor signaling between microtissues containing different cell types. (B) Single microtissue scale (Chapter 3): selecting microtissue populations with tightly gated parenchymal and stromal cell densities per microtissue. (C) Within microtissues (Chapter 4): pre-stabilized cell-cell contacts for improved viability and function.

Chapter 2: Microtissue Fabrication and Templated Assembly

2.1 Introduction

The three-dimensional microscale architecture of living tissues provides vital environmental cues, including extracellular matrix, soluble factors and cell-cell interactions.[94, 180] Paracrine and autocrine cell signaling are critical factors guiding tissue development[181, 182] and maintenance,[61, 183] and dysregulation of these cues contributes to the pathogenesis of diseased states such as cancer.[184-186] Understanding and emulating these cell-cell interactions has been shown to be critical in engineering functional tissues in both 2D[146, 187-189] and 3D[82, 114, 190] systems. In 3D culture, top-down approaches for organizing multiple cell types such as dielectrophoresis,[153, 191] photopatterning,[113, 192] and microfabrication[193] provide high-precision control over cell placement, but are challenging to scale-up for the assembly of mesoscale tissues.

In contrast, bottom-up methods, wherein small tissue building blocks are assembled into larger structures, have potential for creating multicellular constructs in a facile, scalable fashion.[194-198] Living tissues are comprised of repeating units on the order of hundreds of microns; therefore, synthetic microtissues comprised of cell-laden hydrogels in this size range[149] represent appropriate fundamental building blocks of such bottom-up methods. Synthetic microtissues of this size have been previously assembled in packed-bed reactors[194, 199] or by hydrophobic/hydrophilic interactions[196, 200] but without the ability to specify the placement of

many different microtissues relative to one another. One potential method for controlled assembly of heterostructures would be to incorporate the specificity of biomolecular interactions with surface templating to direct assembly. This approach could allow for scalable patterning of multiple cell types into arbitrary architectures with high precision.

In this chapter, we harness the well-characterized molecular recognition capabilities of DNA to achieve rapid templated assembly of multiple microtissue types (**Fig. 2.1**). This method is enabled by the high-throughput production of spherical cell-laden microtissues from a microfluidically-derived, monodispersed emulsion of a photocurable hydrogel. Cell-laden microtissues are derivatized with single-stranded oligonucleotides and integrated with custom DNA microarray templates. Orthogonal DNA sequences are used to specify the assembly of multiple cell types over large (~mm) length scales with high capture efficiency. This fusion of "bottom-up" (templated assembly) and "top-down" (microfluidics and robotic spotting) approaches allows for unprecedented control over mesoscale tissue microarchitecture and exemplifies the potential of integrating disparate fabrication strategies.

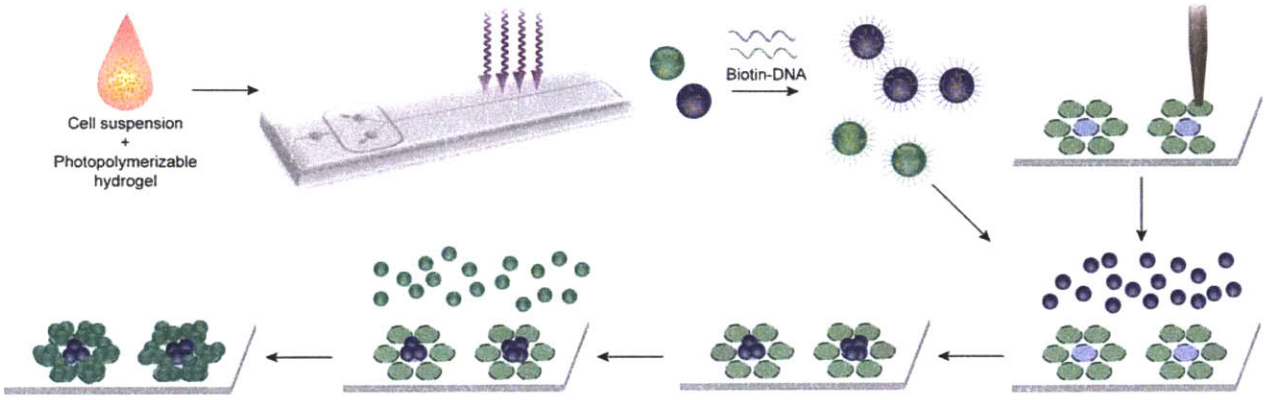

Figure 2.1. Schematic of microtissue encapsulation, functionalization, and DNA-templated self assembly. Cells are injected with a photopolymerizable hydrogel prepolymer into a high-throughput microfluidic encapsulation device. Droplets of the cell-prepolymer mixture are exposed to UV on-chip to form streptavidin-containing microtissues which are then coated with 5′-biotin terminated oligonucleotides. Encoded microtissues containing different cell types are seeded on a DNA microarray template which directs the binding of microtissues to specific spots on the templating surface, attaining sequential DNA-templated patterning of cell-laden microtissues.

2.2 Materials and Methods

Device fabrication

Microfluidic device masters were fabricated on 4 inch silicon wafers using standard photolithographic methods, with SU-8 2050 photoresist (Microchem, MA) spin coated at 1200 rpm to create 125 μm tall features. Masters were coated with trichloro perfluorooctyl silane (Sigma-Aldrich) for 1 hr in a vacuum dessicator prior to casting polydimethylsiloxane (PDMS, Dow Corning) devices. Cured devices with inlet holes made by a 20G dispensing needle (McMaster-Carr) were bonded to glass slides following air plasma treatment. In order to ensure

a hydrophobic surface for droplet generation, Aquapel (PPG Industries) was briefly injected into the device and flushed out with nitrogen.

Ligand conjugation

Acrylate-PEG-RGDS peptide was prepared as previously described.[114] To conjugate streptavidin with acrylate groups, streptavidin was dissolved in 50 mM sodium bicarbonate (pH 8.5) at 0.8 mg/ml. Amine-reactive acrylate-PEG-SVA (3.4 kDa, Laysan) was added at a 25:1 molar ratio and allowed to react with the protein at room temperature for 2 hours. Conjugated acrylate-PEG-streptavidin was purified from unconjugated PEG by washing in PBS with a 30,000 MWCO spin filter (Millipore). The acrylate-PEG-streptavidin conjugate was then reconstituted to 38 μM streptavidin in PBS, sterile filtered, and stored at -20°C.

Microtissue polymerization

Irgacure-2959 initiator (Ciba) was dissolved at 100 mg/ml in n-vinyl pyrrolidinone accelerator (Sigma-Aldrich) to make photoinitiator working solution. The basic 2x concentrated prepolymer solution consisted of 20% w/v poly(ethylene glycol) diacrylate (PEG-DA, 20kDa, Laysan) and 2% v/v of photoinitiator working solution. Additional prepolymer ingredients included 38 μM of acrylate-PEG-streptavidin conjugate, 10 mM acrylate-PEG-RGDS, and/or 1% v/v of fluorescent microspheres (2% solids, Invitrogen) as markers.

The final 2x prepolymer solution was injected into the microencapsulation device in parallel with, for cell-free microtissues, a 1:1 diluting stream of PBS. Syringe pumps were used

to control the flow rates of the aqueous phases and the oil phase, which consists of the perfluoro polyether, Fomblin (Y-LVAC, Solvay Solexis), with 0-2 w/v% Krytox 157 FSH surfactant (DuPont). Prepolymer droplets were gelled on-chip by exposure to 500 mW/cm^2 of 320-390 nm UV light (Omnicure S1000, Exfo) for an approximately one second residence time under typical flow conditions. Cell-free microtissues were collected in handling buffer (PBS with 0.1% v/v Tween-20), allowed to separate from the oil phase, and washed on a 70 μm cell strainer to remove un-polymerized solutes.

Bead hybridization

To stain for the surface-availability of ssDNA bound on microtissues, 1 μm NeutrAvidin biotin-binding beads (yellow-green, Invitrogen) were coated with the complementary 5′-biotin-DNA (IDT). The original suspension of beads (1% solids) was diluted 1:10 with BlockAid blocking solution (Invitrogen), sonicated for 5 minutes, and then incubated with a final concentration of 4 μM 5′-biotin-DNA for 1 hour at room temperature. Beads were then washed three times in PBS by centrifugation at 2000xg. DNA-functionalized microtissues were incubated overnight on a room-temperature shaker with coated beads resuspended to 0.1% solids in BlockAid.

Microarray spotting

Microarray templates were printed in-house using a contact-deposition DNA spotter (Cartesian Technologies) with a 946MP10 pin (Arrayit). Complementary pairs of single-

stranded oligonucleotides used to functionalize microtissues and template their assembly are listed below and consisted of a poly-A linker followed by a heterogeneous 20 nucleotide sequence. The 20-nucleotide binding region of A and A′ are complementary, B and B′, etc. Sequences were modified with 5′-amino groups for microarray spotting, and 5′-biotin groups for microtissue functionalization.

Label	Sequence
A	5′- AAAAAAAAAAGCCGTCGGTTCAGGTCATA-3′
A′	5′- AAAAAAAAAAATATGACCTGAACCGACGGC-3′
B	5′- AAAAAAAAAAAGACACGACACACTGGCTTA-3′
B′	5′-AAAAAAAAAATAAGCCAGTGTGTCGTGTCT-3′
C	5′-AAAAAAAAAAGCCTCATTGAATCATGCCTA-3′
C′	5′-AAAAAAAAAATAGGCATGATTCAATGAGGC-3′
D	5′-AAAAAAAAAATAGCGATAGTAGACGAGTGC-3′
D′	5′-AAAAAAAAAAGCACTCGTCTACTATCGCTA-3′

5′-amino oligonucleotides (IDTDNA) for templating were dissolved in 150 mM phosphate buffer (pH 8.5) at concentrations up to 250 μM, and spotted on epoxide coated slides (Corning) at 70% RH. Patterned slides were then incubated for 12 hours in a 75% RH saturated NaCl chamber, blocked for 30 minutes in 50 mM ethanolamine in 0.1M Tris with 0.1% w/v SDS (pH 9), and rinsed thoroughly with deionized water.

DNA-directed assembly

Microtissues containing PEG-streptavidin were incubated with 1 nmol of 5′-biotin

oligonucleotides per 10 ul of packed microtissues for one hour at room temperature or overnight at 4°C. Un-bound oligonucleotides were removed by washing microtissues on a 70 μM cell strainer or using 100,000 MWCO spin filters. Multi-well chambers (ProPlate, Grace Bio-Labs) were assembled over templating slides, and DNA-functionalized microtissues were seeded in a concentrated suspension over the microarray patterns. Microtissues quickly settled into a monolayer, which was visually confirmed under a microscope. Unbound microtissues were washed off the template by gently rinsing the slide with several ml of handling buffer. Capture efficiency was quantified by the average capture density over replicate spots on a slide, divided by the average seeding density of settled microtissues in a 4x microscope field of view. Percent of maximum packing fraction was calculated as the ratio of capture density to the theoretical density of close-packed circles.

Cell culture

J2-3T3 fibroblasts were cultured in Dulbecco's Modified Eagle Medium (DMEM, Invitrogen) with 10% bovine serum (Invitrogen), 10 U/ml penicillin (Invitrogen), and 10 mg/ml streptomycin (Invitrogen). TK6 lymphoblasts (suspension culture) and A549 lung adenocarcinoma cells were cultured in RPMI 1640 with L-glutamine (Invitrogen) and 10% fetal bovine serum (Invitrogen), 10 U/ml penicillin, and 10 mg/ml streptomycin. All cells were cultured in a 5% CO_2 humidified incubator at 37°C.

Cell encapsulation

Prior to encapsulation, adherent cells (J2-3T3 and A549) were detached with 0.25% trypsin-EDTA (Invitrogen). Cell pellets were resuspended at cell densities between $10x10^6$ cells/ml and $30x10^6$ cells/ml in an isopycnic injection medium consisting of 20% v/v OptiPrep (Sigma-Aldrich) in serum-free DMEM. Isopycnic cell suspensions were injected into microencapsulation devices in place of the diluting stream of PBS, along with 2x prepolymer solution. Gelled microtissues were collected and handled in culture media. To assess cell viability after 3 hours, microtissues stained with calcein AM (1:200, 1 mg/ml in DMSO, Invitrogen) and ethidium homodimer (1:400, 1 mg/ml in DMSO, Invitrogen) for 15 minutes at 37°C. Alternatively, microtissues for DNA-templated assembly were marked with CellTracker Green CMFDA (1:200, 5 mg/ml in DMSO, Invitrogen) or CellTracker Blue CMAC (1:200, 5 mg/ml in DMSO, Invitrogen) for 1 hour at 37°C.

Imaging and visualization

Images were acquired with a Nikon Ellipse TE200 inverted fluorescence microscope, a CoolSnap-HQ Digital CCD Camera, and MetaMorph Image Analysis Software. NIH software ImageJ was used to uniformly adjust brightness/contrast, and pseudocolor, merge, and quantify images. Confocal images were acquired with an Olympus FV1000 multiphoton microscope and Olympus Fluoview software. NIS-Elements software was used to pseudocolor and reconstruct maximum intensity, slice, and volume views.

2.3 Results and Discussion

2.3.1 High-throughput microtissue fabrication

One factor restricting the application of bottom-up assembly to tissue engineering has been the low throughput of typical microtissue fabrication approaches to date, many of which are batch processes.[149, 194, 201] We first sought to design a microfluidic chip to rapidly produce uniform microtissues. Droplets generated by flow focusing of aqueous/oil phases are monodisperse and amenable to photopolymerization.[202] Thus, we fabricated a device to shear photopolymerizable poly(ethylene glycol) diacrylate (PEG-DA) prepolymer containing cells into droplets in oil for downstream gelation by UV-light (**Fig. 2.2a**). Concentrated pre-polymer was injected into the microencapsulation device as a separate stream from the cell suspension (PBS for cell-free microtissues), where the two aqueous streams were designed to meet before reaching a flow-focusing junction (**Fig. 2.2b**). With a 60 μm nozzle, shear forces were sufficient to disperse the aqueous combination into droplets that passed through a corrugated serpentine channel[203] to thoroughly mix the cell-prepolymer solution (**Fig. 2.2c**). The droplets were then polymerized by UV irradiation for 1 second during transport to the outlet. Resulting microtissues were uniformly spherical and monodisperse (**Fig. 2.2d**). We observed that by adjusting aqueous vs. oil phase flow rates (**Fig. 2.2e**) and oil-phase surfactant concentrations (**Fig. 2f**), we could finely control droplet diameter, and hence microtissue size, between 30-120 μm.

At a typical prepolymer flow rate of 200 ul/hr, our device was capable of achieving a production throughput of 6000 microtissues/min (~10^5/hr), two orders of magnitude faster than other continuous systems such as stop-flow lithography[156] (~10^3 particles/hr) or batch fabrication processes.[149] Microtissue fabrication by microfluidic droplet photopolymerization provides precise control over microtissue shape and size, whereas photolithographic[149] and molding[194, 196] techniques do not produce spherical gels and can suffer from resolution limits. Planar microtissue surfaces tend to adhere non-specifically to hydrophilic surfaces due to the high water content (>90%[204]) of the hydrogel material, whereas the low contact area of spherical microtissues reduces capillary adhesion during both handling and assembly. Droplet-based gels have previously been made using agarose[205] or alginate;[141] here, we chose a PEG hydrogel material for its biocompatibility and biochemical versatility. PEG-diacrylate hydrogels have high water content, are non-immunogenic and resistant to protein adsorption, and can be easily customized with degradable linkages, adhesive ligands, and other biologically or chemically active factors.[131]

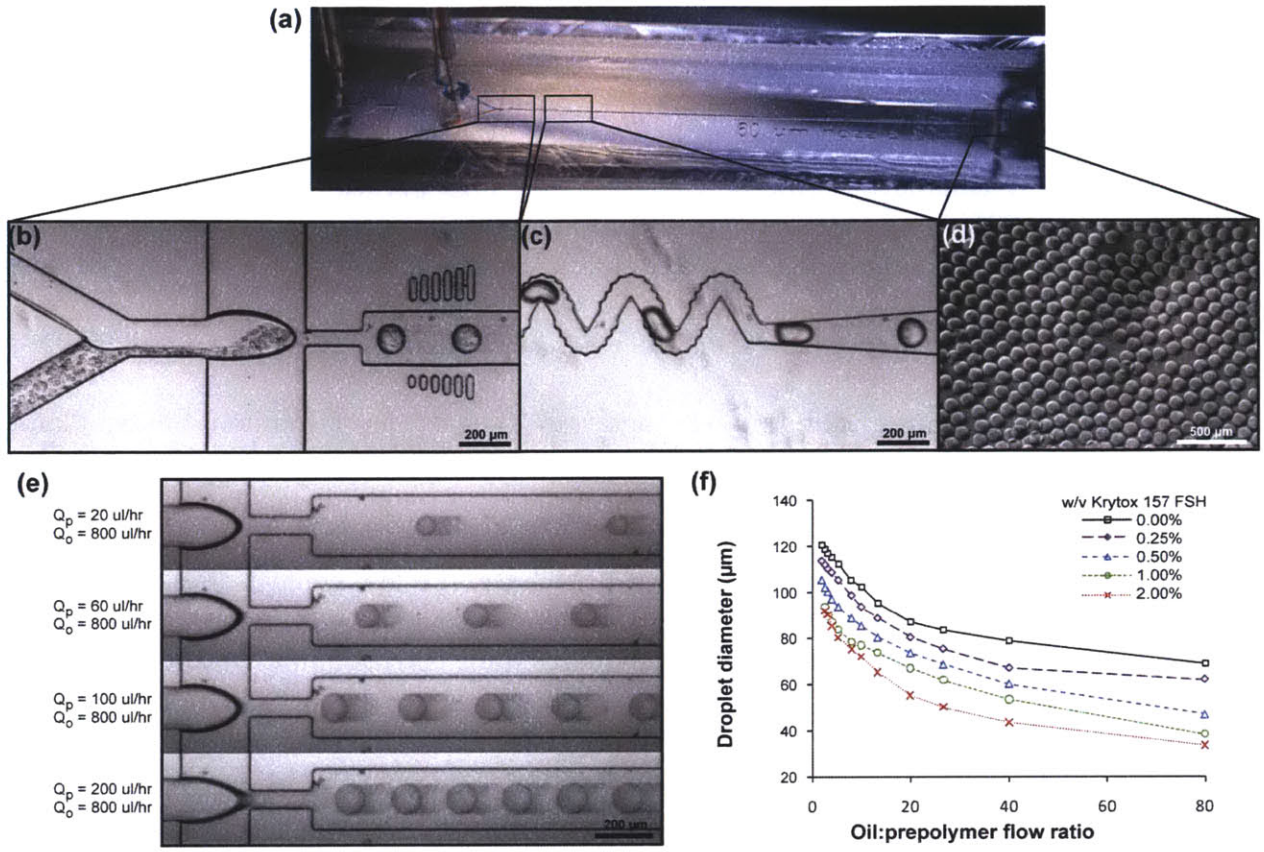

Figure 2.2. Microencapsulation device. (a) Overview of device showing two aqueous input streams (red, blue) dispersed by shear flow from an oil stream into droplets that mix (purple) and travel down the UV-exposure channel. (b) Prepolymer (2x concentrated) and a cell suspension meet and flow into a 60 µm droplet generating nozzle. Vertical columns on either side of the channel provide visual references (50-100 µm below, 100-150 µm above) for real-time adjustment of droplet size. (c) Droplets pass through a bumpy serpentine mixer section to thoroughly disperse cells in prepolymer and are then polymerized by UV irradiation from a curing lamp. (d) Microtissues collected from the device (6000/min) are spherical and monodisperse. (e) Microtissue size is controlled by the relative flow rates of the combined aqueous phase (Q_P) and the continuous oil phase (Q_O), and increases with prepolymer:oil flow ratio. (f) Adding small amounts of Krytox 157 FSH fluorosurfactant into the oil decreased droplet diameter at all flow ratios, allowing higher prepolymer flow rates for a given microtissue size.

2.3.2. *Microtissue functionalization with surface-encoding DNA*

Having established a method to uniformly produce microtissues, we next sought to

modify our microtissues with streptavidin for binding biotinylated DNA. To accomplish this, streptavidin was incubated with amine-reactive acrylate-PEG-SVA (3.4 kDa). Following purification, the acrylate-decorated streptavidin was then mixed into the prepolymer and covalently bound into the acrylate-PEG-acrylate hydrogel network during gelation by acrylate polymerization (**Fig. 2.3a**). Cell-free PEG-SA microtissues containing conjugated acrylate-PEG-streptavidin were stained to verify biotin-binding capacity using biotin-4-fluorescein.We also confirmed the surface-availability of streptavidin with an anti-streptavidin antibody , which was size restricted to only the surface of the microtissue (~7 nm mesh size[204]) . Both biotin fluorescence and antibody staining intensities increased with the volumetric concentration of conjugated streptavidin (**Fig. 2.3b**).

With streptavidin incorporated into the hydrogel network, we were able to encode the microtissues post-polymerization with 5′-biotin terminated oligonucleotides (**Fig. 2.3c**). Streptavidin-biotin based DNA-functionalization of microtissues is simple, modular, and cytocompatible. Post-polymerization encoding of microtissues with biotin-DNA avoids UV damage that would occur by pre-mixing acrylated-DNA into the prepolymer,[206, 207] and allows the same batch of microtissues to be labeled after culture in various conditions. Other bioconjugation methods exist to modify hydrogel networks post-encapsulation, such as

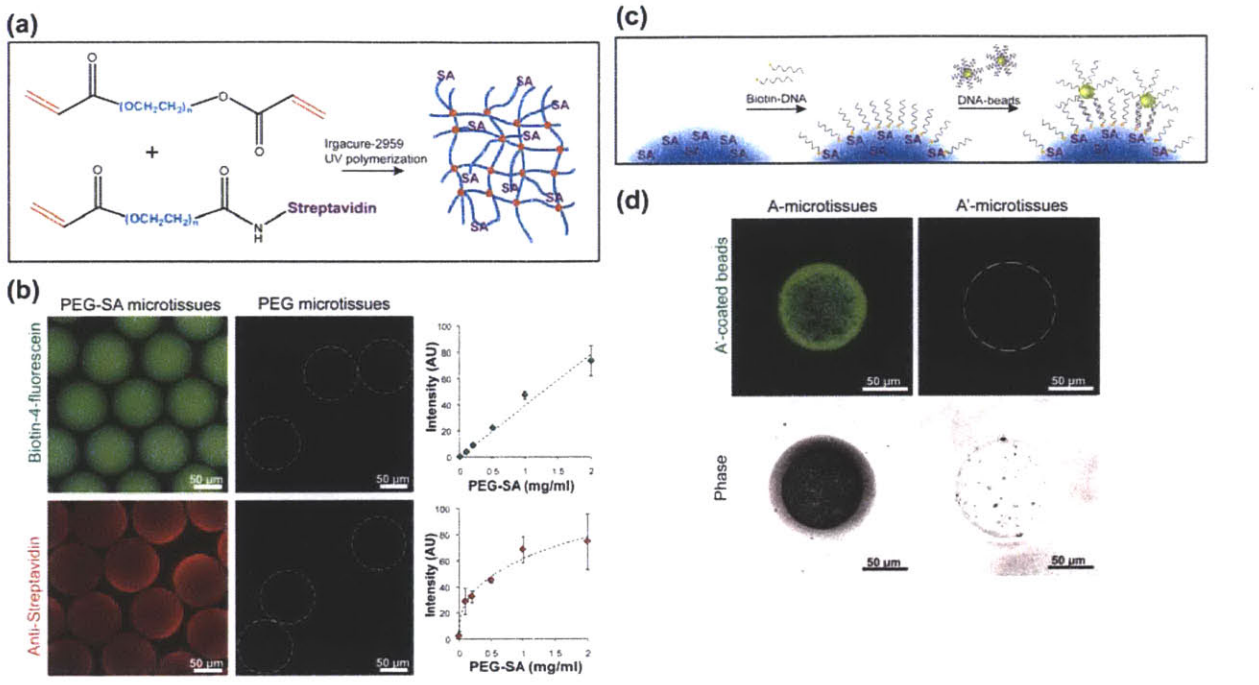

Figure 2.3. Microtissue functionalization with streptavidin and DNA. (a) The primary hydrogel component, acrylate-PEG20k-acrylate macromonomer, was mixed with conjugated acrylate-PEG-streptavidin (0-2 mg/ml) before photo-initiated free radical polymerization, forming a hydrogel network that is decorated with pendant streptavidin proteins. (b) PEG-streptavidin microtissues stained with biotin-4-fluorescein, which can freely diffuse through the hydrogel network, and anti-streptavidin IgG which is restricted to the surface of the microtissues. The intensity of biotin-4-fluorescein staining increased linearly with the bulk concentration of covalently-bound streptavidin, while antibody stains for surface concentration increased only as a power of bulk concentration. (c) PEG-SA microtissues are further functionalized with biotin-ssDNA. The availability of this ssDNA to hybridize with a templating surface was tested using 1 µm fluorescent beads coated with DNA. (d) Microtissues with the appropriate complementary sequence were coated with hybridized beads. No beads hybridized to control-sequence microtissues, which remained dark in the green channel and showed only encapsulated marker beads in the phase image.

maleimide or NHS chemistries[208] but often require reaction conditions that are incompatible with maintaining the viability of encapsulated cells. To ensure that DNA bound to microtissues using the streptavidin-biotin interaction was available to hybridize with DNA displayed on a surface, we incubated DNA-encoded microtissues with 1 µm polystyrene beads coated with the

complementary oligonucleotide (**Fig. 2.3c**). After washing to remove non-specifically bound material, microtissues encoded with the complementary sequence were thoroughly coated with beads visible as bright, punctate spots (**Fig. 2.3d**). Conversely, beads did not specifically hybridize to control microtissues (**Fig. 2.3d**). In order to maximize bead-microtissue hybridization, we investigated conjugating acrylate-PEG-SVA to streptavidin at several molar ratios (**Fig. 2.4**). As expected, microtissues incorporating streptavidin with few acrylate pendants (10:1 molar ratio, mobility shift assay) did not promote bead hybridization as effectively as streptavidin modified with a higher number of acrylate groups (25:1 to 50:1 molar ratio), which was used for all further studies. Gels with over-decorated streptavidin (1000:1 molar ratio) were also not as efficient in mediating bead-microtissue hybridization, suggesting that overmodification and/or steric hindrance plays an important role in DNA-binding capacity.

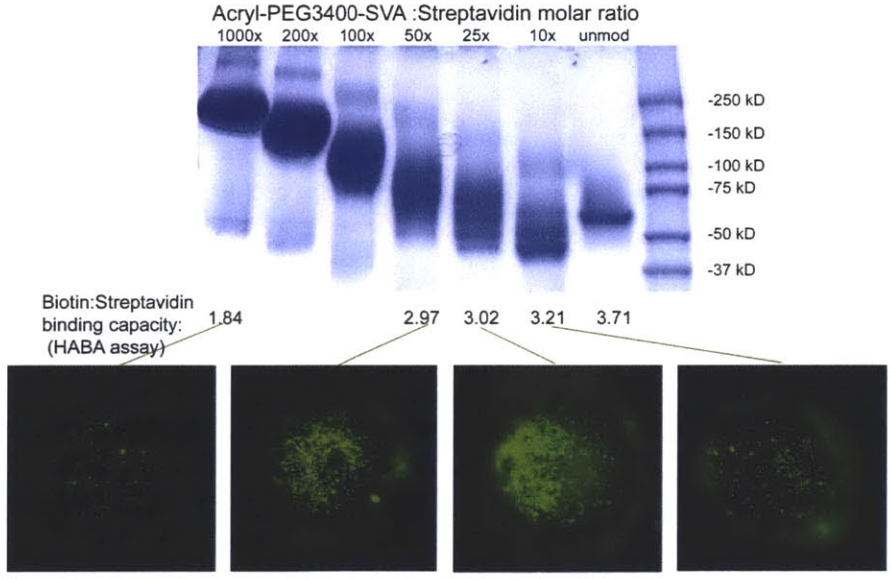

Figure 2.4. Optimization of acrylate-PEG-streptavidin conjugation. Non-denaturing PAGE gel (top) of purified products from varying molar ratios of reactants. At low ratios, discrete bands of protein with 1-5 modified amines are visible. At higher ratios, streptavidin is overmodified and biotin-binding capacity is significantly reduced. Reaction conditions of interest were further tested by incorporating products into microtissues, binding biotin-DNA, and staining by hybridization with DNA-coated beads (bottom).

2.3.3 *Binding efficiency and specificity of DNA-templated assembly*

Having shown that cell-free microtissues can be coated with DNA and hybridize specifically to complementary beads, we next investigated the potential of microtissue assembly into mesoscale patterns determined by an encoded template. To create such a template, we spotted increasing concentrations of DNA (sequence A') onto a functionalized glass slide using conventional microarray technology. DNA-functionalized microtissues (A; containing green marker beads) were allowed to settle onto microarray slides from suspension, at which time non-hybridized microtissues were gently washed off the slide. The number of microtissues bound to templating array spots increased with higher spotting concentrations of templating ssDNA (**Fig. 2.5a**), plateauing at 250 μM, an order of magnitude higher than typical epoxy-silane based microarray spotting concentrations. Spots were fully covered by microtissues at this highest DNA density. To determine the capture efficiency, we seeded microtissues at varying densities (microtissues per mm^2, **Fig. 2.5b**). At contact-limited (hexagonally close-packed) seeding concentrations, we achieved 100% capture efficiency, indicating that if a microtissue settled onto a complementary spot, hybridization and binding would occur.

Similar efficiencies have been observed during the DNA-templated assembly of materials ranging in scale from molecules to nanoparticles to single cells[195, 209-214]. Until now, DNA-templated assembly has not been extended to larger units such as microtissues (100 μm), which present unique challenges in mass transport.[215] At these mesoscopic scales, gravity and friction become important factors in the ability of DNA-coated surfaces to sufficiently interact. During washing steps, stronger viscous drag forces on the microtissues necessitate a large number of hybridization bonds between the microtissues and templating surface to overcome

microtissue removal. Here, to compensate for microtissue size, we optimize microtissue DNA functionalization and template spotting to achieve high DNA surface densities, enabling the first demonstration of large structure DNA-templated assembly.

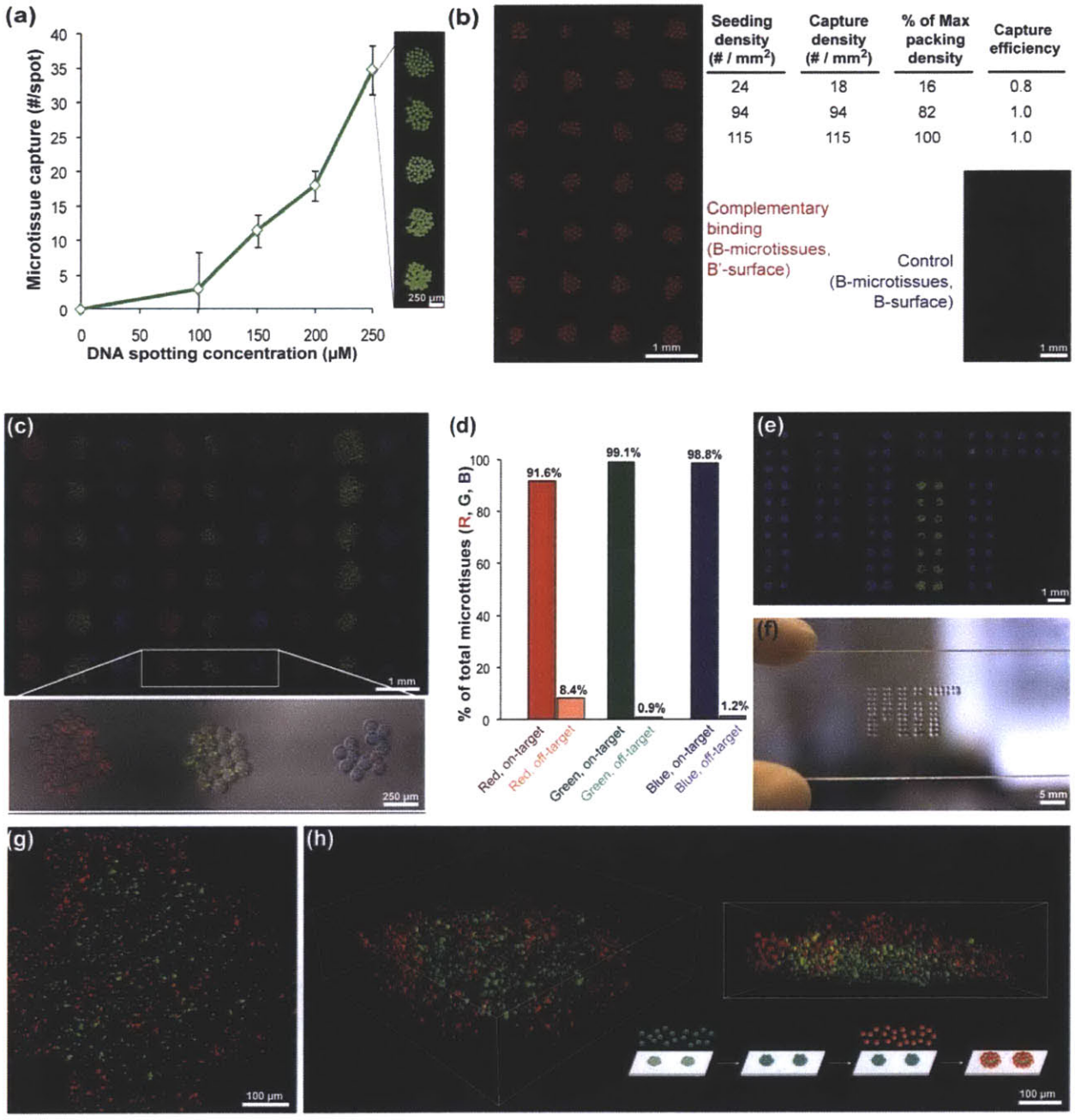

Figure 2.5. Capture efficiency and specificity of DNA-directed microtissue assembly. (a) Number of DNA-functionalized microtissues containing fluorescent beads as markers captured on microarray spots with increasing spotting concentration of complementary oligonucleotide. (b) Quantified assembly results from microtissues seeded over an array of complementary spots at low, medium (shown on the left), and high (close-packed) % surface coverage. Control arrays of non-complementary spots remained blank. (c) Three-color (RGB) microtissue assembly using a set of orthogonal oligonucleotide sequences: B (red), C (green), and D (blue). Microtissues contain encapsulated marker beads. (d) Quantified percentages of microtissues on target spots (1 column) vs. off-target spots (2 columns). (e) MIT logo assembled in microtissues of C (green) and D (blue), and (f) photograph of templating slide illustrating scale of assembled microtissue patterns. (g) Maximum intensity projection and (h) volume reconstructions from multi-photon scans of 3D microtissue structure formed by templating a first layer of microtissues (B, green) and then assembling a second layer of complementary microtissues (B′, red).

During our assembly process, minimal microtissue binding was observed between spots and on non-complementary templating spots (**Fig. 2.5b**), which was largely made possible by our control over microtissue shape. This low background binding allowed us to sequentially pattern multiple microtissue types, each encoded with an orthogonal oligonucleotide sequence, with over 90% specificity (**Fig. 2.5c, d**) and across large areas in under 15 minutes (**Fig. 2.5e, f**). Furthermore, we were able to build 3D structures (**Fig. 2.5g, h**) by filling template spots (B′) with a layer of microtissues (B), and then seeding a second layer of complementary microtissues (B′) that bind on and around microtissues in the first layer. Together, these experiments demonstrate the ease of achieving organizational control at macroscopic length scales by microtissue assembly.

2.3.4 DNA-templated assembly of multicellular tissue constructs

In order to apply DNA-templated patterning to the assembly of multicellular constructs, we next focused on encapsulating cells into uniform and highly viable cell-laden microtissues.

To improve the consistency of cell encapsulation (**Fig. 2.6**), we increased the specific gravity of our cell suspensions to prevent cell settling during injection. We chose a density gradient medium (OptiPrep), based on an iodinated small molecule, that increases specific gravity without affecting viscosity or cross-linked hydrogel network density, and easily diffuses out of the polymerized microtissues. With these changes, we attained cell encapsulation matching a Poisson distribution (**Fig. 2.7b**). In addition, we replaced the hydrocarbon oil phase with an oxygen-permeable fluorocarbon oil (Fomblin) to allow immediate quenching of excess free radicals post-UV exposure.[216] Notably, using fluorocarbon oil, cells were able to tolerate a wide range of total UV exposures (mJ/cm^2) while maintaining >90% viability (**Fig. 2.7c**). As a result of these changes, several adhesive and suspension cell lines, including adherent mesenchymal (fibroblasts), nonadherent mesenchymal (lymphoblasts) and adherent epithelial (adenocarcinoma), were uniformly encapsulated into microtissues with consistently high viability (**Fig. 2.7a**). Variations in average viability between cell types (e.g. J2-3T3 vs. TK6) could be due a number of cell type differences including susceptibility to DNA damage.[217] For cell lines sensitive to UV, photoinitiators in the visible-light range could be substituted into our material system.[218]

These are many advantages associated with patterning cellular microtissues rather than single cells.[211, 212] Firstly, cells can be encapsulated in a modular scaffold with customized ECM molecules (e.g. RGDS) to promote certain phenotypes. As an example, we added acrylated RGDS peptide to the prepolymer during fibroblast encapsulation. By Day 2 post-encapsulation, fibroblasts began spreading within these adhesive microtissues (**Fig. 2.7d, Fig. 2.8**). Secondly, microtissues containing one cell type can be first cultured separately to stabilize homotypic

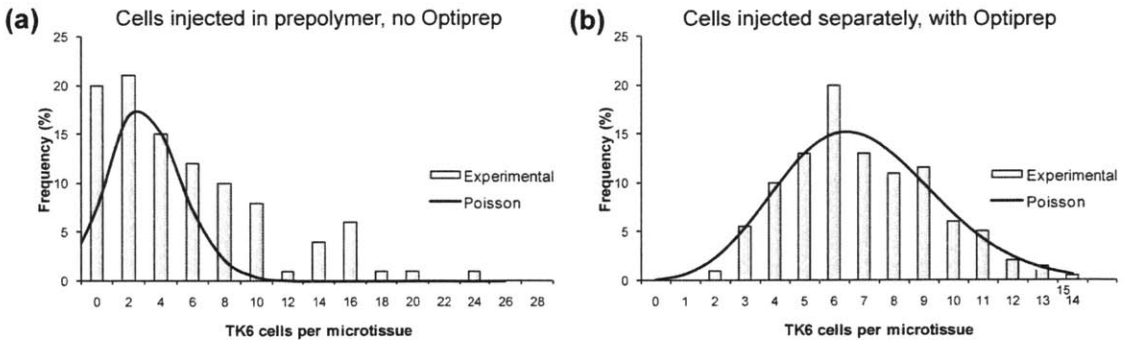

Figure 2.6. Distribution of cell encapsulation numbers within microtissues. (a) Prior to process modifications, cells that were suspended in prepolymer settled within tubing between the syringe and the device, resulting in oscillating cell density reaching the nozzle and an uneven number of cells per microtissue. (b) When cells are injected in an isopycnic medium, and as a separate stream from concentrated prepolymer, the distribution narrowed to the Poisson limit.

interactions before they are self-assembled with other microtissues to activate heterotypic interactions. For instance, when cultured for several days, adenocarcinoma cells encapsulated from a single-cell suspension formed multicellular spheroids (**Fig. 2.7e**). In addition, encoding DNA is bound to the hydrogel scaffold rather than directly onto the cell membrane,[211, 212] where covalently bound ligands may be susceptible to recycling or may potentially modify cell function. Encoded microtissues can remain in assembled patterns for an extended period of time without additional measures for immobilization (e.g. embedding in agarose[195]), and then removed for further culture, isolation, and biochemical analysis.[149] DNA provides a way for programmed detachment via dehybridization (e.g. competitive binding with free ssDNA) or cleavage (e.g. restriction enzymes).[211] Alternatively, patterned microtissues could be stabilized into a contiguous tissue by a secondary hydrogel polymerization[200] or cell adhesion between microtissues to form 3D sheets for implantation (**Fig. 2.9**).

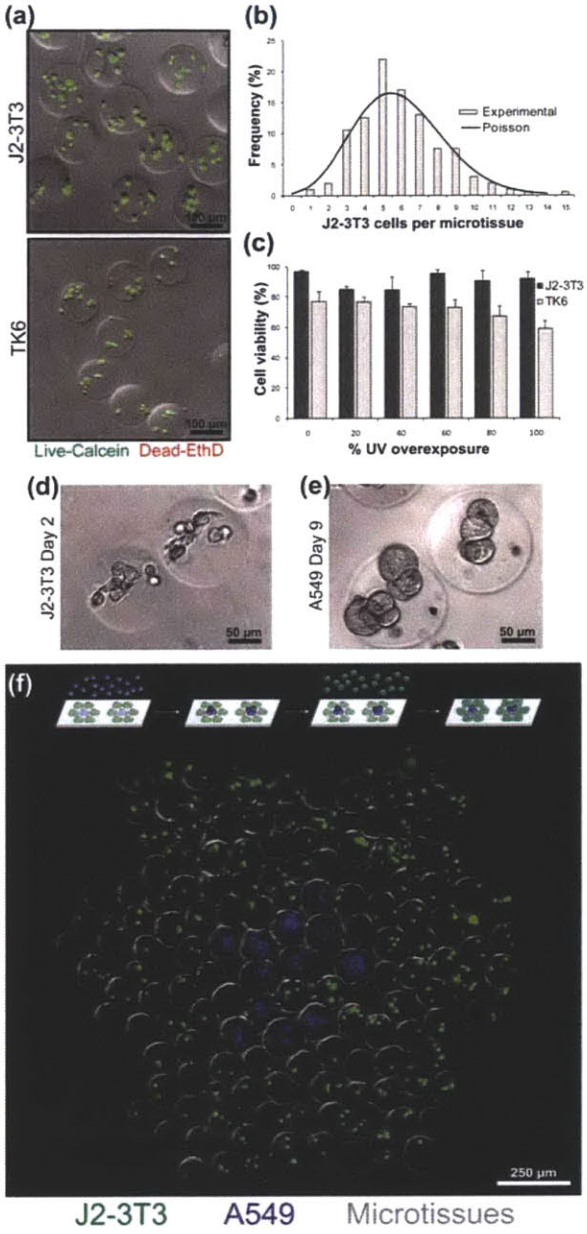

Figure 2.7. Cell encapsulation and microtissue culture. (a) Rat fibroblast (J2-3T3) and human lymphoblast (TK6) cell lines uniformly encapsulated within microtissues and stained for viability. (b) Histogram of J2-3T3 distribution within microtissues and comparison to optimal Poisson statistics. (c) Viability of J2-3T3 and TK6 cells three hours post-encapsulation at increasing % UV overexposure past the minimum intensity required to fully polymerize microtissues. (d) J2-3T3 cells attached and spread within microtissues decorated with RGDS peptides. (e) Human lung adenocarcinoma (A549) cells aggregated to form multicellular tumor spheroids within microtissues. (f) Microtissues encapsulating either J2-3T3 (CellTracker Green) or A549 cells (CellTracker Blue) were self-assembled into composite hexagonal clusters.

Finally, to demonstrate DNA-templated positioning of microtissues containing distinct cell types into pre-defined patterns, we encapsulated adenocarcinoma cells (blue) and fibroblasts (green) into separate microtissues and encoded them with orthogonal DNA sequences (C and D respectively). These microtissues were then seeded onto an array printed with hexagonal clusters of complementary DNA (C′ centered within 6 spots of D′), forming co-cultures of the two cell types representative of a tumor nodule surrounded by stromal cells (**Fig. 2.7f**). Multicellular constructs patterned using this method could be relevant model systems for studying cancer-stroma interactions in 3D. Notably, although DNA-templated microtissues are patterned on a 2D template, cells are encapsulated and respond to a locally 3D microenvironment, e.g. developing into tumor spheroids (**Fig. 2.7e**) rather than growing as a 2D monolayer.[82] Heterotypic signaling from stromal cells has been shown to contribute to tumor invasion and metastasis.[186] The combination of precise spatial control, similar to that achieved in 2D,[146] but with a 3D environment, will be critical toward elucidating such cell signaling mechanisms.

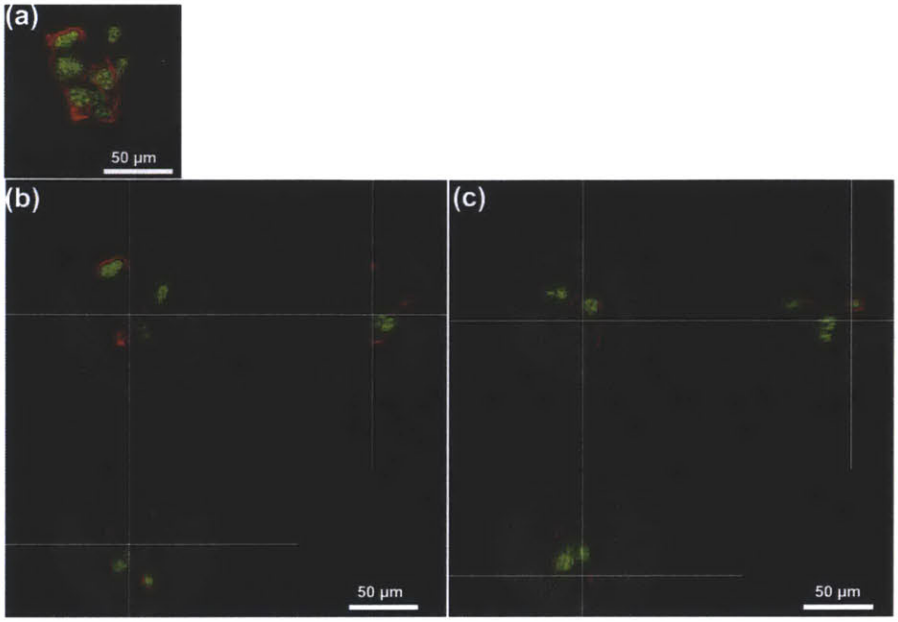

Figure 2.8. Multi-photon images of fibroblast spreading within RGDS microtissues. (a) Maximum intensity projection and (b) slice images of J2-3T3 fibroblasts spreading on Day 4 post-encapsulation. Red: actin (phalloidin), green: hydrogel (biotin-4-fluorescein), bright-green: nuclei (Hoecht).

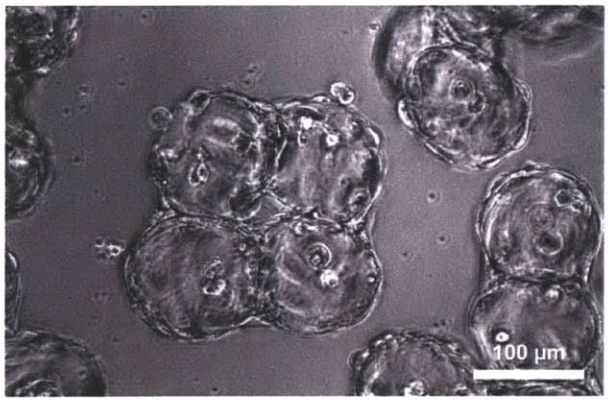

Figure 2.9. Fibroblast-laden, RGD-decorated microtissues cultured in close contact and in the presence of non-encapsulated fibroblasts. Contiguous microtissue-assembled structures linked by adherent cells formed by D1 post-encapsulation.

2.4 Conclusion

We have described a method to organize multiple cell types within a 3D microenvironment that integrates the top-down patterning of a DNA microarray template with the bottom-up assembly of DNA-encoded, cell-laden microtissues. This is the first demonstration of microtissue assembly that is directed by specific biomolecular interactions. The speed and scalability of the assembly process is compatible with DNA templates that can be fabricated by other top-down techniques, such as microfabrication and micro-contact printing, for a diverse range of features and patterning resolution. The programmable molecular interaction of DNA to direct assembly has the potential to be extended to even larger sets of encoding sequences to create more complex heterogeneous structures. The ability to precisely control cell-cell interactions (e.g. cancer-stromal cell, hepatic-nonparenchymal cell) via microfluidic cell encapsulation and DNA-templated microtissue assembly provides a unique opportunity to increase our fundamental understanding of complex diseases or to construct highly functional tissue-engineered implants.

2.5 Acknowledgements

Dr. David Wood and Caroline Hsu were co-authors on this work. We thank Dr. Alice A. Chen and Dr. Gabriel A. Kwong for helpful discussions and editing, and Dr. Bevin P. Engelward (MIT) for providing the TK6 cell line. We acknowledge the Swanson Biotechnology Center (SBC) of the Koch Institute at MIT for the use of microscopy facilities. This work was

supported by the NIH (grants R01-DK56966, R01-EB008396) and Stand Up to Cancer (SU2C). C.Y.L. acknowledges support from the NDSEG and NSF Graduate Fellowships. D.K.W. acknowledges support from the Kirschstein NRSA Fellowship. S.N.B. is an HHMI Investigator.

Chapter 3: Flow Analysis of Microenvironmental Effects on Tumor Proliferation

3.1 Introduction

The cellular microenvironment, which includes soluble signals such as growth factors and hormones, as well as insoluble signals such as cell-cell and cell-matrix interactions, regulates key aspects of healthy and diseased tissue functions. This observation is particularly relevant in cancer, where the microenvironment has been shown to play a critical role in tumor development, metastasis, and drug resistance[38-41]. For example, drug resistance in tumor cells can be modulated by the addition of stromal cells[219] as well as culture in 3D spheroids[86, 89, 101, 220] or encapsulation in synthetic or natural extracellular matrix (ECM)[82, 221]. The unique phenotypes demonstrated in 3D cell culture are due to changes in a variety of microenvironmental factors, including altered cell-cell contacts, diffusion of nutrients and signaling mediators[92], and integrin ligation with growth factor pathway crosstalk[83, 92, 222, 223]. Because cellular behavior is dependent on architectural cues, studying microenvironmental influences on cancer progression in 3D could offer unique opportunities. Animal models inherently include critical microenvironmental cues and three-dimensional tissues, but they lack the throughput required for many applications. *In vitro* tumor models that allow us to control microenvironmental cues specifically in a 3D context may provide a complementary tool to bridge 2D and *in vivo* studies, and may more accurately predict *in vivo* cancer progression and response to therapeutics.

Systematic exploration of microenvironmental cues for many applications, such as drug screening, requires high-throughput platforms that incorporate rapid production and analysis of combinatorial 3D tissue constructs. Microscale versions (100-500 μm) of cell-laden gels ("microtissues") can incorporate a range of co-encapsulated stromal and external diffusible cues. Microtissues have been fabricated by various methods including photolithography[156, 224], micromolding[152], and emulsification[157], but the majority of these techniques are limited in throughput or result in extremely polydisperse microtissue populations. A promising method for high-speed production of microtissues is droplet-based cell encapsulation, wherein a cell-prepolymer mixture is emulsified on-chip by a shearing oil stream and polymerized while in droplets[225]. This process has been demonstrated for a variety of ECM materials, including polyethylene glycol (PEG)[225], alginate[141, 226], collagen[227], and agarose[139], is compatible with a range of cell types (>90% encapsulation efficiency), and rapidly produces large numbers of monodisperse microtissues (6000 gels/min). Although droplet devices facilitate high throughput microtissue fabrication, to date analysis of droplet-derived microtissues has relied on serial imaging. While imaging is information-rich, it is labor-intensive and would become a bottleneck in the context of high throughput screening, especially with large numbers of microtissues. One solution for increasing analytical throughput is the use of an in-flow sorting and analysis system, similar to flow cytometry, that can analyze and sort microtissues on multiple parameters, such as cell density, size and composition based on time-of-flight, extinction, absorbance, and fluorescence. The capability of such a system to quantify fluorescent reporter expression has been demonstrated using microtissues that represent stages of liver development and disease ($n \geq 102–103$, fabricated by photolithography)[149]. Combining high-

speed in-flow analysis with a high throughput microtissue fabrication would produce an ideal system for combinatorial microenvironmental modulation that could be used in high-throughput biology and screening cancer therapeutics.

In this chapter, we combine microfluidic cell encapsulation with large-particle flow analysis to present an integrated platform for studying the effects of microenvironmental cues (cellular, ECM, growth factors, drugs) on tumor cell proliferation in various 3D contexts. To specifically interrogate the impact of various microenvironmental inputs, tumor and stromal cells were incorporated into droplets at high densities and cell-ECM interactions were controlled by physically entrapping full-length matrix proteins within the encapsulating hydrogel. Furthermore, we exploited the native stochasticity generated during microfluidic encapsulation to generate diverse subpopulations of microtissues that contain varied degrees of homotypic and heterotypic interactions, and we isolated those subpopulations using flow sorting to generate highly defined microenvironments. As the primary readout, sorted populations cultured with and without exposure to a panel of soluble factors were re-examined via flow analysis to rapidly record large-scale population data (n>500 events). Finally, we applied this platform to investigate the influence of TGF-β signaling, which is known to be strongly context-dependent and can be either tumor suppressing or cancer promoting, on tumor cell proliferation. We report the outcome of a proof-of-principle drug candidate screen on $Kras^{LSL\text{-}G12D/+};p53^{flox/flox}$ mouse non-small-cell lung cancer (NSCLC) derived cell lines[16]. This screen revealed differing sensitivities of these particular lines to TGF-β signaling in 3D that were not observed in 2D. Our ability to study tumor biology and to develop effective new therapies will require systematic study of tumor cells within a microenvironmental context. The platform that

we have developed provides a high-throughput method to study drug response and tumor biology within highly-defined microenvironmental niches.

3.2 Materials and Methods

Tunable microtissue synthesis

Microfluidic device fabrication and cell encapsulation have been described previously[225]. Briefly, cells or a mixture of cells were injected into the device as an isopycnic suspension and mixed on-chip with 2x concentrated photopolymerizable polyethylene glycol prepolymer. For microtissues functionalized with matrix proteins, collagen I (rat tail, BD Biosciences), fibronectin (human, Millipore), or laminin (murine, Sigma) were included in the concentrated prepolymer at 40 μg/ml. The combined aqueous stream, consisting of 10% (w/v) PEG-DA (20kDa, Laysan), 0.1% (w/v) Irgacure-2959 (Ciba), 1% (v/v) n-vinyl pyrrolidone (Sigma-Aldrich), up to 20 μg/ml ECM proteins, and up to $50x10^6$ cells/ml, was sheared into droplets by fluorocarbon oil at a flow-focusing junction. Downstream, ultraviolet light (Exfo Omnicure, 500 mJ/cm^2) was used to crosslink droplets into spherical cell-laden hydrogels. Microtissue size was controlled by adjusting the oil/prepolymer flow rates (typically 800 μl/hr and 200 μl/hr, respectively) to produce monodisperse microtissues between 50-120 μm that were collected and washed in media before preliminary analysis and sorting.

Large particle flow cytometry

Microtissue reporter and cell fluorescence levels were quantified using a complex object parametric analyzer for handling 500 μm objects (COPAS Select, Union Biometrica) according to the manufacturer's instructions. Samples were first gated by Time of Flight (size) *vs.* Extinction (optical density) to exclude cell debris and aggregates. Gated microtissues were then analyzed for Green (gain: 300) and FarRed (gain: 850, -50% Green compensation) fluorescence and sorted into multiwell plates filled with media. Post-sorting, microtissues were washed in PBS by filtering through 40 μm nylon strainers, resuspended in media, and transferred to low-attachment plates for culture and treatment. COPAS data was re-gated and processed using custom MATLAB code.

Cell culture

Murine cell lines 393T5 and 394T4 have been previously described[16]. Briefly, tumors were initiated in $Kras^{LSL\text{-}G12D/+};p53^{flox/flox}$ mice with intratracheal lentiviral-*Cre* vectors. Tumors were then excised from the mice, enzymatically digested, and subsequently plated onto tissue culture treated plastic to generate cell lines. Cell lines were transfected with ZsGreen[33] and subsequently cultured in Dulbecco's Modified Eagle Medium (DMEM, Invitrogen) with 10% fetal bovine serum (Invitrogen), 10 U/ml penicillin (Invitrogen), and 10 mg/ml streptomycin (Invitrogen). J2-3T3 fibroblasts were cultured in DMEM with 10% bovine serum (Invitrogen), 10 U/ml penicillin, and 10 mg/ml streptomycin. All cells were cultured in a 5% CO_2 humidified

incubator at 37°C. To label fibroblasts prior to encapsulation, cells were detached with 0.25% trypsin-EDTA (Invitrogen) and resuspended in PBS. CellTracker Far Red DDAO-SE (Invitrogen, 1.18 mM in DMSO) was added to the cell suspension (1:625 dilution) and incubated for 45 minutes at 37°C. The cell pellet was then centrifuged, washed, and either re-plated (the dye was stable for several days) or used immediately.

Growth factors and inhibitors

Microtissues were cultured in 10% serum media and treated with growth factors EGF, TGF-β, VEGF, or HGF (R&D Systems) at 50 ng/ml. Small molecule inhibitors were dosed into the microtissue media to a final 10 μM in 0.2% DMSO: SB525334 (Tocris), SJN2511 (Tocris), LY2157299 (Selleckchem), dorsomorphin dihydrochloride (Tocris), DMH-1 (Tocris), or GW5074 (Tocris).

Tumor cell proliferation in 2D

393T5 cells were detached with 0.25% trypsin-EDTA (Invitrogen) and replated at a density of 4000 cells/well into 96-well plates. One day post-seeding and daily thereafter, fresh media and drugs were added and ZsGreen fluorescence was measured using a microplate reader (Molecular Devices).

Microtissue staining and visualization

Live microtissues were imaged directly for ZsGreen-labeled tumor cell line fluorescence or CellTracker Far Red-labeled fibroblasts. Alternatively, microtissues were fixed and permeabilized in order to count embedded cell nuclei. To bypass any difficulties preserving ZsGreen protein fluorescence after fixation, microtissues containing ZsGreen-labeled cells were additionally incubated with CellTracker Green CMFDA (Invitrogen) prior to being fixed (4% paraformaldehyde). Microtissues were then permeabilized (0.05%Triton X-100), and stained with Hoechst 33342 (Invitrogen). Images were acquired with a Nikon Ellipse TE200 inverted fluorescence microscope, a CoolSnap-HQ Digital CCD Camera, and MetaMorph Image Analysis Software. NIH software ImageJ was used to uniformly adjust brightness/contrast, pseudocolor, and merge images.

Statistical analysis

Data are presented as mean ± SEM, except for microtissue cell counts which are described as mean ± standard deviation. Samples were compared using one-way ANOVA, with p-values of <0.05 considered statistically significant.

3.3 Results and Discussion

3.3.1 Platform design

Many techniques for 3D tumor culture have been developed, including encapsulating cells within bulk hydrogels of specific scaffold materials, to control stiffness and ECM

composition. However, these systems do not miniaturize readily for high-throughput studies, especially in situations when cells or reagents are limiting. Further, readouts for larger gels often require imaging[15], which is slow and laborious, or biochemical assays that provide only a global measurement averaged over many local microenvironments. Alternatively, formation of 3D tumor spheroids[7] has been useful in elucidating the importance of architecture on tumor phenotype. Unfortunately, these niches do not incorporate the kind of microenvironmental control that is available through tuning the physical and biochemical properties of engineered scaffolds.[228]

To generate homogeneous populations of defined microtissues for evaluating proliferative potential under designated microenvironmental and soluble cues, we established an experimental workflow that can be divided into five phases (**Fig. 3.1**). First, fluorescently labeled tumor cells are microfluidically encapsulated with the desired combination of stromal cells or ECM into synthetic 3D microtissues (**Fig. 3.1a**). We chose poly(ethylene glycol) diacrylate (PEG-DA, 20kDa) as the hydrogel material because it provides a biocompatible, non-stimulatory background, and unlike other scaffold materials, such as collagen or agarose, PEG can be chemically decorated with integrin binding peptides[114], proteins[229], and other ligands[131].

In the second phase, a large-particle flow analyzer is used to initially characterize freshly generated microtissues in multiple channels of embedded-cell fluorescence (**Fig. 3.1b**). Defined populations of microtissues are selected and sorted by tumor and/or stromal cell density (**Fig. 3.1c**). These steps are required because microfluidic cell encapsulation is an inherently stochastic process: for small numbers of cells, a wide range of cell numbers will be encapsulated in each

microtissue. In the best-case scenario, theory suggests that the distribution of cells within microtissues will be determined by Poisson statistics[225]. However, due to issues of cell settling and aggregation at high cell densities, the cell distribution will often be much more variable in practice. Systems have been optimized to encapsulate single cells[230, 231], but controllably encapsulating 10-100 cells, which are closer to the cell density used in spheroid culture[220], is more challenging. While working in this cell density regime, unavoidable variations in microtissue density and composition of different cell types can reduce the statistical power of the analysis. For example, if a microtissue population (n=500) immediately post-encapsulation has a standard deviation that is 3x the mean fluorescence (σ/μ=3), one could measure a 40% difference in proliferation with 80% statistical power. Since the population spread usually increases over the course of the experiment due to biological variation, this power would decrease even further for later time points. By contrast, using a pre-sort, initial spreads are constrained to approximately σ/μ=0.2, with final standard deviations between σ/μ=0.5 to 1. With these sorted populations, even changes as small as 13% could be detected with 80% statistical power. Further, we take advantage of the initial heterogeneity of the population to produce multiple "bins" of encapsulated cell numbers from a single encapsulation step.

In the next phase, sorted microtissues are collected in tissue-culture wells for 2-6 days of culture, during which they can be treated with soluble growth factors or drugs (**Fig. 3.1d**). During this time, cells proliferate within the microtissues and can be visualized by microscopy. At the desired time point, treated microtissues are collected and re-analyzed by large particle cytometry for changes in overall fluorescence of the embedded cells (**Fig. 3.1b**). This method

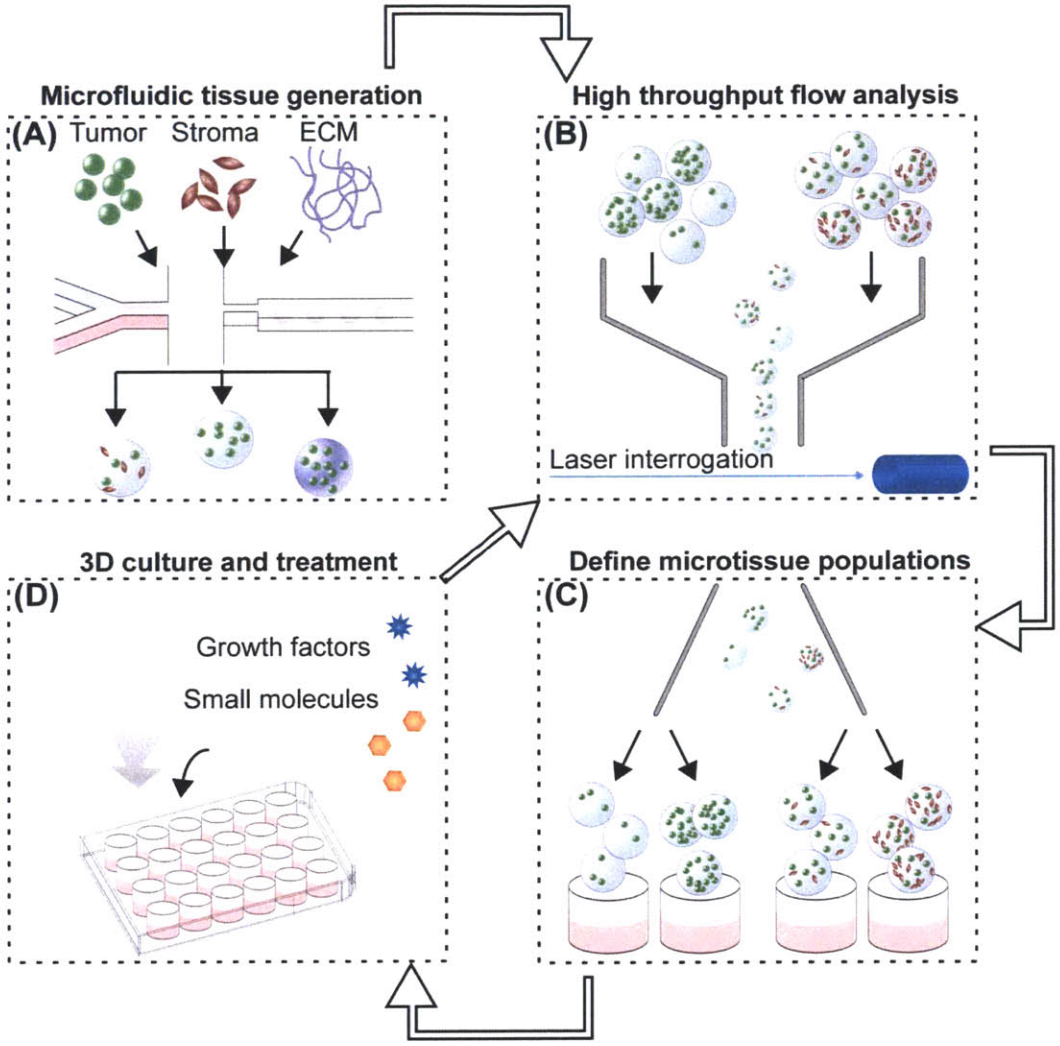

Figure 3.1. 3D tumor microenvironment screening platform. (A) Microfluidic droplet-based encapsulation of tumor cells into microtissues that can be tuned with co-encapsulated stromal cells or entrapped ECM molecules. (B) Produced microtissues are rapidly interrogated in multiple fluorescent channels using large-particle flow analysis. (C) Cytometry-like flow sorting separates and defines microtissues with controlled levels of homotypic and heterotypic interactions. (D) Cellular microenvironment within microtissues is further modulated by soluble factors such as cytokines or small molecule drugs. The extent of cell proliferation within individual microtissues is then detected by flow analysis (B) to collect population-level data on responses to microenvironmental conditions.

offers higher throughput than methods that require serial imaging as a readout, and unlike traditional bioassays that require release of cells from the microgels, our whole-microtissue flow measurement is non-destructive. After every analysis step using our platform, each microtissue population can be re-collected for additional culture periods and subsequent analysis, allowing us to study the evolution of a single population over time.

3.3.2 Controlling tumor homotypic and heterotypic interactions

Cell-cell interactions, both homotypic and heterotypic, are among the most potent modulators of cellular function. Our platform was designed to generate uniform populations of microtissues of user-defined tumor cell (homotypic) and/or accompanying stromal cell (heterotypic) densities. To demonstrate control over homotypic density, we generated a parent population of microtissues, incorporating a range of numbers of murine non-small cell lung cancer cells (393T5) bearing a constitutive fluorescent reporter protein (ZsGreen). The 393T5 NSCLC cell line was established from a primary tumor that formed distant metastases[16]. Because total microtissue fluorescence, as measured using the COPAS, exhibits a linear correlation with cell number (**Fig. 3.2**), we divided our parent population into multiple subpopulations by enriching each bin for a particular range of encapsulated cells (**Fig. 3.3a**). Examination of subpopulations immediately post-sorting reveals three distinctly separated, narrow peaks (**Fig. 3.3a**). After three days in culture, cell growth within microtissues yields populations that remained separable, demonstrating the ability to control homotypic density over time (**Fig. 3.3a**). During these several days in 3D culture, tumor cells that were originally

encapsulated as single cells (**Fig. 3.3b**) gave rise to tumor spheroids within the microtissues (**Fig. 3.3c**), whereas the same cells typically grow as a monolayer when placed in 2D culture[232]. Compared to spheroid models, which require several days to form 3D aggregates, multicellular microtissues in our platform are formed with no time delay. Furthermore, the size and cellular density of spheroids may vary over time due to proliferation and/or contractile forces. The microtissues formed in this study display 3D growth features and allow control of volumetric cell density and interstitial scaffold material.

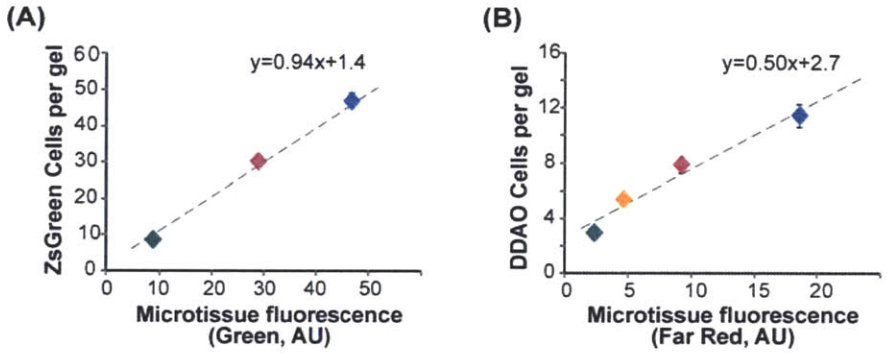

Figure 3.2. Correlation of number of (A) ZsGreen expressing 393T5 cells or (B) CellTracker FarRed. DDAO-stained J2-3T3 fibroblasts encapsulated per microtissue as quantified by nuclear staining and microscopy, with microtissue fluorescence in the corresponding channel as detected by flow analysis.

In addition to the influence of homotypic interactions, stromal cells exert a significant effect on tumor growth and the potential for metastasis[39, 41, 233]. In order to study the impact of these cellular interactions, previous studies have varied the stromal cell to parenchymal cell composition within microgels, albeit at lower cell densities, by changing the flow rates of two corresponding cell streams[139]. This "pre-encapsulation" control strategy yields desired stromal:parenchymal cell compositions, at least on average, but the specific ratio in a given

microgel varies widely across the population. For example, if two cell types are mixed at a density to give on average 8 cells per gel at a 1:1 ratio, Poisson statistics dictate that only 14% of the resulting gels will actually have equal numbers of the two cells. For an average 1:3 stromal to parenchymal ratio, even fewer gels will contain 1:3 cell numbers, with many gels containing no stromal cells at all[24]. To exert finer stoichiometric control of tumor and stroma "post-encapsulation", we incorporated stromal cells into our microtissue models by mixing and co-encapsulating the 393T5 cells with J2-3T3 murine fibroblasts, and generated a parent population of microtissues from one prepolymer mixture with a range of tumor to stroma ratios.

Subsequently, we performed a 2-parameter sort with green and far red fluorescence representing the number of cancer cells and co-encapsulated fibroblasts, respectively (**Fig. 3.3d**). We were able to separate the parent population into low (2.5±0.3 cells/gel) and high (5.0±1.7 cells/gel) numbers of fibroblasts, while holding the number of the cancer cells constant (7.0±2.7 cells/gel), thus generating distinct populations with a two-fold range of stromal to cancer ratios, but consistent cancer cell density (**Fig. 3.3e**). By defining stromal composition "post-encapsulation" rather than "pre-encapsulation," we take advantage of the stochasticity of encapsulation to generate multiple populations with different ratios from a single microfluidic process. This allows us to establish populations with a wide dynamic range of absolute cell numbers as well as cellular composition patterns. Further, the tunability of the sorting parameters (**Fig. 3.4**) allows user-defined tolerances to set the desired spread of cell ratios, which will in general be tighter than those achieved using control over average cell concentrations alone. Therefore, by controlling the bin thresholds, subsequent studies can be

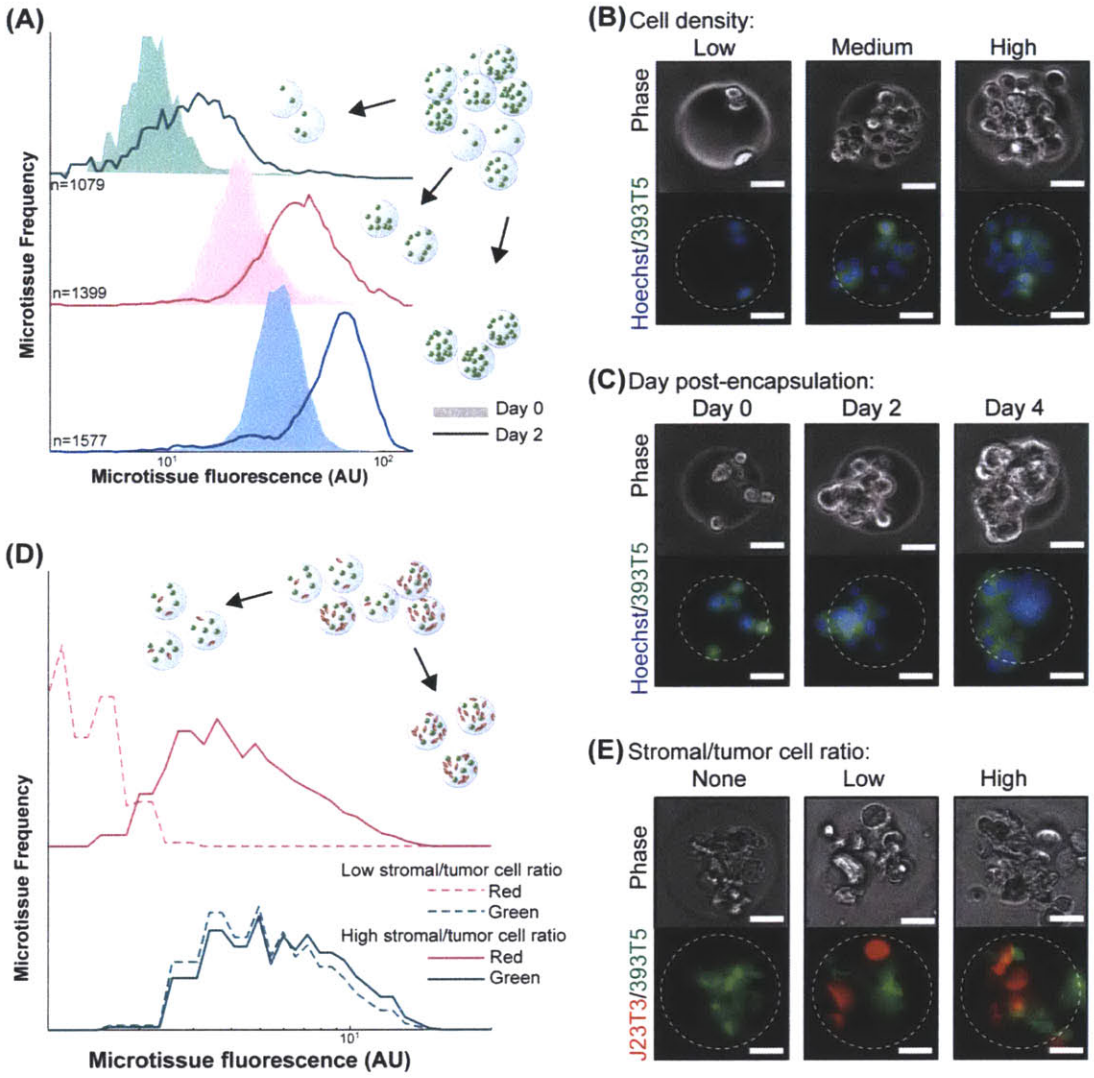

Figure 3.3. Control over homotypic and heterotypic microtissue composition. (A) Histograms of ZsGreen-labeled 393T5 (lung cancer-derived cell line) microtissue populations, using sorted ZsGreen fluorescence as a measure of homotypic density, before (Day 0) and after (Day 2) proliferation. (B) Phase and epifluorescence images of 393T5 cells embedded within microtissues at various cell densities and stained with CellTracker Green CMFDA. (C) Growth of CellTracker CMFDA stained 393T5 cells within microtissues into spheroids over four days. (D) Microtissues containing 393T5 cells co-encapsulated with CellTracker FarRed stained fibroblasts, sorted by stromal cell density (Red fluorescence) while maintaining desired tumor cell density (ZsGreen fluorescence) to achieve a two-fold change in stromal:tumor cell ratio between the High vs. Low populations (E) Phase and epifluorescence images of 393T5 cells (ZsGreen) co-encapsulated with J2-3T3 cells at different ratios. All scale bars: 50 μm.

performed on populations in which every individual, sorted microtissue contains stromal cells at a particular ratio.

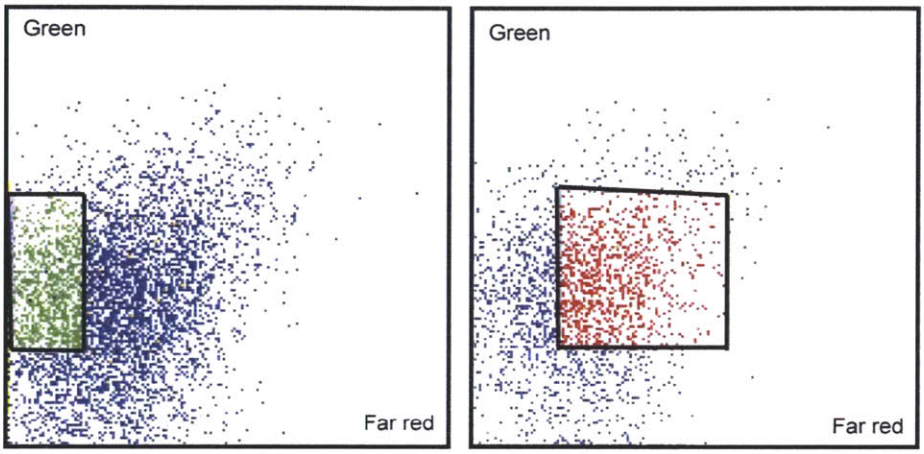

Figure 3.4. Flow analysis and sorting of microtissues containing co-encapsulated tumor (393T5) and stromal (J2-3T3) cells. Individual microtissues (blue events) displaying variations in number of each cell type. Y-axis = Green 393T5 cell density, X-axis = FarRed J2-3T3 cell density. Low stromal ratio and high stromal ratio populations were defined by gating in both channels, maintaining the same y-axis range in both gates, but shifting the x-axis gate to the left (green events) for lower stromal density, and to the right (red events) for higher stromal density.

3.3.3 Modulating cell proliferation with microenvironmental factors

At the molecular level, ECM and soluble factors play a large role in modulating cellular function. In cancer, VEGF secretion stimulates angiogenesis, which is a critical component of tumor growth[234]. Similarly, matrix remodeling is correlated with a more invasive phenotype[41, 235]. We were interested in the ability to test how cytokines and ECM modulate metastatic potential in a 3D context, using proliferation as a surrogate for invasive growth. The composition of our PEG-DA hydrogels (10 wt%, 20kDa) was chosen to form a semi-permeable network (7 nm mesh size[236]) that allows diffusion of soluble proteins with sizes up to 100 kDa[237],

which includes most cytokines. First, we encapsulated 393T5 cells in microtissues, and we sorted them to enrich for a particular homotypic density (17.4±3.4 cells/gel), which we held constant across experiments. Then we cultured the enriched microtissue population for two days in media supplemented with growth factors that have been widely implicated in cancer progression: 50 ng/ml of EGF, HGF, VEGF, or TGF-β (**Fig. 3.5A**). Exposure to EGF, HGF, and VEGF had no significant effect on proliferation as compared to vehicle control-treated microtissues. The lack of impact of EGF is consistent with the fact that these cells overexpress *Kras*, which is downstream of the EGF receptor[16, 234]. Interestingly, treatment with TGF-β led to a significant reduction in proliferation ($p < 10^{-10}$). TGF-β is known to have a tumor suppressor effect in some early-stage cancers but has also been shown in other cases to promote metastasis, leading to epithelial to mesenchymal transition, especially in later stage cancers[238]. While the 393T5 cell line was derived from a primary tumor with proven metastatic potential, our data suggests that the primary tumor still displays an early-stage phenotype that can be suppressed by TGF-β, consistent with observations of other primary lung cancer models[239].

In addition to examining the impact of soluble factors, we also applied our platform to study the effect of ECM proteins on metastatic potential in 3D. ECM interactions with cell integrins are known to not only trigger direct downstream signaling, but also to modulate the response of cells to other inputs such as drugs and growth factors through pathway crosstalk[240, 241]. To include ECM in our microtissues, we co-encapsulated 393T5 cells with collagen I (300 kDa), laminin (850 kDa), or fibronectin (440 kDa), adding 20 μg/ml of the protein to the pre-polymer mixture so that it is physically incorporated within microtissues during

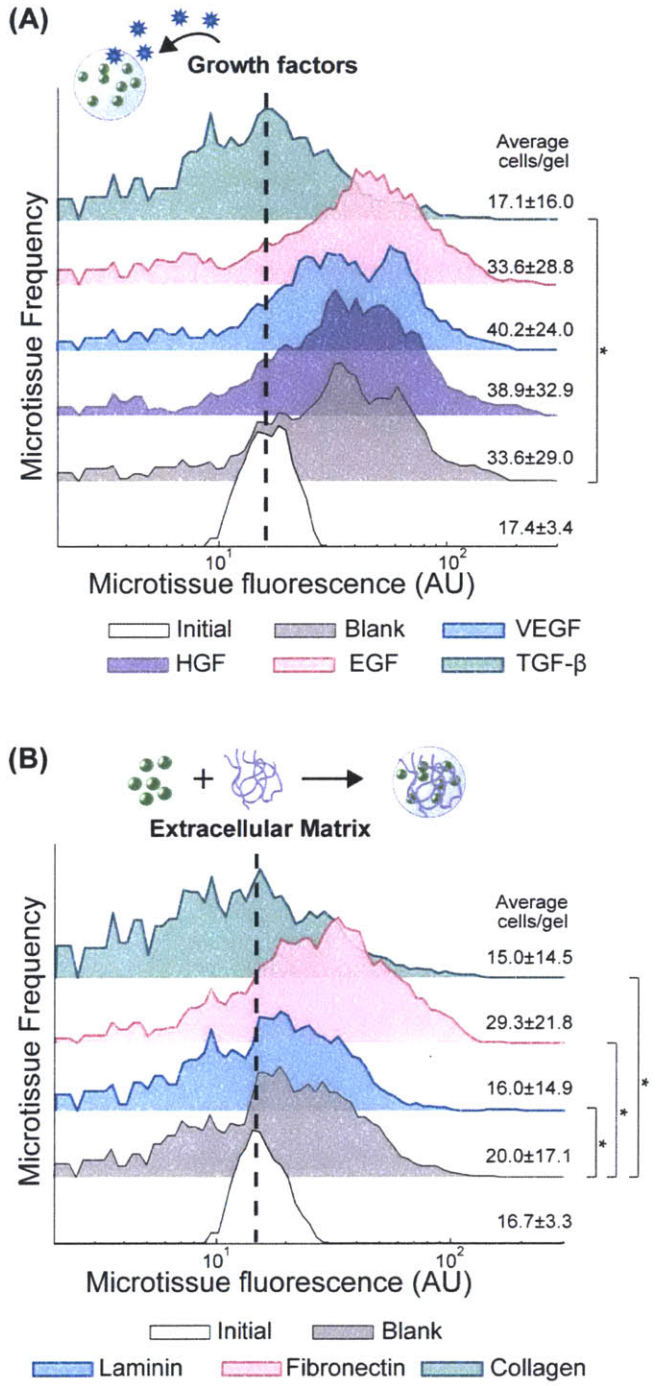

Figure 3.5. Modulation of tumor cell proliferation by cytokines and ECM. 393T5 growth within microtissues (initial 17.4+/-3.4 cells/gel) when (A) cultured in media containing 50 μg/ml VEGF, HGF, EGF, or TGF-β, or (B) encapsulated in the presence of to 20 μg/ml of laminin, fibronectin, or collagen-1 that remain physically entrapped within the hydrogel scaffold. Average number of cells per gel calculated from microtissue fluorescence using linear regression. * indicates $p < 0.01$.

photopolymerization. Due to the size of the hydrogel network, large proteins (>150 kDa) are able to diffuse only very slowly through the gel (**Fig. 3.6**). Therefore, we expect that the even larger ECM proteins remain effectively entrapped in the microtissues over the timescale of our experiments. Also, at this low concentration, the ECM proteins are unlikely to significantly impact the physical properties of the 100 mg/ml PEG-DA hydrogel. Thus, baseline nutrient diffusion and cell growth rates are comparable, allowing a horizontal comparison of ECM molecule signaling effects in 3D using minimal amounts of expensive ECM materials, and without the confounding factor of varying mechanics (e.g. collagen gels vs. fibrin gels) or network properties. ECM-functionalized microtissues enriched for a specific homotypic density were sorted and cultured for 2 days **(Fig. 3.5b).** Consistent with their pro-metastatic phenotype, the tumor-derived cells exhibited significantly elevated proliferation in the presence of fibronectin ($p < 10^{-10}$), which has been shown previously to correlate with metastatic activity[242, 243]. In contrast, growth was inhibited in the presence of both laminin ($p < 0.01$) and collagen I ($p < 10^{-4}$), again demonstrating a tumor cell preference for proliferation in an invasive-supporting matrix over basement membrane proteins. Additionally, collagen I has been reported to induce TGF-β3 expression in some lung cancer cells[244], which could lead to an indirect growth inhibition mediated by this ECM, consistent with our observations in response to TGF-β3 exposure, described above (**Fig. 3.5a**).

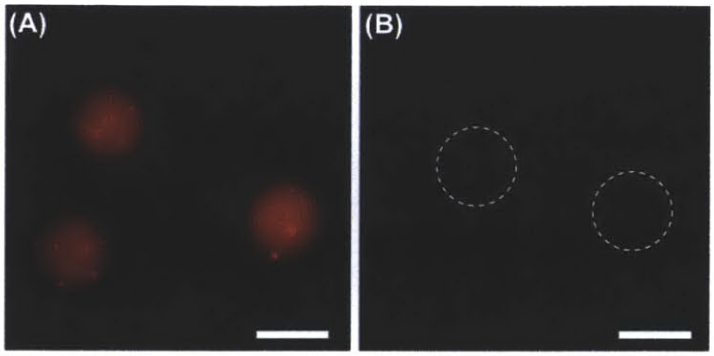

Figure 3.6. Epifluorescence microscopy of cell-free microtissues containing encapsulated proteins. Microtissues are formed from either (A) prepolymer containing 20 μg/ml of Texas Red labeled antibody (rabbit, polyclonal IgG), or (B) control blank PEG prepolymer. Microtissues were washed in PBS for 24 hours post-polymerization. Scale bar = 100 μm.

3.3.4 Microenvironmental modulation of tumor drug response

Having demonstrated that our sortable microtissue platform can be used to assess the responsiveness of tumor cell populations to soluble as well as embedded matrix proteins, we sought to apply this system to conduct a small-scale pilot drug screen. In contrast to conventional 3D gels, miniaturized tumor microtissues offer the advantage for screening purposes in that reagent costs can be reduced, especially with respect to the amount of drug needed to treat a certain media volume, while the number of replicates is maximized. Combined with its high-throughput readout that will reduce experimental time and effort needed per drug, our platform offers extreme scalability to support even broader screens. As a first proof of concept, we hypothesized that this platform could be used to probe candidate drugs that impact tumor cell proliferation specifically in a 3D architecture, as opposed to any outcomes observed in conventional 2D culture conditions. Given that exogenously supplied TGF-β inhibited 393T5 proliferation (**Fig. 3.5a**), and perturbations in TGF-β signaling have been

found to be strongly tumor- and context-dependent[238], we selected several small-molecule inhibitors that disrupt aspects of the TGF-β signaling pathway: SB525334 (TGFβR1), SJN 2511 (TGFβR1), and LY2157299 (TGFβR2, TGFβR1). Dorsomorphin (AMPK, ALK2, ALK3, ALK6), DMH-1 (ALK2), and GW5074 (c-raf) were also tested and all treatments were compared to the growth of DMSO vehicle-treated microtissues, or TGF-β as a negative control for 3D growth. For 3D assays, encapsulated 393T5 cells were sorted for a specific population density and cultured for several days in the presence of 10 μM of the inhibitors. Proliferation was assayed based on the change in microtissue fluorescence over time. We compared these results to those found in a 2D assay, where 393T5 cells were seeded on tissue culture microplates and proliferation was tracked by microplate well fluorescence[219].

Using this assay, we detected statistically significant alterations in microtissue proliferation in response to several of the drug candidates, relative to untreated and DMSO controls (**Fig. 3.7a**). The TGFβR1 inhibitor, SB525334, was one of several compounds that exerted similar effects in both 3D and 2D conditions, in that it led to reduced proliferation in each case (**Fig. 3.7b**). Dorsomorphin caused cell death in both geometries, and GW5074 elicited little to no anti-proliferative effect (**Fig. 3.7a,b**). However, we noted marked differences between 2D and 3D responses to TGF-β and LY2157299. Specifically, while TGF-β inhibited proliferation in 3D as observed previously, the cytokine did not exert any significant effect in 2D. The opposite trend was observed in response to the TGFβR1/TGFβR2 inhibitor, LY2157299, in that it inhibited proliferation in 2D cultures, but did not alter 3D microtissue growth (**Fig. 3.7a, b**). We extended our observations by repeating the drug screen using a second cell line isolated from a mouse with the same genetic background (394T4). Consistent results were obtained when the

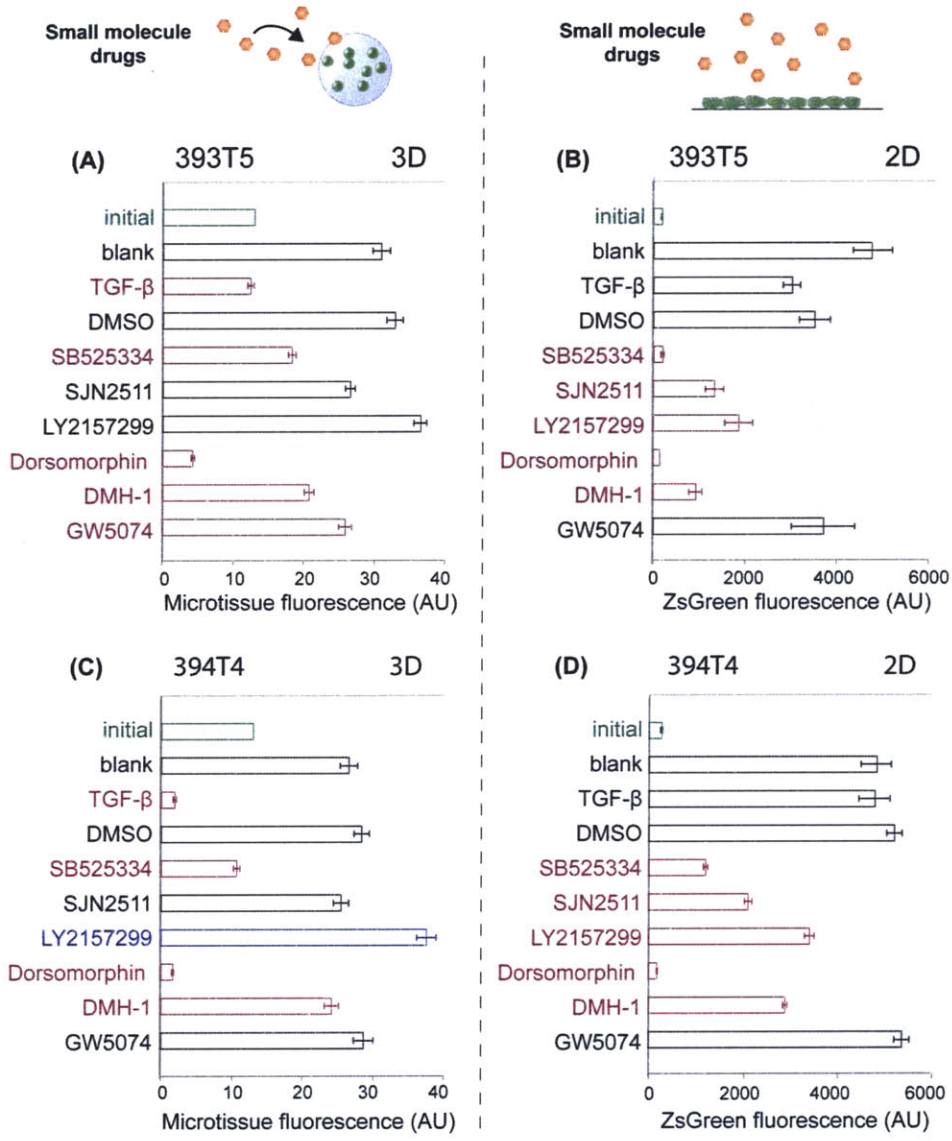

Figure 3.7. Comparison of 393T5 (A-B) and 394T4 (C-D) lung cancer cell response to drugs when cultured in 3D microtissues (A,C) vs. in 2D monolayers (B,D). Cells were treated in both formats with 10 μM of SB525334 (TGFβR1), SJN 2511 (TGFβR1), LY2157299 (TGFβR2, TGFβR1), Dorsomorphin (AMPK, ALK2, ALK3, ALK6), DMH-1 (ALK2), or GW5074 (c-raf), or 50 ng/ml of TGF-β. Microtissue or tissue-culture well fluorescence for each condition are shown after 3 days of culture for 393T5 cells and 5 days of culture for 394T4 cells, which proliferate slower in control conditions, so that the two cell lines undergo the same number of population doublings during each assay. Initial conditions are labeled in green (3D: 13.5 +- 2.5 cells/gel, 2D: 26×10^3 cells/cm^2). Gray rectangles indicate the range of p=0.05 significance by ANOVA with Tukey post-hoc test compared to DMSO controls. Red conditions had significantly reduced cell numbers compared to DMSO controls, whereas blue conditions had significantly increased proliferation rates.

growth responses of drug-treated, sorted microtissues bearing 394T4 cells were compared to 2D cultures (**Fig. 3.7c, d**). LY2157299 is a clinically relevant compound undergoing trials for use in a variety of cancer patients[245-247], and has been reported to bind to both receptors, but to TGFβR2 with greater specificity (IC50 2 nM vs. 86 nM for TGFβR1)[248]. Canonically, TGF-β binds to TGFβR2, which then recruits and phosphorylates TGFβR1. However, it is known that specific TGF-β receptors regulate different activities induced by TGF-β, possibly due to the recruitment of alternative signaling complexes[249]. Specifically, several published accounts point to TGFβR2 primarily regulating DNA synthesis, whereas TGFβR1 has been suggested to have a greater impact in mediating matrix synthesis or degradation[250-252]. This distribution of functions could be one explanation for why only LY2157299 (inhibiting TGFβR2 for DNA synthesis in addition to TGFβR1) would exhibit the context-dependent but opposing effects on proliferation compared to direct TGF-β treatment, whereas the TGFβR1-only inhibitors (SB525334, SJN2511) did not.

Given the vast, and often contradictory, published literature regarding the roles of TGF-β and its receptors, particularly in cancer biology, the impact of drugs may be highly contextual and dependent on tumor models, culture conditions or architectures. This pattern is particularly well-illustrated in our current results and also serves to emphasize the value and importance of evaluating drug candidates in multiple in vitro model systems – perhaps in parallel with established therapeutics in order to calibrate the specific assay readout. In this case, the observation that a TGF-β receptor inhibitor exerts opposing effects on tumor cell proliferation when compared with responses to its ligand is perhaps not unexpected. However, the fact that

this same pattern is consistently reversed in our 2D *in vitro* architecture raises important caveats with respect to the potential responsiveness of tumor cells when this pathway is manipulated *in vivo* in a clinical setting. Notably, a finding consistent with our result was observed by another group examining a mouse model of metastatic breast cancer[253]. In their system, activated TGFβR1 delayed primary tumor growth and accelerated formation of lung metastases, whereas addition of dominant-negative TGFβR2 had the opposite effect. The authors speculate that TGF-β functions as a tumor suppressor in a primary lesion, but promotes metastasis dissemination, which is consistent with our findings that primary-tumor derived lung cancer cells remain responsive to TGF-β stimulation.

3.4 Conclusion

We have demonstrated a platform that integrates microfluidic droplet encapsulation to produce microscale tunable microenvironments with a high speed analytical system based on in-flow sorting and analysis of microtissues. This platform utilizes tissue engineering materials and methods as well as microfluidic technology, but obviates common problems with 3D tissue engineering constructs, such as laborious fabrication, low-throughput imaging analysis, and low statistical power. The capacity for high-speed analysis enables the detection of hundreds to thousands of individual events in order to assay the impact of microenvironmental conditions on proliferation. Moreover, by sort-based enrichment of defined microtissue populations to limit variability in cell number and/or composition, our platform reduces noise while increasing replicates, which offers the potential to achieve strong statistical significance in biological

studies. We used this platform to explore the impact of TGF-β signaling on non-small cell lung cancer proliferation. We demonstrated microenvironmentally-mediated modulation of tumor cell proliferation in this platform and we observed context-dependent signaling via the TGF-β pathway in our model cell line. Modification of the microtissue scaffold with collagen-1, or treatment of microtissues with TGF-β, diminished cancer cell proliferation uniquely in the 3D setting. Furthermore, a TGFβR1/TGFβR2 inhibitor (LY2157299), but not TGFβR1-only inhibitors, decreased proliferation in 2D yet promoted growth in a 3D context. Based on these results, we predict that the anti-proliferative influence of TGF-β observed in 3D may be mediated by TGFβR2. An interesting extension of these findings would be to conduct a related *in vivo* preclinical experiment by treating the tumor-prone genetic mouse model[16], which gave rise to our 393T5 and 394T4 lines, with oral LY2157299. Based on our findings, one might predict that the drug might limit or at least delay the appearance of distant metastases, but may not impact the development of primary lung tumors. Future work involving the combined flow-enrichment of subpopulations of microtissues will apply our platform to explore combinations of microenvironmental conditions, such as drug responsiveness in the presence of particular ECM combinations or ratios of heterotypic stromal cell contacts. To support an expanded screen of cues, a microfluidic combinatorial mixer could be incorporated upstream of droplet encapsulation so that ECM and stromal composition could be controlled on-chip. Also, new encapsulation devices including multiple parallel droplet nozzles could augment the microtissue fabrication rate for a full-scale drug screen. Further utility of this platform may be found in extension to other tissues and disease contexts including stem cell or other

developmental biology settings, in which the influence of microenvironmental signals has been challenging to study in a methodical, manipulable and screen-compatible fashion.

3.5 Acknowledgements

Dr. David Wood and Joanne Huang were coauthors on this work. We thank Nathan Reticker-Flynn (MIT) for helpful discussions, and Dr. Heather Fleming (MIT) for critical readings. We thank Dr. Monte Winslow (Stanford) and Dr. Tyler Jacks (MIT) for the 393T5 and 394T4 cell lines, and we thank Dr. Richard Hynes (MIT) for providing the ZsGreen vector. We thank the Massachusetts Institute of Technology Laboratory for fabrication support. This work was supported by the Stand Up to Cancer Charitable Initiative from the American Association for Cancer Research. Individual fellowship support was provided by the National Institute of Biomedical Imaging and Bioengineering National Research Service Award fellowship (D.K.W.), the Mazumdar-Shaw International Oncology Fellows Program (D.K.W.), and the National Science Foundation Graduate Research Fellowship Program (C.Y.L.). S.N.B. is an HHMI investigator.

Chapter 4: Hepatocyte Microtissues for Toxicity Screening and Drug-drug Interactions

4.1 Introduction

Unpredicted liver toxicity is a major cause of drug development failures and post-market withdrawals.[11] Animal models often fail to fully reflect the complexities of human liver behavior due to cross-species differences in hepatocyte function, underscoring the need for human-specific pre-clinical models. Current *in vitro* models such as liver slices and microsomes are not amenable to long-term studies of intact cell behavior, while cell lines do not reflect the full phenotype of primary hepatocytes. Thus, primary hepatocytes are ideal candiates for drug development applications but undergo a rapid loss of differentiated function and viability once *ex vivo*.[27, 28] This has led to various approaches to stabilize hepatocyte function by recreating microenvironmental factors typically found in native liver, such as cell-cell interactions (both homotypic[24] and hetereotypic[56-60]), cell-matrix interactions,[48, 254] and tissue architecture[105]. In many cases it was found that hepatocyte phenotype and function were influenced by culture in a 3D rather than 2D system, for example when cultured as spheroids,[46, 68, 255-259] sandwich gels,[49-52] porous scaffolds,[71-73] or encapsulation in in natural[53-55, 106] or synthetic hydrogels.[75, 114, 115] Hepatocytes cultured in 3D may be more representative of *in vivo* behavior, but many of these strategies were developed for cell-based regenerative therapies, in which the major challenge is scale-up of tissue size.

Miniaturization of cell-laden hydrogels into <250 μm units, called "microtissues," is a promising new approach to tissue engineering that provides several distinct advantages over both scaffold-free 3D culture (i.e.. spheroids) and conventional hydrogels. The cell-encapsulating hydrogel serves a shear-protective function during perfusion, spinner culture, or general handling.[260-262] It also prevents aggregation even during culture in small volumes so that remaining transport of oxygen and nutrients is not limiting.[260, 263] Further, functionalization of the scaffold enables controlled addition of exogeneous factors to tune the microenvironment, such as such as entangled whole ECM proteins,[126, 264] adhesive peptides, [114, 116, 123] or tethered cell signling factors.[132-134] Due to the miniaturized format, microtissues are amenable to multiplexed[149] and high-throughput flow analysis,[264] bypassing more time-consuming readouts such as confocal microscopy[125] Finally, there has been extensive interest in using microtissues as building blocks for bottom-up assembly of patterned tissues[154, 172, 225] and packed-reactor-like devices.[148, 194, 199] However, these studies have thus far used only the more robust and readily cultured hepatocellular carcinoma-based cell lines, and have yet to be extended to primary hepatocytes.

In this chapter, we report the fabrication of microtissues comprised of primary mammalian hepatocytes that can be mass-produced for drug screening applications. To stabilize hepatocyte function post-isolation, we first developed a method to form small (<10-cell) aggregates, called "pucks," by patterning hepatocytes on collagen microislands and then detaching the confluent islands. These micropatterned cell-cell interactions enabled survival hepatocyte survival in bulk PEG hydrogel as well as in 100 μm microtissues, which were

produced in mass by continuous microfluidic droplet-based cell encapsulation. Hepatic microtissues exhibited intact hepatocellular activity as characterized by albumin production and species-specific induction of drug metabolism enzymes. Finally, leveraging the dynamic gene expression and intact cellular machinery of primary hepatocytes, we demonstrate for the first time that hepatic microtissues can be used to predict hepatotoxicity and known drug-drug interactions.

4.2 Materials and Methods

Plate patterning

Topographically patterned polydimethylsiloxane (PDMS, Dow Corning) masking molds that defined collagen microislands were cast from silicon masters. Standard photolithographic methods were used to fabricate the masters with 50 μm tall raised circular pillars of SU-8 2050 photoresist (Microchem, MA). Intermediate PDMS "negatives" were cast from the master and coated with (tridecafluoro-1,1,2,2-tetrahydrooctyl)-1-trichlorosilane (UCT Specialties) for 1 hour in a vacuum desiccator. Final PDMS masking molds were then cast from the negatives to again have raised pillars, and cut into appropriate discs to fit into 6-well plates.

Ultra-Low attachment plates six well plates (Corning) were coated with 0.15 mg/ml Type I collagen (rat tail, BD Biosciences) at 37°C for 1 hour. Wells were rinsed with deionized

water and dried with nitrogen. PDMS masking molds were carefully placed into each well, using gentle pressure to ensure that all parts of the pattern adhered to the well, and the entire plate was subjected to air plasma treatment (SPI Supplies) for 15 seconds. Non-patterned control plates meant to have a homogenous collagen surface coating did not undergo this last step. Masking molds were removed from wells for reuse, and plates were sterilized by 15 minutes of UV exposure prior to use.

Cell culture and puck formation

Hepatocytes were isolated from 2- to 3-month-old adult female Lewis rats as previously described.[49, 265] Hepatocyte culture medium consisted of Dulbecco's Modified Eagle Medium (DMEM, Invitrogen) with 10% fetal bovine serum (Invitrogen), 0.5 U/ml insulin (Lilly), 7 ng/ml glucagon (Bedford Laboratories), 7.5 μg/ml hydrocortisone (Sigma), 10 U/ml penicillin (Invitrogen), and 10 mg/ml streptomycin (Invitrogen). J2-3T3 fibroblasts were cultured in DMEM with 10% bovine serum (Invitrogen), 10 U/ml penicillin, and 10 mg/ml streptomycin. mCherry J2-3T3 fibroblasts were generated by ViroMag R/L (Oz Biosciences) mediated transduction of lentivirus containing mCherry under control of the EF1alpha promoter (Promega). Transduced mCherry fibroblasts were subsequently selected by puromycin followed by fluorescence-activated cell sorting. All cells were cultured in a 5% CO_2 humidified incubator at 37°C.

To seed freshly isolated hepatocytes, cells were first pelleted at 50xg for 5 minutes and resuspended in hepatocyte medium without serum at a cell density of $2x10^6$ hepatocytes/ml. One ml of this suspension was added to each well of a patterned or non-patterned 6-well plate.

Hepatocytes were allowed to attach for 2 hours to any adhesive regions of the plate in the incubator, with gentle linear shaking every 15 minutes to re-disperse unattached cells. Progress of seeding was monitored under a microscope. After microislands were seeded to confluence, each well was rinsed twice with 2 ml of medium to remove any remaining unattached cells. Cell number on each island was manually counted three hours after initial plating,when cells were firmly attached but individual cell borders could be easily distinguished. For hepatocyte-only pucks, the seeded cells were then cultured in 1 ml of full hepatocyte medium with serum overnight. To form pucks that contain both hepatocytes and fibroblasts, J2-3T3 cells were then added to each well ($0.5x10^6$ cells in 1 ml hepatocyte medium) and allowed to seed overnight, with gentle shaking every 15 minutes for the first 2 hours.

Encapsulation in bulk PEG gels

Hepatocytes that had been cultured on patterned or non-patterned 2D plates for 24 hours were detached using 2 mg/ml collagenase (Type IV, Invitrogen) in DMEM. Within 5 minutes, multicellular pucks lifted from the plate but did not dissociate into single cells. Pucks or unpatterned cells were diluted in hepatocyte medium, pelleted (50xg, 5 min), and then resuspended at an effective cell density, calculated from the number of microislands per well and the number of cells per island, of $8x10^6$ cells/ml in PEG prepolymer. The prepolymer solution consisted of 100 mg/ml PEG-diacrylate (20 kDa, Laysan Bio) in heavy DMEM (DMEM adjusted to have a specific gravity of 1.06 by OptiPrep density medium, Sigma) with 1:100 v/v photoinitiator working solution (100 mg/ml Irgacure 2959, Ciba, in *n*-vinyl pyrrolidone, Sigma). The adhesive peptide RGDS was incorporated by also including 10 mM of Acrylate-

PEG(3.4kDa)-RGDS monomers that were prepared as previously described[114] in the prepolymer. For co-encapsulation of fibroblasts with hepatocyte pucks, J2-3T3 fibroblasts were detached with 0.25% Trypsin-EDTA (Invitrogen), pelleted, and also resuspended in prepolymer for a final 1:1 ratio of fibroblasts and hepatocytes ($8x10^6$ fibroblasts and $8x10^6$ hepatocytes per ml).

Disc-shaped, or "bulk" PEG gels were fabricated using hydrogel polymerization apparatus described previously.[113] Briefly, prepolymer solution containing cells was loaded into a 8.5 mm diameter, 250 μm thick silicone spacer, sandwiched between a Teflon base and a glass cover slip, and polymerized by exposure to UV light from a spot curing system with a collimating lens (320-390 nm, 21 mW/cm^2, 12 s; Lumen Dynamics). Each gel was soaked in rinse media for 1 hour to remove any un-polymerized components and was subsequently cultured in 0.5 ml of hepatocyte medium. All experiments were performed with quadruplicate gels for each condition.

Microfluidic encapsulation in microtissues

Droplet-based microfluidic encapsulation devices were fabricated as previously described.[225] For microfluidic encapsulation, hepatocyte-only or hepatocyte-fibroblast pucks were lifted using 2 mg/ml collagenase, pelleted (50xg, 5 min), and then resuspended at an effective hepatocyte density of $30x10^6$ cells/ml in PEG prepolymer. The cell suspension was loaded into a syringe and injected into the device at 200 μl/hr. Simultaneously, fluorocarbon oil (Fomblin Y-LVAC, Solvay Solexis) containing 0.5 w/v% Krytox 157 FSH surfactant (DuPont) was also injected into the device as an oil phase. At a droplet-generating nozzle, the aqueous

cell suspension was broken into 100 μm-diameter droplets of cells and prepolymer in oil, which were then continuously polymerized on chip by exposure to UV light (320-390 nm, 500 mW/cm^2, 0.5 s; Lumen Dynamics) before exiting the device. Microtissues collected from the device were separated from oil and washed on a 70 μm strainer to remove any un-polymerized components. To remove gels that did not contain any cells (due to settling of the pucks during injection), microtissues were centrifuged at 50xg for 5 minutes in a Percoll (Sigma) density medium solution (12.5 μl isotonic 1.12 g/ml density Percoll stock per ml of media). Pelleted microtissues were resuspended in hepatocyte medium and cultured in 40 μm strainer caps (BD Falcon) as inserts for 24-well plates. All experiments were performed with quadruplicate wells for each condition.

Biochemical assays

Supernatant was collected every other day from bulk gels or microtissues. Secreted albumin in the supernatant was quantified by an enzyme-linked immunosorbent assay (ELISA) kit using sheep anti-rat albumin antibodies (Bethyl Labs) and horseradish peroxidase detection (3,3',5,5'-tetramethylbenzidine, Invitrogen).

For enzyme induction experiments, microtissues were pre-treated with inducers for 72 hours beginning at 48 hours post-encapsulation. Stock solutions of inducers were prepared in dimethyl sulfoxide (DMSO) and diluted 1:1000 for final concentrations of 50 μM omeprazole (Sigma), 25 μM rifampin (Sigma), and 10 μM dexamethasone (Sigma). Phenobarbital (Sigma) was dissolved at 40 mM in deionized water and diluted to a final concentration of 200 μM. Vehicle controls were pre-treated with 72 hours of either 1:1000 DMSO or 1:200 water.

Cytochrome P450 activity was assessed with luminogenic P450-Glo kits (Promega) according to vendor instructions for non-lytic assays using cultured cells. Microtissues were incubated with Luciferin-PFBE (1:40 dilution in phenol-free DMEM), Luciferin-CEE (Cyp1A1, 1:66 dilution), or Luciferin-H (Cyp2C9, 1:50 dilution) for 3 hours. Processed medium samples from each strainer of microtissues were collected and luciferin metabolites measured on a luminometer (Berthold, 10 s).

Acetaminophen treatment

For hepatotoxicity experiments, microtissues were cultured for 72 hours post-encapsulation and then exposed to 0 - 40 mM of acetaminophen (Sigma) for 24 hours. All samples contained a final 0.8% v/v DMSO. For drug interaction experiments, microtissues were cultured for 48 hours post-encapsulation, exposed to various inducers or controls for 72 hours, and then dosed with 40 mM of acetaminophen in the presence of inducers for 24 hours.

Large-particle flow cytometry

High throughput analysis of microtissue viability was performed by first staining microtissues in suspension with the live-dead fluorescent stains calcein AM (5 μg/ml) and ethidium homodimer (2.5 μg/ml) for 15 minutes at 37°C. Whole-microtissue levels of fluorescence were detected using a BioSort large particle flow cytometry (Union Biometrica) equipped with a 488 nm excitation laser. Microtissues were gated for on the basis of Time of Flight (size) and Extinction (optical density) to exclude debris. Fluorescent signal acquisition parameters were set as follows: Gains – Green 3, Red 3, PMT control – Green 300, Red 700.

Compensation was applied to subtract 90% of the green signal from red. Scatter plots were created using BioSorter software. Raw data was also exported for processing with custom MATLAB code.

Immunohistochemistry, live-dead staining, and imaging

For immunohistochemistry, fresh isolated hepatocytes or hepatocyte microtissues were fixed in methanol and 10% acetic acid and then gently pelleted in eppendorf tubes. Cell pellets were resuspended in histogel (Thermo Scientific), repelleted, and placed on ice for histogel gelation. Histogel-encapsulated cell pellets were processed, embedded, and sectioned. Sections were incubated with primary antibodies against either pan-cytokeratin (1:800, Sigma) or arginase-1 (1:400, Sigma) and then with species-appropriate secondary antibodies conjugated to Alexa 488 or 555. Images were obtained using a Nikon Ti scanning-confocal microscope.

Cell viability within bulk gels and microtissues was examined using calcein AM (5 μg/ml) and ethidium homodimer (2.5 μg/ml) fluorescent stains (Molecular Probes, incubated with cells for 15 minutes at 37°C) to stain live and dead cells respectively. Images were acquired using a Nikon Ellipse TE200 inverted fluorescence microscope and CoolSnap-HQ Digital CCD Camera. MetaMorph Image Analysis Software was used to uniformly adjust brightness/contrast, pseudocolor, and merge images.

4.3 Results

4.3.1 Control and uniformity of hepatocyte patterning

Collagen micro-islands were defined on tissue culture plates using a soft lithography process[59] wherein a layer of adsorbed collagen is first masked by contact with a PDMS mold (**Fig. 4.1a**). Protruding PDMS posts of various sizes (50, 75, and 100 μm diameters) (**Fig. 4.1b, i-iii**) were used to protect collagen in contacted regions from plasma ablation, resulting in 50-100 μm circles of remaining collagen. This range of island sizes was selected to be compatible with targeted 100 μm diameter microtissues and the 70 μm droplet-generating nozzle during microfluidic encapsulation.

Freshly isolated rat hepatocytes seeded onto micropatterned collagen islands of various sizes (50, 75, and 100 μm diameters). Hepatocytes densely covered and adhered only to the areas of collagen microislands (**Fig. 4.1b, iv-vi**). This patterning and process was robust and scalable to large areas (**Fig. 4.2**), which enabled mass production of patterned hepatic islands. After one day of culture, (**Fig. 4.1b, vii-ix**), hepatocytes spread to form a confluent 2D layer over each microisland. When treated with collagenase to digest underlying collagen, hepatocyte islands, or "pucks," detached from the plate as cohesive units (**Fig. 4.1b, x-xii**) without dissociating into single cells, presumably due to minimal digestion of cell surface proteins by collagenase. Cell number in each puck was directly related to island area and generally followed the Poisson distribution (**Fig. 4.1b, xiii-x**; 5.6±1.7 cells for 50 μm islands, 7.9±2.0 cells for 75 μm islands, and 11.8±2.4 cells for 100 μm islands). All subsequent studies used pucks

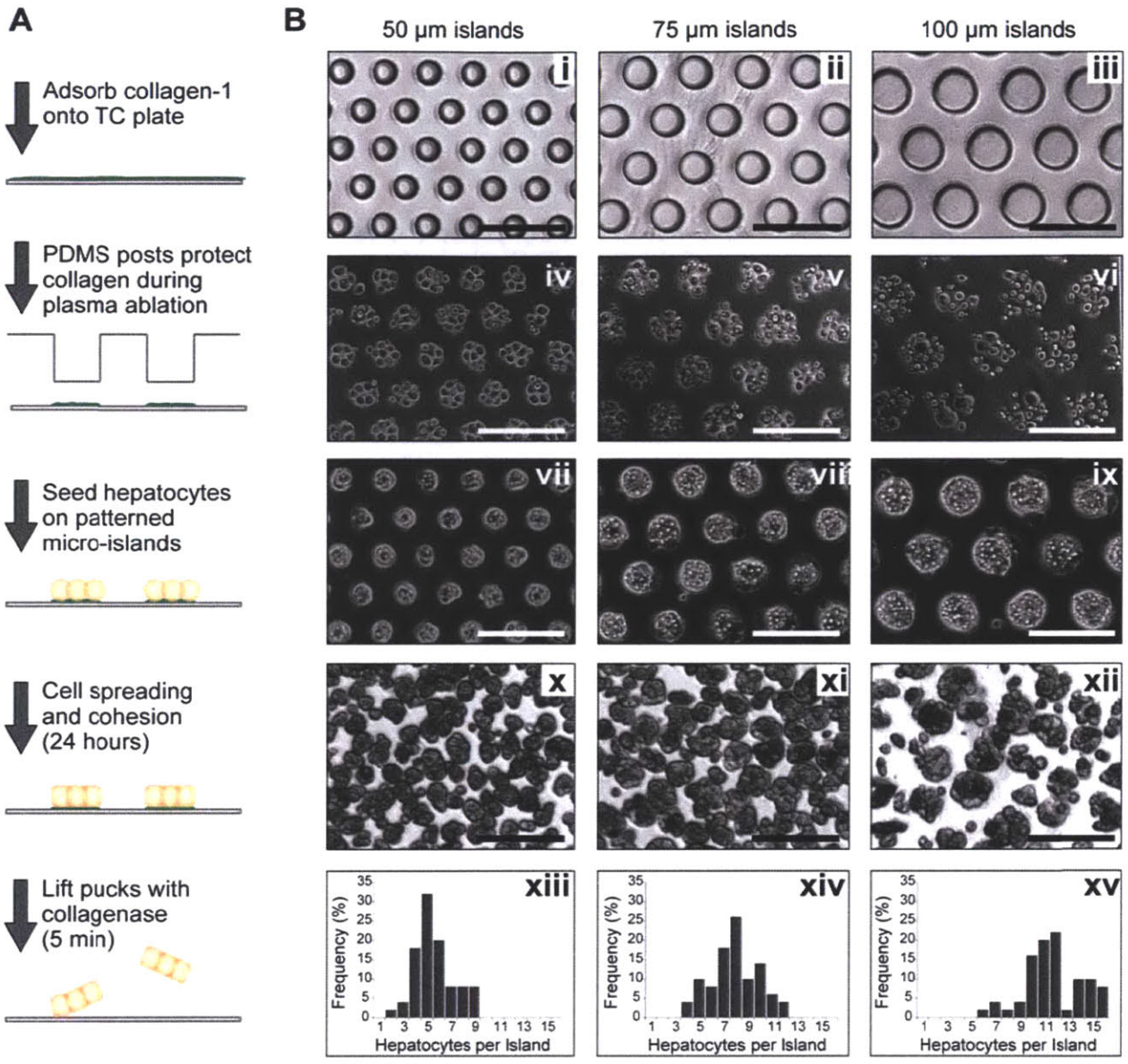

Figure 4.1. Hepatocyte puck formation and detachment from patterned collagen microislands. A) Schematic illustrating the definition of adhesive collagen islands on plastic, hepatocyte seeding and spreading over 24 hours, and detachment with collagenase. B) Phase images showing i-iii) PDMS molds to define island size, iv-vi) primary rat hepatocytes initially seeded on the islands, vii-ix) confluent hepatocyte islands after 24 hours of culture, and x-xii) detached pucks. All scale bars are 200 μm. xii-xv) Histogram of number of the hepatocytes in each size of puck.

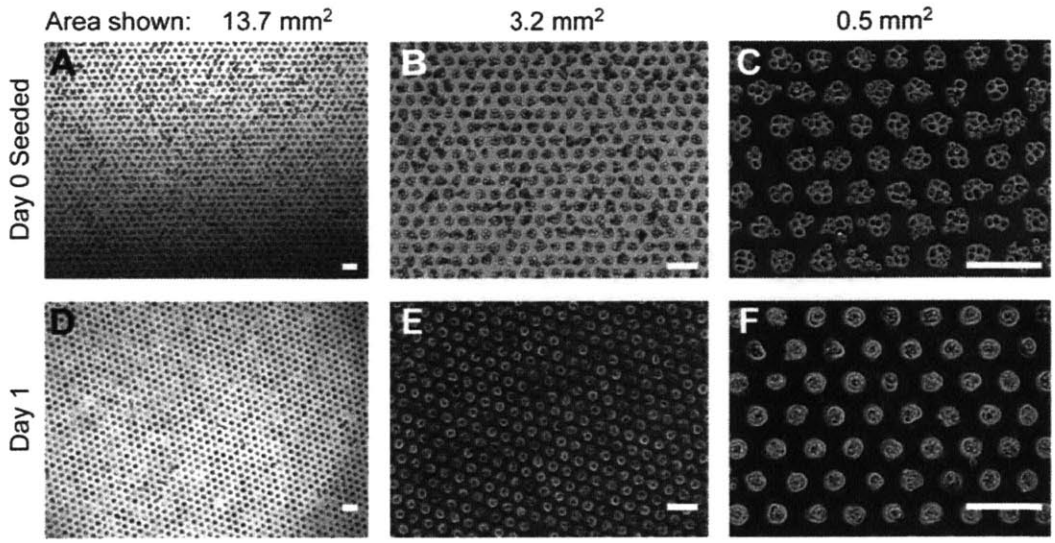

Figure 4.2. Microisland seeding (A-C) and puck formation (D-F) by primary hepatocytes over large areas. All scale bars = 200 μm.

formed by 50 μm islands, which resulted in multicellular pucks (smaller island sizes resulted in many islands only capturing single cells) that remained small enough for facile microfluidic handling. After removal from collagen substrate, hepatocytes in freely floating pucks expressed both cytokeratin and arginase-1 (**Fig. 4.3**), indicating that puck culture enabled selection for viable hepatocytes after fresh isolation procedures. Taken together, these results show that micropatterning to prompt the formation of cell-cell contacts was facile and effective.

4.3.2 *Effect of homotypic contacts on 3D albumin secretion*

To examine whether pre-clustering of hepatocytes improved hepatic function after encapsulation in a 3D hydrogel, we first tested the albumin secretion of the cells within monolithic, "bulk" PEG gels as a first measure of health and viability. For the hydrogel scaffold

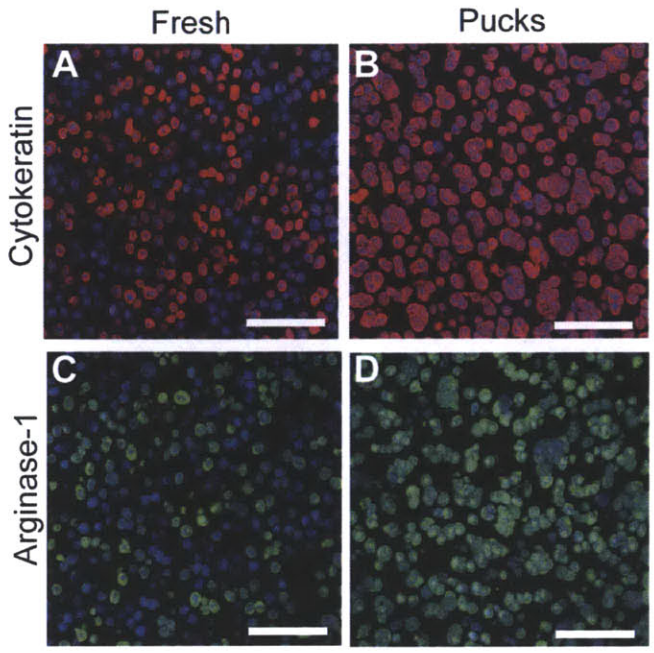

Figure 4.3. Hepatocyte pucks express liver proteins. After removal from collagen substrate, hepatocytes in freely floating pucks expressed both cytokeratin (red) and arginase-1 (green). Expression levels were greater in pucks (right) compared to freshly isolated purified hepatocytes (left), indicating that puck culture selected for viable hepatocytes after isolation procedures.

material, 10 wt% PEG-DA (20k) was chosen because it is 1) loose enough to allow diffusion of oxygen/nutrients/proteins to and from the cells,[204] 2) biologically/immunologically inert, and 3) can be functionalized with acrylate-containing ligands.[116, 131, 135, 136, 266] As a control condition, hepatocytes were randomly seeded in collagen-coated but unpatterned 6-well plates at 600,000 cells/well, which was chosen from the theoretical number of cells that would seed in a 50 μm-island patterned well assuming 5.6 hepatocytes per island. At this density, cells on the unpatterned surfaces are able to make chance cell contacts as they seed in 2D and form loose cords of cells when detached (**Fig. 4.4**).Hepatocytes were randomly seeded ("unpatterned") or micropatterned using collagen islands for 24 hours, lifted by collagenase, resuspended in

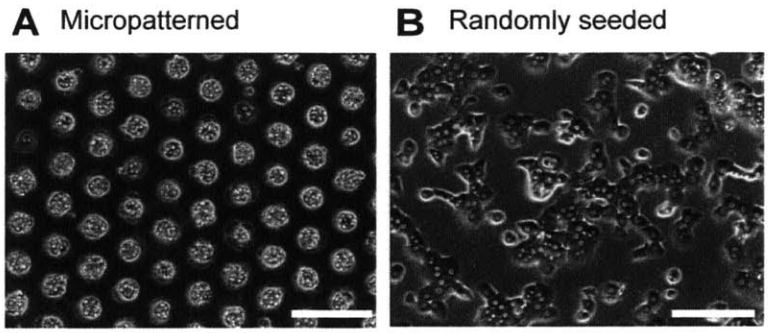

Figure 4.4. 2D culture of hepatocytes on either (A) micropatterned islands, or (B) unpatterned, collagen-coated plastic. All scale bars = 200 μm.

hydrogel prepolymer, and photopolymerized into 14 ul disc-shaped gels (**Fig. 4.5a**). Live/dead staining with calcein AM and ethidium homodimer on the encapsulated pucks indicated >80% viability after 3 hours (which is comparable to the ~80% viability of lifted pucks, indicating that the polymerization process was not additively cytotoxic (**Fig. 4.5b**). Hydrogels containing hepatocyte pucks exhibited increasing albumin secretion during the first week after encapsulation followed by sustained secretion for up to two weeks. Albumin secretion in hydrogels containing pucks was over 3-fold greater compared to control hydrogels containing unpatterned hepatocytes at 8 days ($p = 0.0571$, $n = 4$, Wilcoxon rank sum test). These results demonstrate that micropatterning hepatocytes to form hepatic 'pucks' prior to encapsulation improve hepatocyte phenotype after encapsulation in a 3D hydrogel.

4.3.3 *Effect of other supporting factors in 3D albumin secretion*

Co-culture of hepatocytes with a second cell type,[58, 59] or the presence of adhesion proteins or peptides such as RGDS,[75, 114] have been reported previously to support the

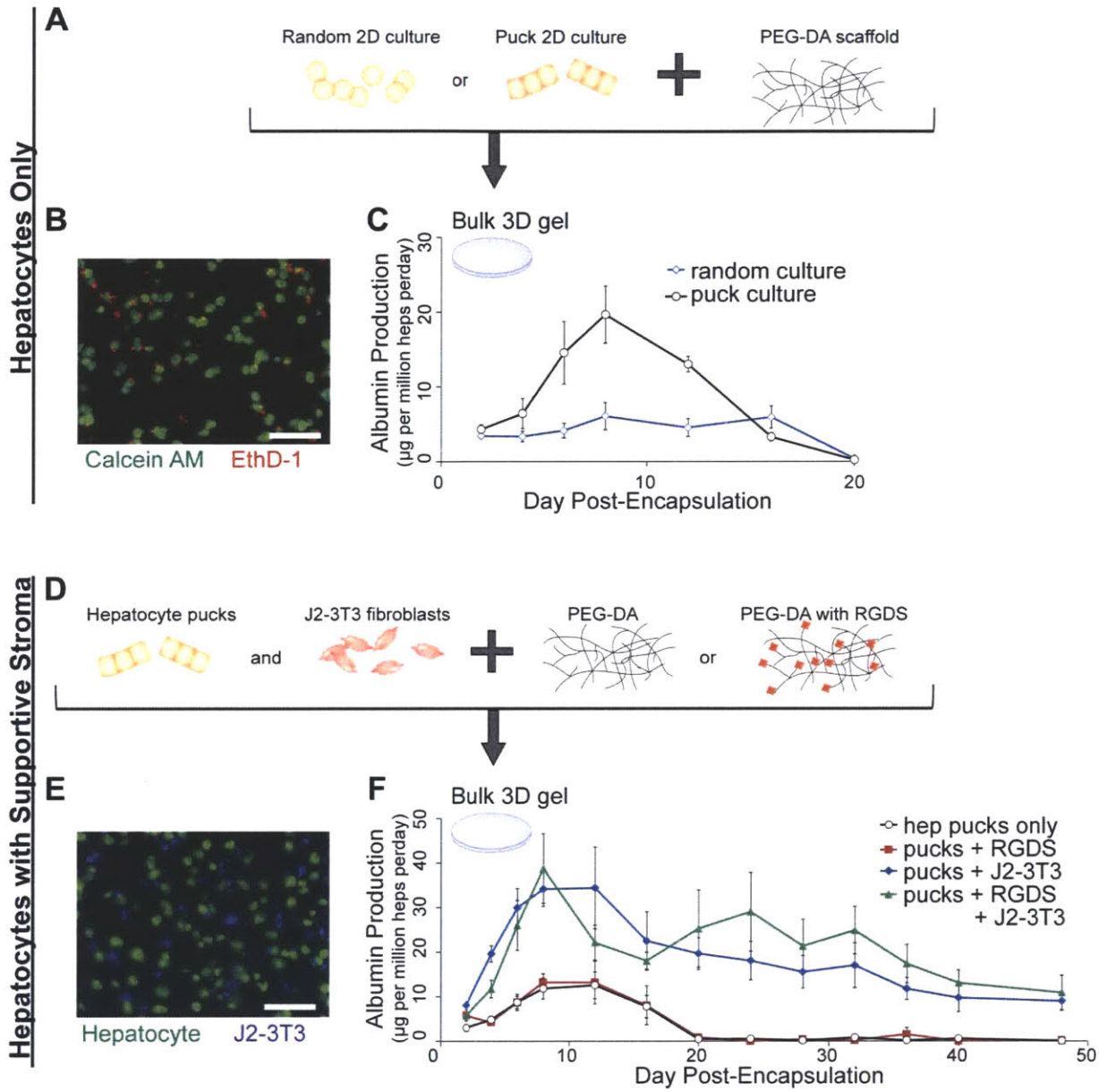

Figure 4.5. Hepatocyte pucks in 8.5mm-diameter bulk PEG hydrogels. A) Hepatocytes were detached from either patterned or random 2D culture after 24 hours and encapsulated in a 3D PEG scaffold. B) Live-dead stain of hepatocyte pucks within PEG hydrogel. C) Albumin secreted into the supernatant from hepatocyte-laden gels (n = 4). D) J2-3T3 fibroblasts were co-encapsulated along with hepatocytes into the hydrogel, which was modified by RGDS adhesive peptides. E) Epifluorescence image of hepatocyte pucks (green, calcein) and fibroblasts (blue, mCherry) co-culture within a gel. F) Albumin secreted into the supernatant from gels containing hepatocyte pucks with additional fibroblasts and/or RGDS (n = 4). Error bars show standard error (SEM). All scale bars are 200 µm.

maintenance of primary hepatocyte function. Thus, we explored the incorporation of both heterotypic cell-cell interactions and extracellular matrix-derived adhesive moieties into the 3D gels (**Fig. 4.5d**). To achieve the former, a single-cell suspension of J2-3T3 fibroblasts expressing mCherry was mixed into the prepolymer used to encapsulate hepatocyte pucks. Resultant gels (**Fig. 4.5e**, shown in blue) contained J2-3T3 fibroblasts distributed throughout the volume of the gel, at length scales (<100 μm from the nearest hepatocyte) that previous studies have demonstrated to enable paracrine signaling through soluble factors[146] as well as, in some cases, immediately adjacent to hepatocytes. Adhesive moieties were incorporated into gels by chemically conjugating acrylate-functionalized RGDS peptides (10 mM) into the hydrogel network. 3D co-culture of fibroblasts with hepatocyte pucks resulted in a greater than 2-fold increase of albumin production relative to hepatocyte-only controls in the first week (**Fig. 4.5f**). More importantly, the maintenance of albumin production over time was extended in the presence of fibroblasts from 20 days to over 7 weeks. Conversely, adhesive peptides did not significantly affect albumin production curves in RGDS-containing gels compared to non-adhesive controls, whether the gels contained hepatocyte pucks only or hepatocyte pucks with fibroblasts (**Fig. 4.5f**). Together, these results demonstrate that supportive cues from J2-3T3 fibroblasts but not RGDS adhesive peptides are crucial for long-term hepatocyte survival in this system.

4.3.4 Microfluidic production of hepatic microtissues

Having verified that hepatocyte pucks retain function when encapsulated with fibroblasts in macroscopic bulk PEG hydrogel, we sought to miniaturize the 3D engineered

tissue into 100 μm-diameter "microtissues." For these studies, we produced individual droplets of prepolymer containing cells and then polymerized these cellular droplets to form "microtissue" hydrogels on-chip (**Fig. 4.6a**). Hepatocyte pucks, fibroblasts, and photopolymerizable prepolymer were mixed to form a combined aqueous stream that was injected into the encapsulation device. This aqueous stream was designed to intersect with an oil stream of oxygen-permeable fluorocarbon oil at a droplet-generating nozzle, such that prepolymer-in-oil droplets were continuously produced. Droplets were subsequently polymerized within the device (**Fig. 4.7**). Polymerized, spherical microtissues containing multicellular pucks were collected from the outlet of the chip. Viability of microtissues as assessed by live-dead staining was similar to that of bulk-encapsulated pucks (**Fig. 4.6b**). Similar to bulk hydrogel studies, the presence of dispersed fibroblasts mixed into the gels significantly increased total albumin produced over 16 days (**Fig. 4.6c**).

Because fibroblasts were found to play such a key supportive role in maintaining hepatocyte puck function, we explored the option provide this heterotypic interaction earlier in the process, during the first 24 hours post-hepatocyte isolation. To include fibroblasts when hepatocytes are stabilizing in 2D, fibroblasts were seeded onto any remaining space on the microislands after hepatocytes had been allowed to attach for 2 hours. When unattached fibroblasts after 2 more hours are rinsed off, 95% of the resulting islands contained both cell types (**Fig. 4.8**), and as before, formed confluent circles of cells over 24 hours that could be discretely detached by collagenase to produce mixed hepatocyte-fibroblast pucks. Microtissues containing hepatocyte-fibroblast pucks, where the two cell types were brought into contact on the day of hepatocyte isolation, will be hereafter referred to as "hepatic microtissues" and

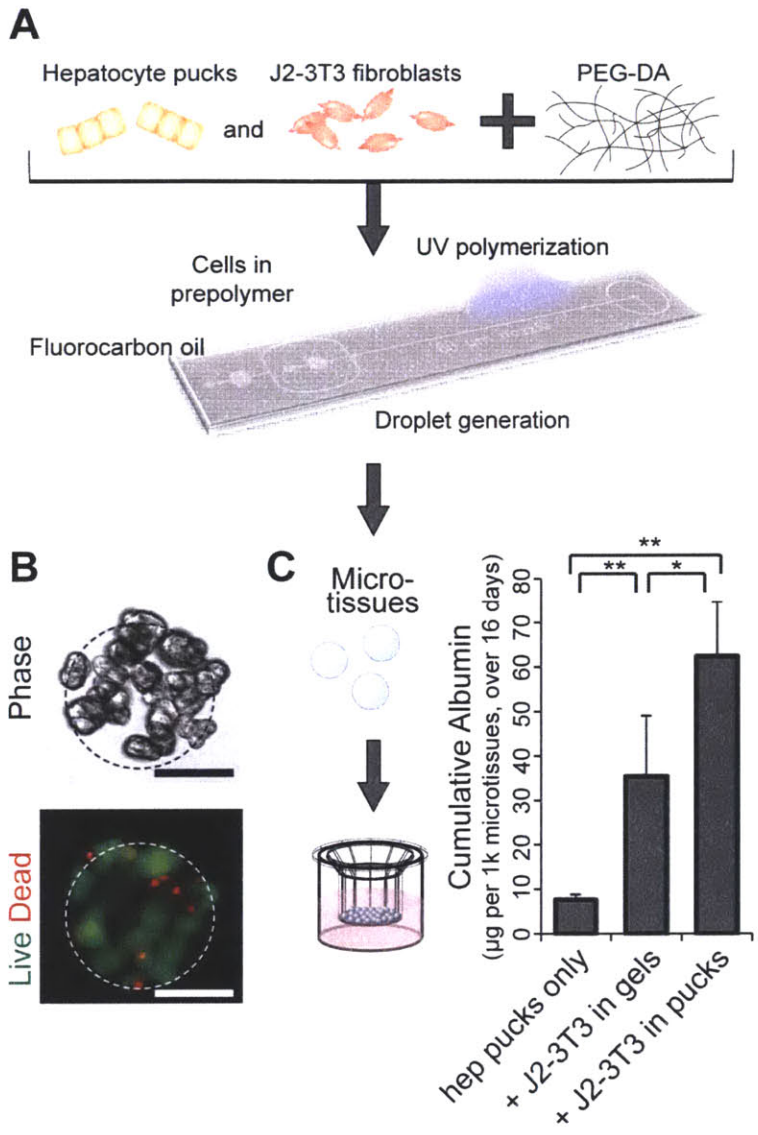

Figure 4.6. Microfluidic encapsulation of hepatocyte pucks. A) A mixture of hepatocyte pucks and fibroblasts are encapsulated using a microfluidic droplet generating device to polymerize ~100 µm –diameter spherical cell-laden hydrogels. B) Phase image and viability staining of an individual microtissue containing several hepatocyte clusters. The dotted line indicates the edge of the hydrogel. Scale bar = 50 µm. C) Secreted albumin quantified from microtissues containing either hepatocyte pucks only, hepatocyte pucks with a single-cell suspension of fibroblasts, or hepatocyte-fibroblast mixed pucks. Error bars show standard error (SEM). n = 4 wells, * p = 0.0571, ** p = 0.0286, Wilcoxon rank sum test for pairwise comparisons.

displayed the most optimal hepatic function as measured by total amounts of secreted albumin, producing 70% more than microtissues containing hepatocyte pucks and fibroblasts mixed 24-hours post-isolation (**Fig. 4.6c**).

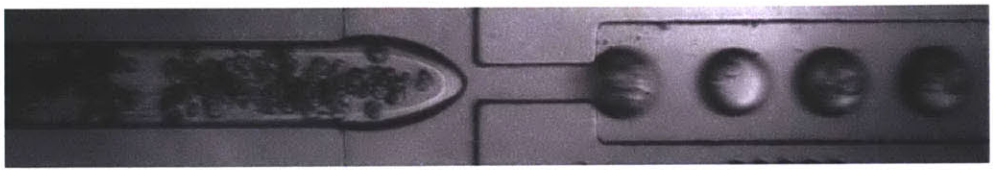

Figure 4.7. Flow-focusing nozzle of microfluidic encapsulation device. Cell-containing prepolymer reaches the junction from the left and is broken into droplets by perpendicular oil streams coming from the top and bottom. 100 μm-diameter droplets suspended in oil leave the junction towards the right and are exposed to UV light immediately downstream.

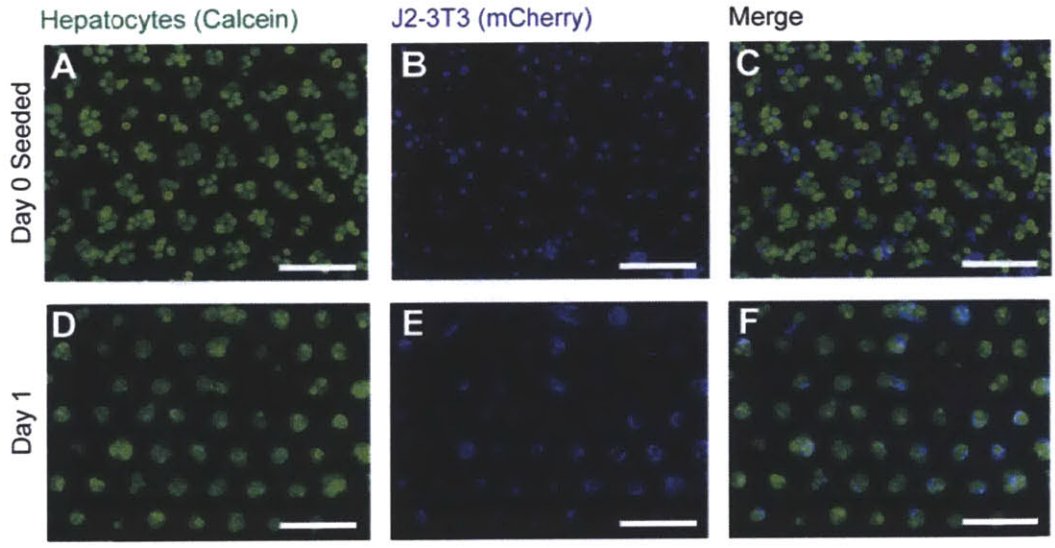

Figure 4.8. Sequential seeding of hepatocytes and fibroblasts to form mixed pucks. A)-C) Fluorescent images of the two cell types right after seeding indicate distribution of fibroblasts into each island. D-F) Cohesive mixed pucks after 24 hours of spreading with both cell types incorporated. All scale bars = 200 μm.

4.3.5 *Species-specific cytochrome P450 enzyme activity*

We further characterized the liver-specific functions of hepatic microtissues by assessing their cytochrome P450 (Cyp) enzyme activity in response to known pharmacological inducers. Microtissues were dosed with inducers omeprazole (50 μM), dexamethasone (10 μM), rifampin (25 μM), or phenobarbital (200 μM) two days after encapsulation. After a 72 hours incubation period, the activity of several Cyp isozymes was quantified and indicated levels of induction that correlated well with the literature:[17, 18, 267, 268] a 9-fold increase in Cyp1A1 activity by omeprazole, a 7-fold increase in Cyp3A4 activity by dexamethasone, a 2-fold increase in Cyp2C9 activity by rifampin, and a 2-fold increase in Cyp3A4 activity by phenobarbital (**Fig. 4.9**).

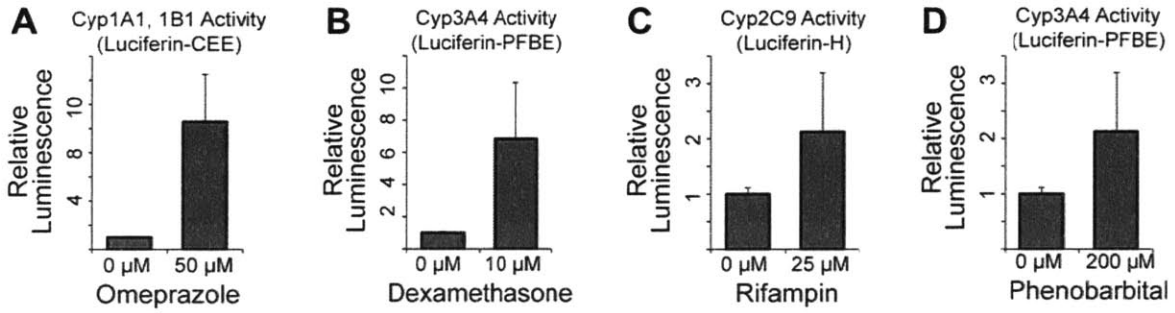

Figure 4.9. Induction of cytochrome P450 activity in hepatocyte-fibroblast mixed-puck microtissues. A) Cyp1A1 activity induced by 50 μM omeprazole. B) Cyp3A4 activity induced by 10 μM dexamethasone. C) Cyp2C9 activity induced by 25 μM rifampin. D) Cyp3A4 activity induced by 200 μM phenobarbital. Luminescent signals were scaled relative to uninduced vehicle controls, all groups were $n = 3$. Error bars show standard error (SEM).

4.3.6 *Acetaminophen toxicity*

To test the suitability of microtissues for 3D drug toxicity studies, we treated microtissues with varying concentrations of the common analgesic, acetaminophen (APAP). Acetaminophen is hepatotoxic only when metabolized by P450 enzymes, including Cyp3A4, Cyp2E1, and Cyp1A2,[269] into the reactive metabolite N-acetyl-p-benzoquinone imine (NAPQI). After treating microtissues with acetaminophen for 24 hours, we co-stained microtissues using calcein AM (live) and ethidium homodimer (dead). The miniaturized 3D format of the microtissues allowed us to use a large-particle flow cytometer for high-throughput detection of individual microtissue viability in each treatment group (**Fig. 4.10a**). At lower concentrations of acetaminophen (0 - 15 mM), the microtissue population was detected with generally high green (live) fluorescence and low red (dead) fluorescence, and cluster in a line when represented on a scatter plot (**Fig. 4.10b**). However, after treatment of microtissues with 40 mM APAP, a population shift downwards (less green) and to the right (more red) indicates a range of reduced viabilities within the microtissue population. By gating the microtissues to separate those with typical post-encapsulation viabilities from those with exhibiting some level of reduced viability, we were able to quantify the number of microtissues that fall above this threshold as "% viable microtissues" (# of microtissue below gate / total microtissues in population) (**Fig. 4.10c**). Microtissues that fall below this gating threshold indicate some level of decreased viability i.e. more dead cells to live cells. Using % viable microtissues as a metric, the dose curve of acetaminophen concentration displays a non-linear toxicity "shoulder" below which there was little effect, but above which hepatotoxicity is observed, as has been reported[59, 270] and is presumably due to depletion of intracellular glutathione.[11, 271]

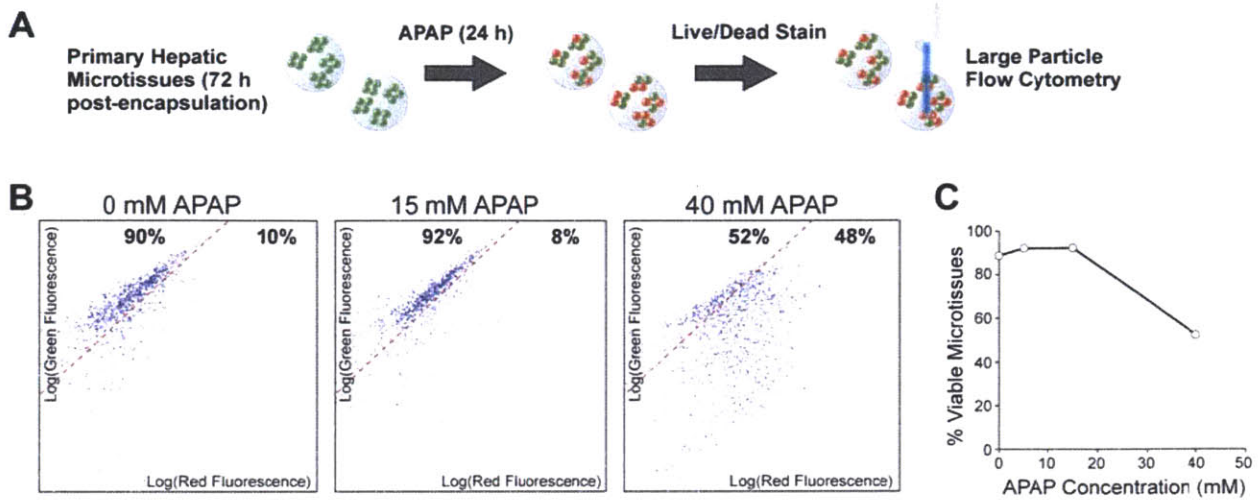

Figure 4.10. Acetaminophen-induced microtissue hepatotoxicity. A) Live-dead staining and large particle flow cytometry to detect level of toxicity on a per-microtissue basis. B) Scatter plots of microtissue fluorescence (green – live, red – dead) after 24 h incubation with various doses of acetaminophen. Upper left gate indicates % of all microtissues in the population that do not show reduced cell viabilities (% viable microtissues). C) Cliff-point for APAP toxicity observed in % viable microtissue dose curve.

4.3.7 Cytochrome P450-mediated drug-drug interactions

We sought to explore a canonical example of drug-drug interactions, in which induction of a Cyp enzyme by one drug may result in faster metabolism of a subsequent drug, affecting its toxicity or efficacy. Since hepatic microtissues were previously responsive to Cyp induction, we simulated co-treatment of the microtissues with 1) a pharmacologic inducer (omeprazole, dexamethasone, rifampin, or phenobarbital), and 2) acetaminophen. Pre-incubation of microtissues with omeprazole, which is reported to induce Cyp1A2,[19] prior to treatment with acetaminophen increased the amount of dead staining and increased the amount of live staining compared to acetaminophen-only treated microtissues (**Fig. 4.11a**) as analyzed by large-particle

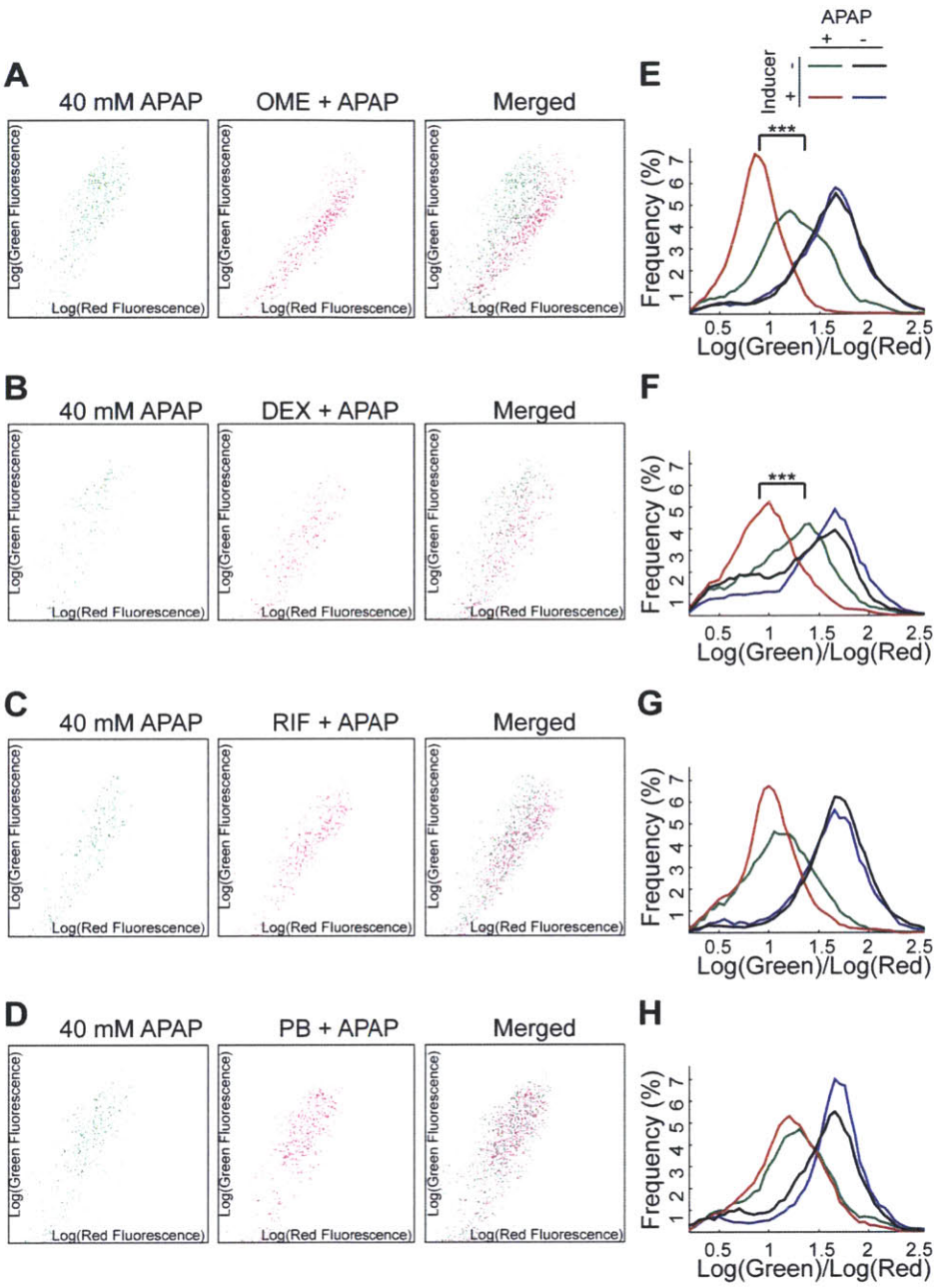

Figure 4.11. Cytochrome P450 inducer interactions with acetaminophen toxicity. A-D) Flow cytometry scatter plots of microtissues treated with 40 mM APAP after 72 hours of induction with A) 50 μM omeprazole, B) 10 μM dexamethasone, C) 25 μM rifampin, or D) 200 μM phenobarbital. Green – calcein, live. Red – ethidium homodimer, dead. E-H) Histogram representation of microtissue populations, quantifying ratio of green vs. red signal with higher ratios indicating a higher percent of viable cells in the microtissues. Treatment and control groups were green: APAP only, red: inducer + APAP, blue: inducer only, black: vehicle control. $n > 1000$, *** indicates p-value $< 10^{-4}$ (One-way ANOVA, Tukey post-hoc test).

flow cytometry. Pre-treatment with dexamethasone, which is known to induce Cyp3A4 activity[17] (**Fig. 4.9b**) also exacerbated acetaminophen-induced hepatotoxicity (**Fig. 4.11b**).

Conversely, rifampin and phenobarbital, which are poor inducers of rat Cyp3A4[17], did not significantly increase acetaminophen toxicity (**Fig. 4.11c,d**). Together, these data indicate that hepatic microtissues are responsive to cytochrome-P450 mediated drug interactions.

4.4 Discussion

It has become increasingly clear that while hepatocellular carcinoma-derived cell lines grow readily in culture, they are inadequate *in vitro* models for liver drug metabolism due to low cytochrome P450 enzyme activity[25], unresponsiveness to induction[31], and reduced sensitivity to hepatotoxins.[32] Primary hepatocytes remain the preferred cell-based model, but are difficult to culture *ex vivo*, undergoing a rapid loss of liver-specific function and viability when conventionally plated.[59] Efforts to maintain freshly isolated hepatocytes have attempted to replace some of the architectural and microenvironmental stimuli surrounding hepatocytes *in vivo*, such as neighboring cells, extracellular matrix, soluble factors, and physical forces.[24, 33] For example, both homotypic and heterotypic cell-cell interactions have been reported to modulate the function of primary hepatocytes in patterned 2D culture[56, 59, 146] as well as in various 3D culture systems.[58, 62, 75, 114, 272]

Based on these reports, we hypothesized that facilitating physical cell-cell contacts would be critical towards the function of primary hepatocyte-derived microtissues. Thus, we chose to pre-aggregate hepatocytes into multicellular units before 3D encapsulation of the cells. Furthermore, we sought to do so in a manner that could form uniform units (<100 μm) for downstream microfluidic processing (i.e. for consistent flow), and was easily scalable to millions of aggregates. Conventional techniques to form 3D aggregates, such as culturing cells in rotational suspension,[263, 273] or on non-adhesive plates,[274] can take multiple days to incorporate all cells, and lead to spheroids that are non-uniform in shape and size.[69, 263] To address this problem, various techniques to enhance spheroid uniformity have been developed such as hanging-drop platforms[275] or centrifugation into pyramidal microwells,[276] but are limiting in both expense and throughput.

In this study, we have described a novel "2D to 3D" fabrication method to produce such aggregates by seeding cells on large arrays of <100 μm micropatterned collagen islands, and detaching intact cell-clusters from each island with collagenase (**Fig. 4.1**). The ability to define different island sizes, and hence the number of cells per aggregate and the size of the detached pucks, illustrates the control that can be achieved over puck characteristics and uniformity. As an alternative to other 3D aggregation methods, our method additionally selects only for adhesive hepatocytes in the freshly isolated population, filtering out any non-viable cells. Most importantly, our method is orders of magnitude higher in throughput compared to hanging drop (96 or 384 spheroids/plate) or microwell plates (28000 spheroids/plate), especially for small aggregates. Using our method, one 6-well plate patterned with 50 μm islands can template over 600,000 pucks, or approximately $3x10^6$ hepatocytes assuming 5 hepatocytes per puck.

To test our original hypothesis that pre-stabilized cell-cell contacts improve hepatocyte function in 3D, we formed 50 μm pucks from primary rat hepatocytes and encapsulated them within macroscopic PEG hydrogels. Using albumin production as a first-pass marker for hepatocyte function, we found that pre-aggregation of the hepatocytes did indeed increase the levels of albumin secreted from cell-laden hydrogels (**Fig. 4.5c**), which is consistent with literature reports on the effects of homotypic hepatocyte interactions.[46, 51, 277] The addition of co-encapsulated J2-3T3 fibroblasts into the hydrogels improved hepatocyte performance even more, corroborating the phenotypic advantage gained from co-culture,[56, 58-60, 62-65, 67] and extended the albumin secretion capabilities of the hepatocytes to over 7 weeks (**Fig. 4.5f**). Interestingly, further functionalizing the PEG hydrogel with adhesive RGDS peptides did not have a significant effect on albumin production by encapsulated hepatocytes. Integrin ligation by RGDS has been reported to confer survival to isolated hepatocytes through the Akt pathway [278]. Also, although cellular response to RGD can depend on how the peptide is presented (e.g. clustering density[111]), we have conjugated RGDS to 10% PEG-DA hepatocyte-laden hydrogels using the same co-polymerization route in the past.[75] That RGDS was not a necessary for optimal hepatocyte function is the present case may be due to cross-talk between cell-matrix and cell-cell interaction pathways,[91, 92, 241] and suggests that cell-cell contacts were sufficient to alleviate the need for any cell-matrix contacts since the PEG hydrogel background is biologically inert. An alternative explanation could be that collagenase detachment of the hepatocyte pucks was sufficiently gentle on any extracellular matrix molecules (ECM) secreted by and attached to the hepatocyte islands, such that the ECM was immobilized with the cells during encapsulation and provided the appropriate matrix attachment cues.[279]

Microfluidic encapsulation of hepatocytes raises several additional factors that must be considered. Foremost among these is that although both microtissues and bulk gels are photopolymerized from the same prepolymer composition, the continuous fabrication of microtissues and therefore the short exposure time of prepolymer droplets in the device necessitate much higher light intensities (500 mW/cm^2 instead of 21 mW/cm^2). Given the theoretical mechanism of photoinitiation and free-radical polymerization, the small length scale of the microtissues requires a higher concentration of radicals during polymerization to overcome diffusion rates of radical-quenching oxygen into the droplet.[216] Furthermore, primary hepatocytes are known to be potentially sensitive to shear stress.[33, 280, 281] Thus, while hepatocytes have been reported to function in macroscale 3D scaffolds, [75, 113, 114] it is non-trivial to implement a continuous, high-throughput fabrication process to miniaturize the gels. Despite these challenges, we have verified by live-dead staining (**Fig. 4.6b**) and albumin (**Fig. 4.6b**) that hepatocytes indeed remain functional as hepatic microtissues. We also determined that the addition of fibroblasts by co-seeding fibroblasts onto hepatocyte islands most effectively supports hepatocyte albumin production in microtissues compared to co-encapsulating fibroblasts 24 hours post-hepatocyte isolation. This finding is consistent with the rapid decline of hepatocytes without fibroblasts in 2D culture, where early physical contact, as opposed to only soluble signaling, was critical in the first 18 hours post-isolation.[146] By patterning co-cultured pucks, we introduce supportive fibroblasts both earlier and in a closer configuration (contact vs. paracrine), and further ensure that the two cell types do not separate during microfluidic injection from size and density differences.

Of the 500+ metabolic functions that hepatocytes perform in the body, xenobiotic detoxification is essential in an *in vitro* model for drug development. We have shown activity in the optimized hepatic microtissues of several major isozymes: Cyp1A1, Cyp3A4, and Cyp2C9 (**Fig. 4.9**). Moreover, we have demonstrated induction in metabolic activity in response to omeprazole, dexamethasone, rifampin, and phenobarbital. Given these intact drug metabolism characteristics, the miniaturized 3D format of microtissue culture enables high-throughput toxicity and drug-drug interaction screens. Advantages of the microtissue system for such purposes include being amenable to fast flow cytometry-like fluorimetric readout that provides populational data. Experiments can be designed with large numbers of replicate gels for statistical power but using reduced amounts of compounds, which may be limiting especially earlier in the development process. For spheroid cultures, uncontrolled aggregation often results in large spheroids with necrotic cores;[259, 260, 263, 280, 282] hepatic microtissues are protected from both shear and aggregation, and can be cultured in small volumes without such consequences.

As a proof of concept, we have illustrated a toxicity dose experiment with the hepatoxic drug acetaminophen (**Fig. 4.10**). Overall levels of live (green) and dead (red) staining were measured for each microtissue in control or APAP-exposed populations. Compared to pooled biochemical assays such as MTT assays on 2D hepatocytes[59], this data provides information on not only the average amount of hepatotoxicity observed but also the spread of responses from the microtissue population (**Fig. 4.10b**). We have also executed a 6-day drug-drug interaction experiment, in which we observed that omeprazole or dexamethasone pre-treatment exacerbated acetaminophen toxicity (**Fig. 4.11**). Combined, these results suggest the utility of

this system for screening new drug candidates, with the potential for longer treatment times and complex dosing schemes (multiple doses, drug co-treatment) that cannot be performed in short-lived liver slices or microsomes.

Throughout this study, primary rat hepatocytes were used to establish patterning and encapsulation techniques. It is notable that the resulting hepatic microtissues effectively reflect their species-specific origin. In our microtissues, we measured a 7-fold induction of Cyp3A4 by dexamethasone, which is comparable to the fold inductions reported for rat hepatocytes (~3-8 fold from various donors while no induction was observed for human hepatocytes[17]). Accordingly, dexamethasone induction increased hepatotoxicity from acetaminophen exposure (**Fig. 4.11b**), which is known to be metabolized through Cyp3A4. Phenobarbital and rifampin on the other hand are strong Cyp3A4 inducers for human hepatocytes but less so for rat hepatocytes[18], with phenobarbital causing only a 2-fold induction of Cyp3A4 in microtissues (**Fig. 4.9d**). Thus as expected, phenobarbital and rifampin did not significantly affect acetaminophen hepatotoxicity (**Fig. 4.11c,d**). Therefore, although the hepatic microtissues characterized here may not be directly predictive of human clinical outcomes, these results suggest that microtissues derived from human hepatocytes could potentially display human-specific induction patterns.

4.5 Conclusion

In this study we utilized an array of microfabrication and microfluidic techniques to encapsulate, for the first time, primary hepatocytes within PEG microtissues for stabilized long-

term function. We have described a novel 2D to 3D method to facilitate the formation of cell-cell contacts in a controlled and scalable manner. We have examined the influence of these homotypic interactions as well as other factors on the survival and function of primary hepatocytes when encapsulated in a 3D PEG scaffold, observing that hepatocyte-hepatocyte contacts seem to alleviate the need for scaffold adhesion. After establishing an optimal microtissue composition comprising mixed hepatocyte-fibroblast pucks, we have demonstrated that these primary hepatic microtissues maintain their phenotype and display species-specific responses to known inducers, and allow for a high-throughput detection of acetaminophen-induced hepatotoxicity and CYP450-mediated drug interactions. Collectively, these techniques present a versatile platform to model drug metabolism and toxicity. Future work will incorporate automated liquid handling and more specialized fluorescent indicators of hepatocyte injury.[283]

4.6 Acknowledgements

Dr. Robert Schwartz, Dr. Kelly Stevens, Joanne Huang, and Brian Alejandro were co-authors on this work. We thank Lia Ingaharro (MIT) for performing hepatocyte isolations and general technical support, Dr. Heather Fleming (MIT) for editing the manuscript, Dr. Kathleen Christine (MIT) for the mCherry J2-3T3 line, and Shengyong Ng (MIT) for insightful discussions. We also thank MIT's Microsystems Technology Laboratories for microfabrication

facilities, and Dr. Salil Desai (MIT) and Kartik Trehan (MIT) for fabrication assistance. The J2-3T3 fibroblast cell line was kindly provided by Dr. Howard Green (Harvard). This work was supported by the National Institutes of Health. R.E.S. is supported by the American Gastroenterological Association Research Scholar Fellowship. C.Y.L. is supported by the National Science Foundation Graduate Research Fellowship Program. S.N.B. is an HHMI Investigator.

Chapter 5: Modular Construction of a Primary Human Liver-on-a-Chip

5.1 Introduction

Nearly half a billion dollars of development cost is lost every time a drug fails in late-phase development or is withdrawn from the market.[1] The most common cause for such drug candidate failure is unexpected liver toxicity,[11] often arising from reactive metabolites[33] that were not observed in pre-clinical animal models and highlighting the need to assess human responses to drugs. *In vitro* models based on human hepatocytes have the potential to model human *in vivo* ADME/TOX (absorption, distribution, metabolism, and excretion/toxicity) more quickly and accurately, reducing the need for and costs of animal testing. However, human hepatocytes are notoriously difficult to culture *ex vivo* and rapidly lose their liver-specific phenotype under conventional culture conditions.[27, 33] This has led to a variety of efforts to optimize the culture conditions of human hepatocytes such as by providing media supplements[24, 284], extracellular matrix, or co-culture with non-hepatic cell types[24, 33]. In this body of work, it has been found that three-dimensional culture configurations, which better reflect the natural architecture of the liver *in vivo*, improve maintenance of hepatocyte function compared to that in 2D culture.[24, 75, 255, 274, 285-288] The perfusion of hepatocyte cultures, which allows constant waste removal and stricter control of the culture microenvironment, has also been reported to further improve many hepatocyte functions including albumin, urea, and drug metabolizing activity compared to static cultures.[33, 255, 289-295]

Microfluidic perfusion systems have been developed that benefit from the general advantages of perfusion,[296, 297] but have been scaled down for drug development, requiring only small volumes of reagents and offering the potential for integration with downstream organs to study organ-organ interactions and integrated pharmacokinetic/pharmacodynamics modeling (PK-PD)[298, 299]. As perfusion of hepatocytes in 2D monolayers[297, 300, 301] can incur shear stress-induced damage[302] and display architecture-dependent phenotypic differences,[289] most efforts have cultured cells in 3D formats, [298, 299, 301, 303-307] though many use hepatocarcinoma-derived cell lines [298, 299, 303] that inadequately represent primary hepatocyte drug metabolism.[25, 29-32] Recently, several groups have reported devices containing primary hepatocytes trapped between microfabricated baffles simulating the hepatocyte-endothelial sinusoid barrier.[304-307] While promising, this approach puts strict constraints on the specified device architecture, and is difficult to extend to multi-organ systems. Additionally, microfluidic liver models in general are frequently complex to use and limited by technical difficulties in cell loading.

Here, we report the microencapsulation of human hepatocytes with J2-3T3 fibroblasts in poly(ethylene glycol) hydrogel to form 3D "microtissue" units (~100 μm diameter). These pre-stabilized hepatic microtissues are modular[148, 199] and can be easily seeded into various perfusion configurations, allowing versatile forms of co-culture with other cell types on-chip, or "un-loading" and sampling of the microtissues for analysis. If desired, these modular liver units can also be independently cultured and treated off-chip before loading into devices. To evaluate the liver-specific activity of our microtissues, we characterize albumin production, Phase I drug metabolism enzyme activity, and response to known hepatotoxins. By choosing to use primary

hepatocytes as the cells in our model, we are able to detect human-specific enzyme induction profiles, as well as donor-specific differences in metabolism. Finally, we demonstrate microfluidic perfusion culture of the microtissues in a device consisting of an array of microtissue traps, with intact drug metabolism, enzyme induction, and hepatocyte viability persisting for over 3 weeks.

5.2 Materials and Methods

Cell culture

Cryopreserved human hepatocytes were purchased from Invitrogen. Donor lot Hu1434 was used for all experiments unless otherwise specified (see **Table 1**). Hepatocyte medium consisted of high-glucose Dulbecco's Modified Eagle Medium (DMEM, Invitrogen) with 10% v/v fetal bovine serum (Invitrogen), 1% v/v ITS Premix (insulin, human transferrin, and selenous acid, BD Biosciences), 0.49 pg/ml glucagon, 0.08 ng/ml dexamethasone, 0.018 M HEPES, 10 U/ml penicillin, and 10 mg/ml streptomycin.

J2-3T3 fibroblasts (used at passage < 18) were a gift of Dr. Howard Green (Harvard) and were cultured in DMEM with10% bovine serum (Invitrogen), 10 U/ml penicillin, and 10 mg/ml streptomycin. Huh7.5 cells were generously provided by Dr. Charles Rice (Rockefeller) and were cultured in DMEM with 10% fetal bovine serum (Invitrogen), 10 U/ml penicillin, and 10 mg/ml streptomycin. All cells were cultured in a 5% CO_2 humidified incubator at 37°C.

Donor	Age	Ethnicity	Gender
Hu1420	68	Caucasian	Female
Hu1434	55	Caucasian	Male
Hu4175	3	Caucasian	Male
Hu4197	31	Caucasian	Female
Hu4248	12	Caucasian	Female
Hu8132	57	Caucasian	Female

Table 5.1. Donors of cryopreserved human hepatocytes.

Spheroid formation

Plates for spheroid formation[276] containing continuous arrays of 100 μm side-length pyramidal microwells in 6-well plates were provided by Dr. Peter Zandstra (Toronto). Before use, microwell surfaces were sterilized under UV for 15 minutes, passivated by soaking in 5% w/v Pluronic F-127 (Sigma) in water for 1 hour at room temperature, and rinsed at least three times in DMEM.

Freshly thawed human hepatocytes were resuspended with detached J2-3T3 fibroblasts (0.25% trypsin-EDTA, Invitrogen) at a cell density of 500,000 cells/ml for each cell type (total $1x10^6$ cells/ml). This mixed cell suspension was then transferred to the pyramical microwell plates (12 ml per 6-well plate) such that theoretical average of 5 hepatocytes and 5 fibroblasts would settle into each microwell. After allowing 15 minutes for cell settling, plates were carefully moved to the incubator for spheroid formation overnight (18-24 hours).

Hepatocyte encapsulation in PEG gels

Spheroids were dislodged from microwells after overnight culture by gentle pipetting and pelleted at 50xg, 5 min. Hepatocyte-fibroblast spheroids were then resuspended at an effective cell density, calculated from initial cell numbers added to the microwells, of $8x10^6$ hepatocytes/ml in PEG prepolymer. The prepolymer solution consisted of 100 mg/ml PEG-diacrylate (20 kDa, Laysan Bio) in heavy DMEM (DMEM adjusted to have a specific gravity of 1.06 by OptiPrep density medium, Sigma) with 1:100 v/v% photoinitiator working solution (100 mg/ml Irgacure 2959, Ciba, in *n*-vinyl pyrrolidone, Sigma). Disc-shaped PEG gels were fabricated using hydrogel polymerization apparatus.[113] Prepolymer solution containing cells was loaded into a 8.5 mm diameter, 250 μm thick silicone spacer, sandwiched between a Teflon base and a glass cover slip, and gelled by exposure to UV light from a spot curing system with a collimating lens (320-390 nm, 21 mW/cm2, 12 s; Lumen Dynamics). Each gel was soaked in rinse media for 1 hour to remove any un-polymerized components, and was subsequently cultured in 0.5 ml of hepatocyte medium. All experiments were performed with quadruplicate gels for each condition.

Microfluidic hepatocyte encapsulation

Huh7.5 microtissues for validation of device design and basic parameters were encapsulated as previously described.[264] For hepatocyte microtissues, spheroids were dislodged from microwells after overnight culture and resuspended in prepolymer solution at a much higher cell density than for disc-shaped PEG gels: assuming spheroids are half hepatocytes and

half fibroblasts, the spheroids were resuspended to $1x10^6$ hepatocytes/26.7 μl PEG prepolymer. Because of the high cell density, the PEG prepolymer for microfluidic encapsulation was adjusted to account for the volume of the cell pellet: the initial prepolymer before adding cells contained only 80% of the appropriate volume of DMEM, but the correct amounts of PEG and initiator, so that the final concentrations with the volume of the cell pellet would be as described above (100 mg/ml PEG-diacrylate, etc.).

The cell-prepolymer mixture was injected into a microfluidic encapsulation device as previously described[308], where the spheroids are encapsulated into droplets of prepolymer in oil and polymerized into microtissues. In a typical encapsulation procedure, spheroids would be encapsulated in batches of $3x10^6$ hepatocytes to reduce the amount of time hepatocytes were out of the incubator and in microfluidic tubing. To minimize the number of empy, cell-free gels that were formed, the flow of spheroids into the device was monitored by microscope and the shutter on the UV lamp was temporarily closed whenever there was a period of low spheroid density.

Microtissues collected from the device were separated from the heavier fluorocarbon oil phase, filtered through a 132 μm nylon mesh to exclude large aggregates or debris, and then washed on a 70 μm nylon mesh (Falcon) to remove any un-gelled cells and unreacted components. For non-perfused culture, at this point microtissues were dispensed and concentrated into 40 μm FACS tube cap strainers (BD Falcon) and cultured in Ultra-low attachment plates (Corning) 24-well plates (650 μl hepatocyte medium/well, changed every 2 days).

Cytochrome-P450 studies

All chemicals were purchased from Sigma and stock solutions were prepared in DMSO at 1000x final concentrations unless otherwise noted. For induction studies, microtissues were cultured in strainers for at least 2-days post-encapsulation and then treated for 72 hours with Cyp450 inducers 25-50 μm rifampin, 50 μm omeprazole, 10 μm dexamethasone, or 200-1000 μM phenobarbital (stock solution 40 mM in water). For inhibition studies, Cyp450 inhibitors 8'methoxypsoralen (25 μM), sulfaphenazole (50 μM), quinidine (10 μM), or thioTEPA (10 μM) were added to microtissues for 1 hour prior to and during incubation with Cyp450 substrates: coumarin (50 μM), ethoxyresorufin (5 μM), bupropion (100 μM), S-mephenytoin (100 μM), dextromethorphan (100 μM), or testosterone (100 μM) for 3 hours at 37°C. Glucoronidase/sulfatase-mediated phase II metabolites from coumarin or ethoxyresorufin were hydrolyzed by incubating with β-glucuronidase/arylsulfatase (Roche) for 2 hours at 37 °C. The metabolites of coumarin and ethoxyresorufin were quantified at wavelengths of 355/460 ex/em and 560/610 ex/em respectively. Metabolites of bupropion, S-mephenytoin, dextromethorphan, and testosterone were quantified by HPLC (Integrated Analytical Solutions). Cyp450 activity was also quantified using P450-Glo assay kits (Promega): microtissues were incubated with substrates luciferin-IPA (1:1000 dilution, Promega), luciferin-H (1:50, Promega), or luciferin-CEE (1:50, Promega) for 3 hours at 37 °C. Corresponding metabolites were detected in the microtissue supernatant using a luciferin detection reagent and a luminometer (10 s integration time, Berthold) according to assay instructions.

Device fabrication and loading

Standard photolithographic methods (SU-8 2050 photoresist, 125 μm thickness) were used to fabricate silicon masters for encapsulation devices and perfusion chamber devices. Sylgard 184 elastomer (PDMS, Dow Corning) devices were cast from the masters and inlet/outlet holes were punched using a 20G dispensing needle (McMaster Carr). Devices were bonded to glass slides after air plasma treatment (5 second) and baked on a 125°C hot plate for 5 minutes to strengthen the bond. Finally, the inner channels of encapsulation devices were coated with a hydrophobic silane (Aquapel). Perfusion devices were sterilized with 70% ethanol just before use, which also served to wet the inner surfaces of the chamber and prevent bubble formation, and was then flushed out of the device with medium. Tubing and connectors were sterilized by autoclave.

Perfusion devices were loaded on the day of microtissue encapsulation, though microtissues could also be cultured off-chip before loading. Newly washed microtissues were transferred off of 70 μm strainers in hepatocyte medium and injected by hand (flow rates ~20 μl/second) into the inlet of each perfusion device. Loading progress of each device was checked under the microscope to verify that all traps were filled. Microtissues that passed through the device without being captured were re-collected at the outlet and re-injected if necessary.

Device operation

Loaded liver-chip devices were cultured in a 5% CO_2 humidified incubator at 37°C. A multi-channeled external pump was connected to the outlet of each device in order to pull media through the device from an inlet reservoir (**Fig. 5.1**).

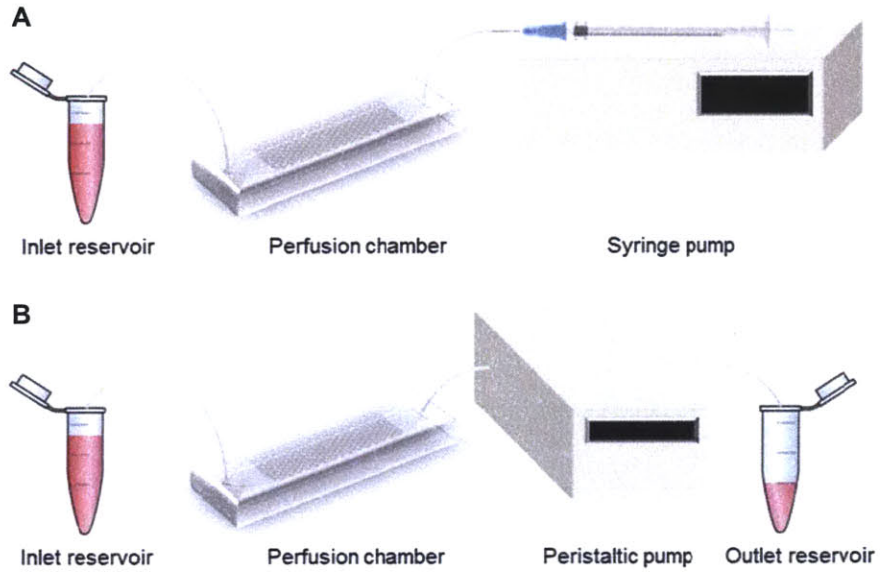

Figure 5.1. Setup and operation of microtissue perfusion chamber. (A) After loading microtissues via the inlet (left side) of each device, devices are connected by tubing to an inlet medium reservoir. A syringe pump actuates flow of the medium through the perfusion chamber (3-121 µl/hr), and spent medium is collected within the outlet tubing between the device and the syringe. (B) For parallel perfusion of multiple devices, a peristaltic pump is used to pull medium from the inlet reservoir through the device into the outlet (24 µl/hr). During metabolism assays, the inlet reservoir is replaced with a solution containing probe substrates, and metabolites are collected in the outlet reservoir.

To perfuse devices with various flow rates simultaneously, a syringe pump (Harvard Apparatus) was set up with syringes (BD, plastic) of several different inner diameters, such that a given linear displacement by the pump would withdraw different volumes of perfusate. Syringes were connected by extensive Tygon tubing to the outlet of each device, and were

initially filled with Fluorinert FC-40 (Sigma). During operation, spent medium that has passed through the device was collected in the long outlet tubing, which was disconnected daily and dispensed into collection tubes. Collected samples were then diluted to an equal final volume in fresh medium.

No-flow control devices that were loaded with microtissues but not perfused contained only the initial 15 μl of hepatocyte medium from the loading process. To prevent evaporation, devices were placed in a dish and submerged in just enough medium to cover the top of the PDMS device. The inlet and outlet holes of the PDMS device were small and, being in silicone, often self-seal when tubing is not connected. Preliminary experiments using food coloring indicated no visible transfer of liquid between inside the device and the submerging medium. Spent media samples from no-flow devices were collected by washing out the retained liquid with a known amount of fresh medium, and then further dilution to the same final volume of perfused media samples.

Simultaneous operation of larger numbers of devices in parallel (up to 24) was performed on a peristaltic pump (Ismatec). Medium was pulled from a reservoir through the devices at 24 μl/hr and directly into collection tubes that were collected daily. To perform biochemical assays on devices, the inlet of the device was moved to pull from another reservoir containing assay reagents rather than medium.

Albumin quantification

To track albumin production from hepatocytes, supernatant was collected every other day from bulk gels or microtissues in strainer, and output perfusate from devices was collected every day. The albumin concentration in each sample was quantified by an enzyme-linked immunosorbent assay (ELISA) using sheep anti-rat albumin antibodies (Bethyl Labs) and horseradish peroxidase detection (3,3',5,5'-tetramethylbenzidine, Invitrogen).

Toxicity experiments

For hepatotoxicity experiments, microtissues were cultured for 72 hours post-encapsulation and then exposed to 0-70 mM acetaminophen, 0-60 mM cyclophosphamide, 0-500 μM troglitazone, 0-350 μM chlorpromazine, or 0-120 μM imipramine for 24 hours (all chemicals purchased from Sigma). Final DMSO was kept under 0.8% v/v in hepatocyte medium. For drug interaction experiments, microtissues were cultured for 48 hours post-encapsulation, exposed to either 2 mM n-acetyl cysteine (NAC) or 1 mM buthionine sulfoximine (BSO) for 24 hours, and then dosed with 40 mM of acetaminophen with continued presence of NAC or BSO for 24 hours.

Large-particle flow cytometry

High throughput analysis of microtissue viability was performed by first staining microtissues in suspension with the live-dead fluorescent stains calcein AM (5 μg/ml) and ethidium homodimer (2.5 μg/ml) for 15 minutes at 37°C. Whole-microtissue levels of fluorescence were detected using a BioSort large particle flow cytometry (Union Biometrica) equipped with a 488 nm excitation laser. Microtissues were gated for on the basis of Time of

Flight (size) and Extinction (optical density) to exclude debris. Fluorescent signal acquisition parameters were set as follows: Gains – Green 3, Red 3, PMT control – Green 300, Red 700. Compensation was applied to subtract 90% of the green signal from red. Scatter plots were created using BioSorter software. Raw data was also exported for processing with custom MATLAB code.

5.3 Results and Discussion

5.3.1 Primary hepatocyte microtissue fabrication

We have previously reported the fabrication and optimization of hydrogel-encapsulated microtissues using primary rat hepatocytes.[308] In that work, we found that establishing cell-cell contacts by pre-aggregating hepatocytes with J2-3T3 fibroblasts before encapsulating was essential towards improving the function of resulting 3D tissues. Extending this principle to human hepatocytes, cryopreserved hepatocytes were thawed and seeded with a 1:1 ratio of fibroblast into 100 μm side length pyramidal PDMS microwells (**Fig. 5.2**). Over 24 hours, cells in each microwell (on average 5 hepatocytes and 5 fibroblasts) formed spheroids that were approximately 50 μm-diameter. In the absence of fibroblasts, hepatocytes-only aggregates did not form compact spheroids within 24 hours (data not shown). For such small spheroids and short times, the 100 μm side length microwells are ideal and increase throughput 16x compared to the commercially available 400 μm side length microwells. However, because the smaller microwells are shallower, they cannot accommodate larger cell numbers per spheroid, and

spheroids are more easily disrupted into nearby wells over multiple days of culture especially during medium changes.

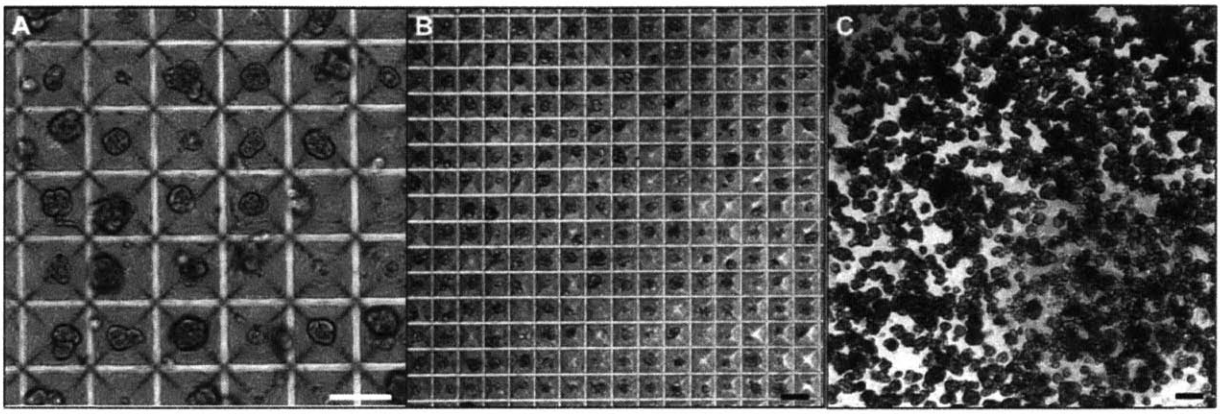

Figure 5.2. Mixed hepatocyte-fibroblast spheroid formation in pyramidal microwells. Freshly thawed hepatocytes and singly-dissociated J2-3T3 fibroblasts were combined at a 1:1 ratio and allowed to settle in pyramidal microwells such that on average, each microwell would contain 5 hepatocytes and 5 fibroblasts. (A-B) Phase contrast microscopy showing spheroid formation after 24 hours. (C) Spheroidal aggregates removed from microwells for subsequent encapsulation. All scale bars = 100 μm.

In our case, hepatocyte-fibroblast spheroids were removed from the microwells after one day and encapsulated within photopolymerized 10% PEG-DA hydrogels using a microfluidic droplet-generating device.[308] Resulting mixed spheroid-laden microtissues secreted albumin for over two weeks (**Fig. 5.3a**), whereas microtissues containing only hepatocyte aggregates were only minimally functional for the first week, confirming the supportive nature of J2-3T3 fibroblasts on human hepatocyte function in the microtissue format. Because donor lots of human hepatocytes can vary in both inherent biology and response to cryopreservation, we repeated this co-culture and encapsulation process with multiple lots (**Fig. 5.3b**). We found that in each case, hepatocyte function was successfully stabilized and albumin was secreted into the

supernatant from PEG-DA gels for over two weeks, confirming that the pre-aggregation and scaffold composition are robust for hepatocytes from a range of donor individuals.

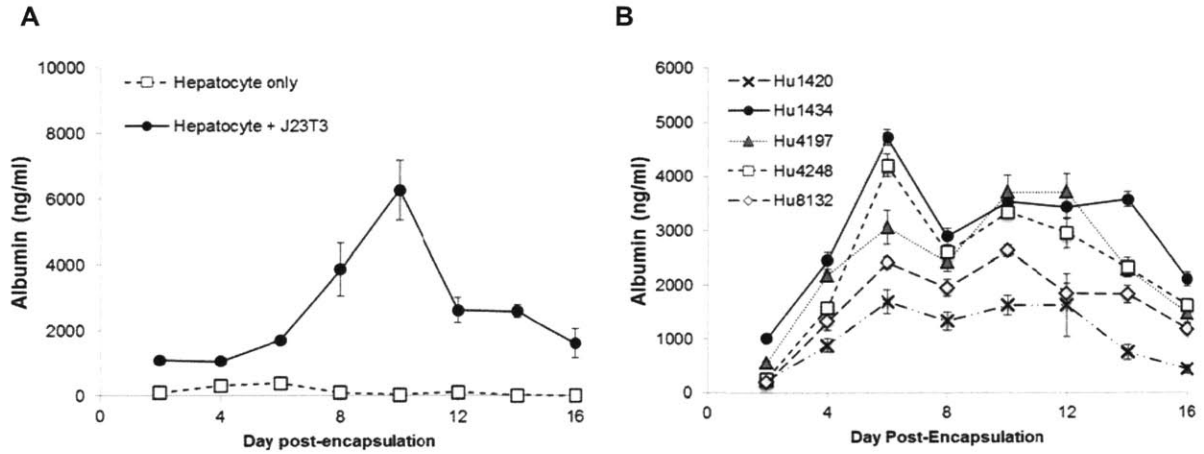

Figure 5.3. Albumin secretion by encapsulated primary human hepatocytes. (A) Supernatant concentrations of albumin from 10% PEG-DA microtissues containing either hepatocyte-only spheroidal aggregates, or hepatocyte-fibroblast spheroidal aggregates. (B) Supernatant concentrations of albumin from 10% PEG-DA gels (8.5 mm-diameter x 0.25 mm thick) with hepatocyte-fibroblast spheroidal aggregates from various hepatocyte donor lots.

5.3.2 Species- and donor-specific drug metabolizing enzyme activity

To assess the utility of hydrogel-encapsulated microtissues as an *in vitro* model of drug metabolism, we characterized microtissue cytochrome P45 (CYP450) activity as a more stringent measure of organ-specific activity beyond albumin production. Cytochrome P450s are a class of Phase I enzymes that are responsible for approximately 75% of total drug metabolism.[33] Many drug interactions leading to changes in drug efficacy or safety are modulated through CYP450 induction or inhibition. Microtissues were first stimulated to upregulate enzyme production using clinical inducers for 72 hours, and then exposed to fluorometric and luminescent

substrates for specific CYP isozymes (**Fig. 5.4).** Induction profiles in the microtissues at Day 5 post-encapsulation correlated well with literature reports: pre-incubation with rifampin induced Cyp3A4 (10-fold),[17, 309] Cyp2A6 (1.5-fold),[310] and Cyp2C9 (3.5-fold).[309] Phenobarbital induced Cyp3A4 (5-fold) and Cyp2A6 (1.7-fold),[310] and omeprazole induced Cyp1A1 (3-fold) and Cyp1A2 (350-fold).[19] The pattern of human CYP450 induction represented here is not generally not observed in hepatocellular carcinoma cell lines,[31, 32] which renders the latter insufficient for predicting CYP450 mediated drug interactions. Furthermore, several of the induction interactions observed here are species-specific. For example, rifampin has been reported to induce Cyp3A4 for human hepatocytes but not rat hepatocytes.[17] Similarly, Cyp1A2 is induced by omeprazole in human hepatocytes but much less so in rat hepatocytes.[19] Conversely, dexamethasone is a strong inducer of Cyp3A4 in rat hepatocytes but not in human hepatocytes[17] (**Fig. 5.4a**). We also tested the inhibition of CYP450 enzymes using several known inhibitors, and observed as expected reduced Cyp3A4 activity in the presence omeprazole (**Fig 5.4a**),[311, 312] Cyp2A6 inhibition by 8-methoxypsoralen[313] (**Fig. 5.4b**), and Cyp2C9 inhibition by sulfaphenazole (**Fig 5.4c**).[314, 315] Taken together, this evidence supports the conclusion that microtissues are effective at stabilizing the drug metabolism functions of primary human hepatocytes, and highlights why *in vitro* human cultures can be more predictive of *in vivo* human liver response than animal models.

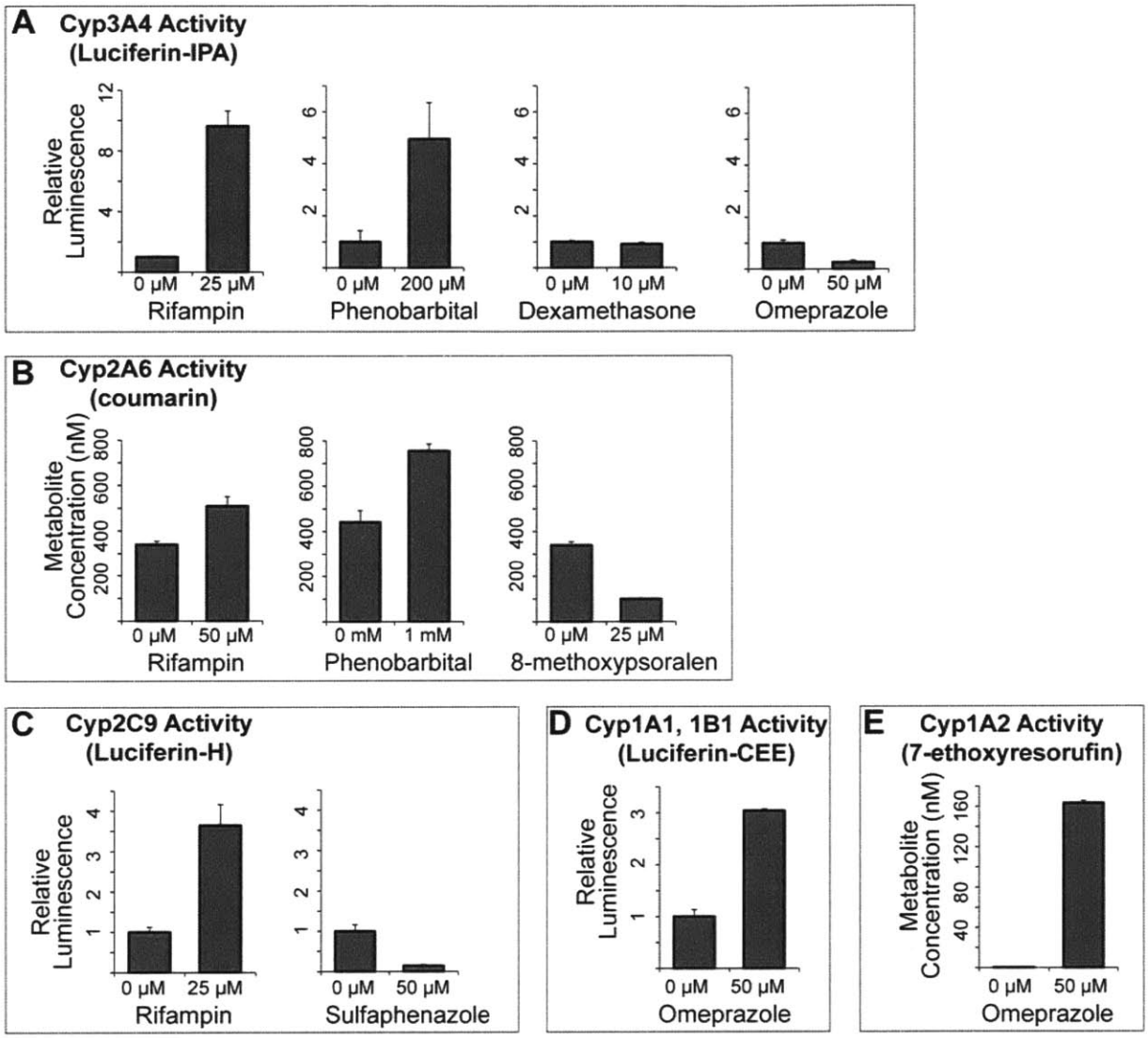

Figure 5.4. Induction of cytochrome P450 activity in primary human hepatocyte microtissues. (A) Cyp3A4 activity as evaluated by luciferin-IPA metabolism in response to inducers (72 hours) rifampin, phenobarbital, or dexamethasone, and weak inhibitor omeprazole. (B) Cyp2A6 activity evaluated by coumarin metabolism to coumarin 7-hydroxylase in response to induction by rifampin and phenobarbital, or inhibition by 8-methoxypsoralen. (C) Cyp2C9 activity evaluated by luciferin-H metabolism as induced by rifampin or inhibited by sulfaphenazole. (D-E) Cyp1A1 and Cyp1A2 activity evaluated by luciferin-CEE and 7-ethoxyresorufin metabolism, respectively, when induced by omeprazole.

We also sought to examine whether microtisuses had the potential to accurately reflect donor specific differences in drug metabolism. On Day 5 post-encapsulation, baseline, induced, and inhibited Cyp3A4, Cyp2D6, Cyp2C19, and Cyp2B6 activities were quantified in microtissues derived from two different donor lots, Hu1434 (Donor A) and Hu4175 (Donor B) (**Fig. 5.5**). CYP2D6 and CYP2C19 are known to have genetic polymorphism, with resulting inter-individual variability in drug clearance through these pathways.[13, 316] In the Caucasian population, to which both donor lots belong, approximately 10% of individuals are considered low 2D6 metabolizers,[317] while approximately 5% are low 2C19 metabolizers[12]. Thus, it is particularly notable that in our microtissue model, Donor A exhibits 3.4-fold higher baseline Cyp2D6 activity than Donor B (**Fig. 5.5c, d**). Cyp2D6 activity metabolized about 25% of clinically used medications[317] and is generally one of the most difficult hepatocyte functions to maintain under non-optimal culture conditions;[295] its presence here speaks to the functional stability of hepatocytes in microtissue culture. The concentration of metabolites processed by Cyp2D6 by Donor B is as low as the activity for either donor in the presence of the inhibitor quinidine (**Fig. 5.5c,d**), suggesting that Donor B may have been an inherently low 2D6 metabolizer. Genotyping of the two donors could confirm this hypothesis. On the other hand, Donor A had almost undetectable Cyp2C19 activity (**Fig. 5.5e**), whereas microtissues from Donor B were 60-fold more active (**Fig. 5.5f**). Similar fold-inductions were observed after 2 weeks of microtissue culture (data not shown). The ability to model such a range of donor characteristics will be crucial in screening drug candidates; for example, a given dose may not affect the average population but could lead to a toxic buildup in low metabolizing individuals.

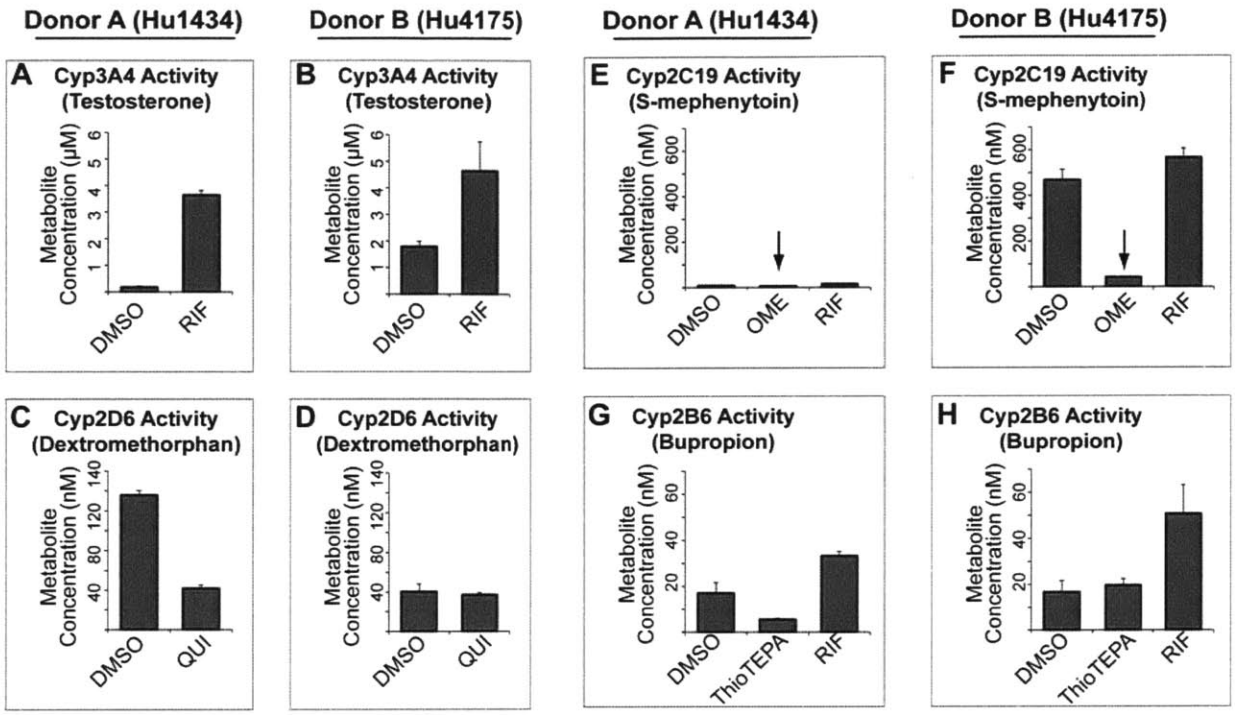

Figure 5.5. Comparison of cytochrome P450 activity (Day 5) between donor individuals. (A,C,E,G) HPLC quantification of metabolites produced by Hu1434 microtissues. (B,D,F,G) HPLC quantification of metabolites produced by Hu4175 microtissues. Arrows in (E) and (F) indicate metabolite concentration below detectable limit. Inducers and inihibitors used were rifampin (RIF), quinidine (QUI), omeprazole (OME), and thioTEPA.

5.3.3 Microtissue response to hepatotoxic drugs and drug interactions

We next treated microtissues with several model hepatotoxins to validate the responsiveness of microtissues to hepatotoxic insults (**Fig. 5.6**). One of these was acetaminophen (APAP), which is itself nontoxic but is converted by CYP450 enzymes in the liver into the reactive metabolite N-acetyl-*p*-benzoquinone (NAPQI)[271]. NAPQI can be inactivated by intracellular glutathione, but accumulates to toxic concentrations when glutathione reserves are depleted[271]. As a first pass, our readout for microtissue toxicity was a live/dead stain using calcein AM (green, live) and ethidium homodimer (red, dead). Microtissues were incubated with a range of acetaminophen concentrations for 24 hours, stained, and analyzed using a large

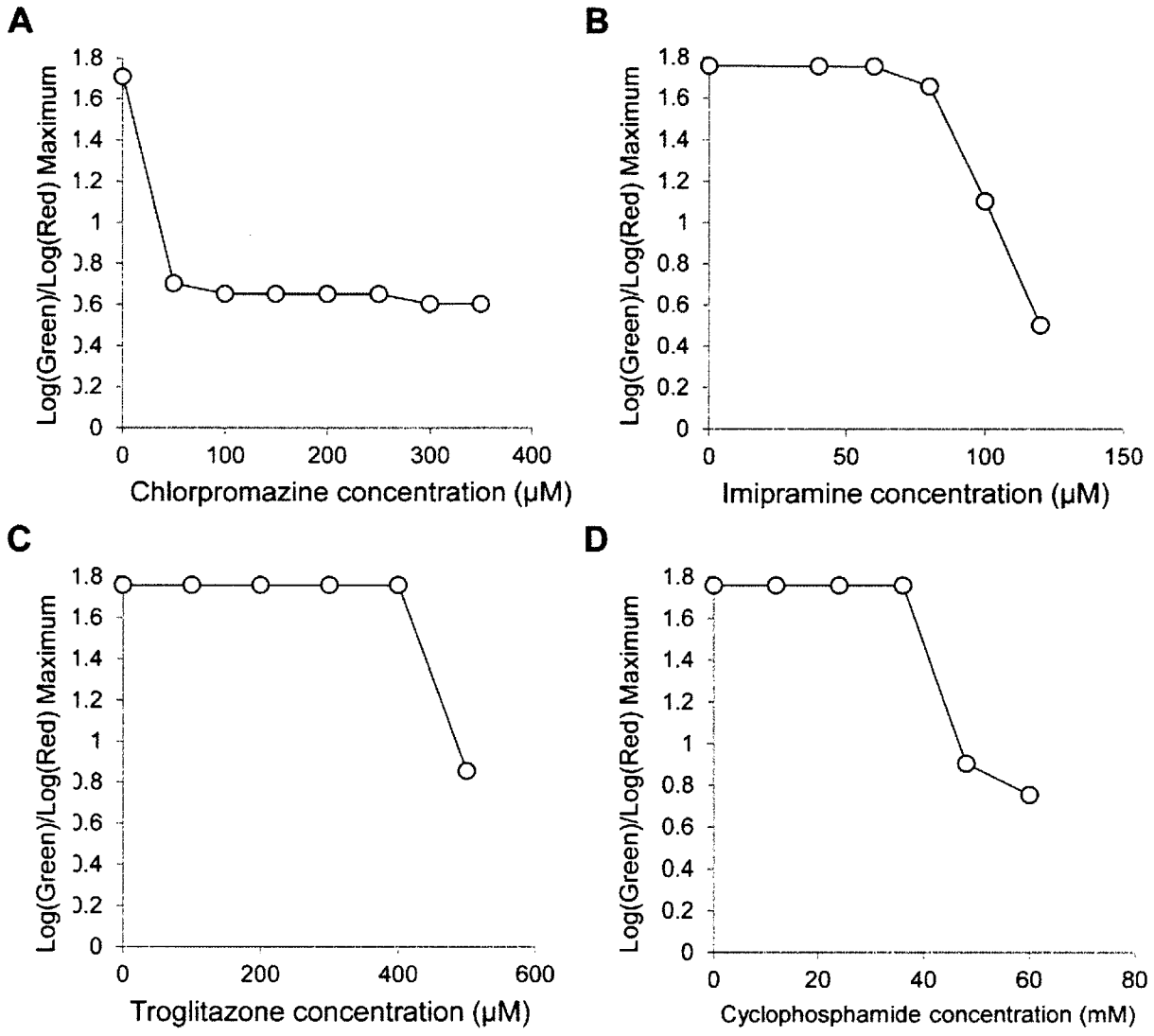

Figure 5.6. Microtissue hepatotoxicity as measured by large particle flow cytometry. Data points indicate shift in peak green/red (live vs. dead) peak location with increasing concentrations of (A) chlorpromazine, (B) imipramine, (C) troglitazone, and (D) cyclophosphamide.

particle flow cytometer. On scatter plots of microtissue fluorescence, dose-dependent hepatotoxicity was observed, with the detected microtissue population shifting farther to the right (more dead staining) and down (less live staining) with increasing concentrations of acetaminophen (**Fig. 5.7a**).When the ratio of green signal vs. red signal is quantified for each

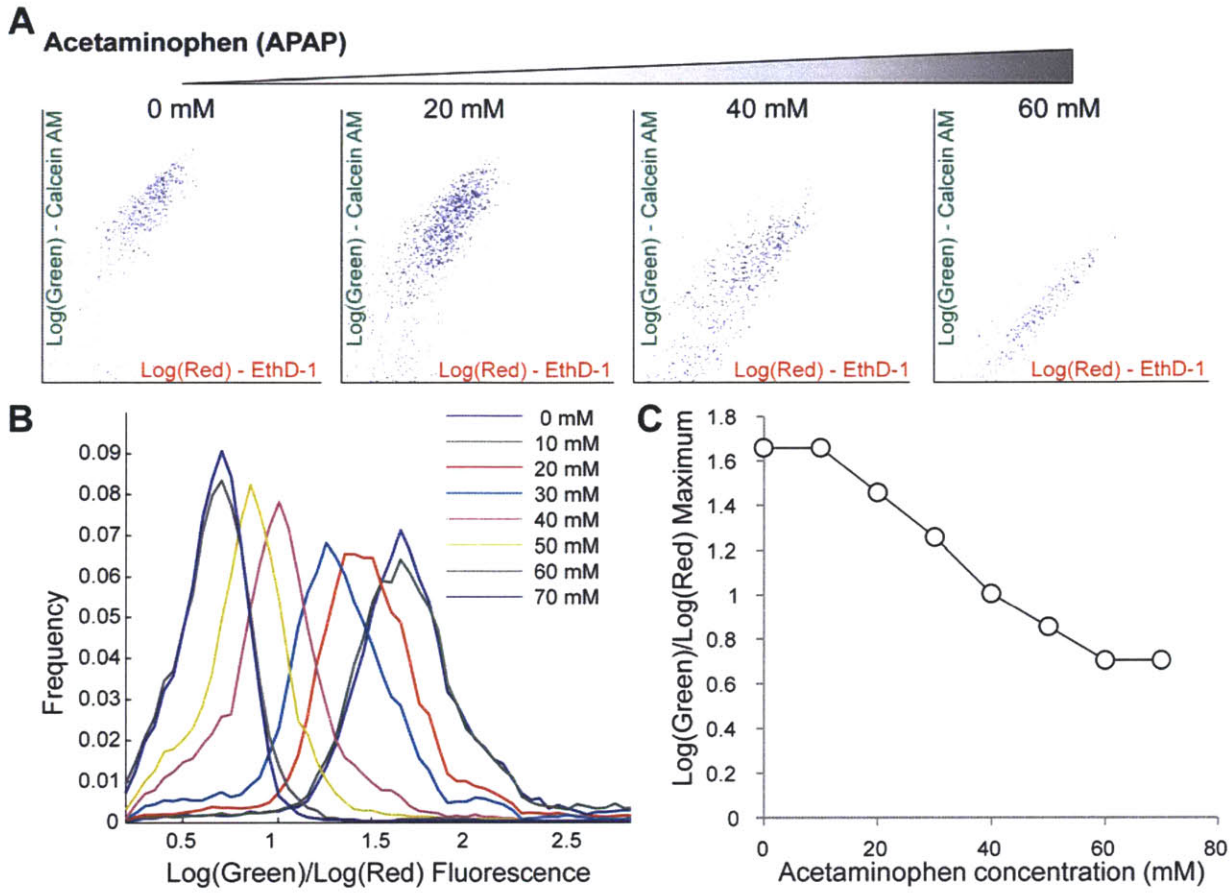

Figure 5.7. Acetaminophen-induced hepatotoxicity in human hepatic microtissues. (A) Large-particle flow cytomettry scatter plots of live/dead (green/red) stained microtissue populations when exposed to increasing concentrations of acetaminophen for 24 hours. (B) Histogram quantification of each microtissue population, measuring the ratio of green to red fluorescence in each microtissue. (C) Plot of histogram peak locations. Initial data point at 0 mM APAP indicates fully viable microtissues, whereas 60 and 70 mM data points indicate toxicity to all cells within each microtissue.

population, as a measure of % cell viability in each microtissue, histograms curves (**Fig. 5.7b**) also display decreasing log(green)/log(red) peak locations (**Fig. 5.7c**) with increasing acetaminophen concentration. To further investigate whether the observed toxicity is consistent with the proposed acetaminophen mechanism, we pretreated microtissues with either

buthionine sulfoximine (BSO), which inhibits glutathione production and thus depletes intracellular glutathione, or N-acetyl cysteine (NAC), which is a glutathione precursor and thus increases the amount available to deactivate, before exposure to acetaminophen. As expected, BSO pre-treatment exacerbated APAP-induced toxicity, while NAC pre-treatment mitigated it (**Fig. 5.8**).

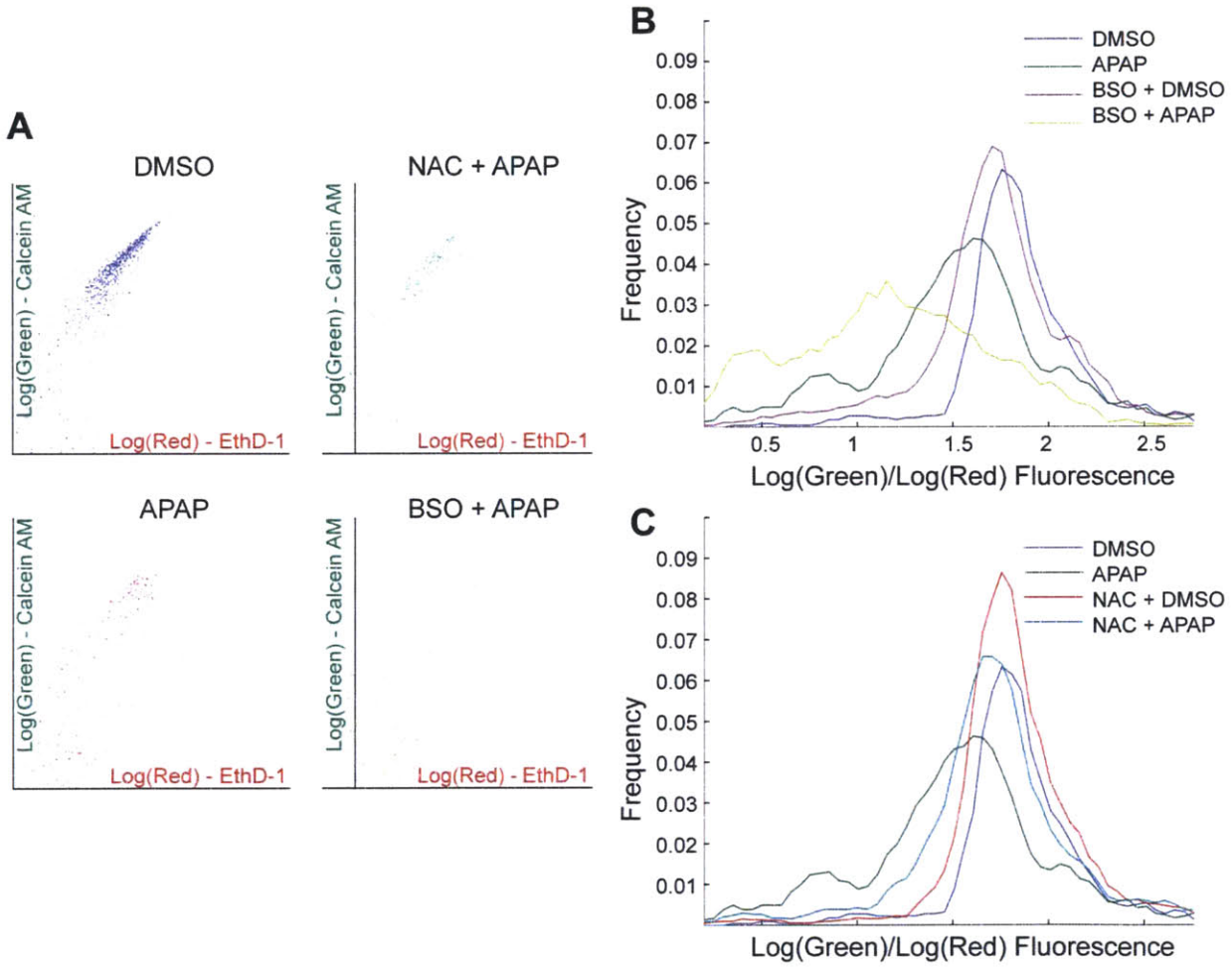

Figure 5.8. Mechanism-based drug interactions with acetaminophen toxicity. (A) Scatter plots of live/dead (green/red) stained microtissues after exposure to acetaminophen or combinations of acetaminophen with N-acetyl cysteine (NAC) or buthionine sulfoximine (BSO). (B) Histogram quantification of treated microtissue populations.

5.3.4 *Design and operation of microfluidic perfusion chamber*

To illustrate the application of hepatic microtissues in a perfused device, we designed a simple microfluidic chamber containing an array of C-shaped microtissue traps (**Fig. 5.9**). The inner diameter of the traps was selected to be 500 μm so that each trap holds approximately 10 microtissues. We chose to trap microtissues in groups of 10 to allow some local interaction between the microtissues via secreted soluble factors, but balancing this against the diffusive distance between the perfusate flow and the center of the microtissue clusters. The shape and spacing of the traps in an array were then optimized for capture efficiency, defined as the number of gels passing through the device that are retained in traps. We found that straight outer edges and backs on each trap helped direct microtissues into the next row of traps: microtissues would need to make nearly a 90° turn to escape (**Fig. 5.9c**). If the edges and bottoms of the traps were semi-circular, laminar flow around the edges helped microtissues establish a sine-like flow path and escape all subsequent traps. During microtissue loading into our final devices (**Fig. 5.9c**), traps fill in rows from the first row (left) backwards, which signifies that microtissues are escaping to subsequent traps only if there is no longer space in the prior traps.

As the supply of human hepatocytes is limited, we first explored the operating parameters of the device using microtissues containing Huh7.5 cells. Devices were loaded with Huh7.5 microtissues and perfused with standard culture medium at various flow rates: 3 μl/hr, 19 μl/hr, 62 μl/hr, and 121 μl/hr. At all flow rates except the highest, microtissues remained viable after 3 days as visualized by calcein staining, and Huh7.5 cells seemed to be proliferating

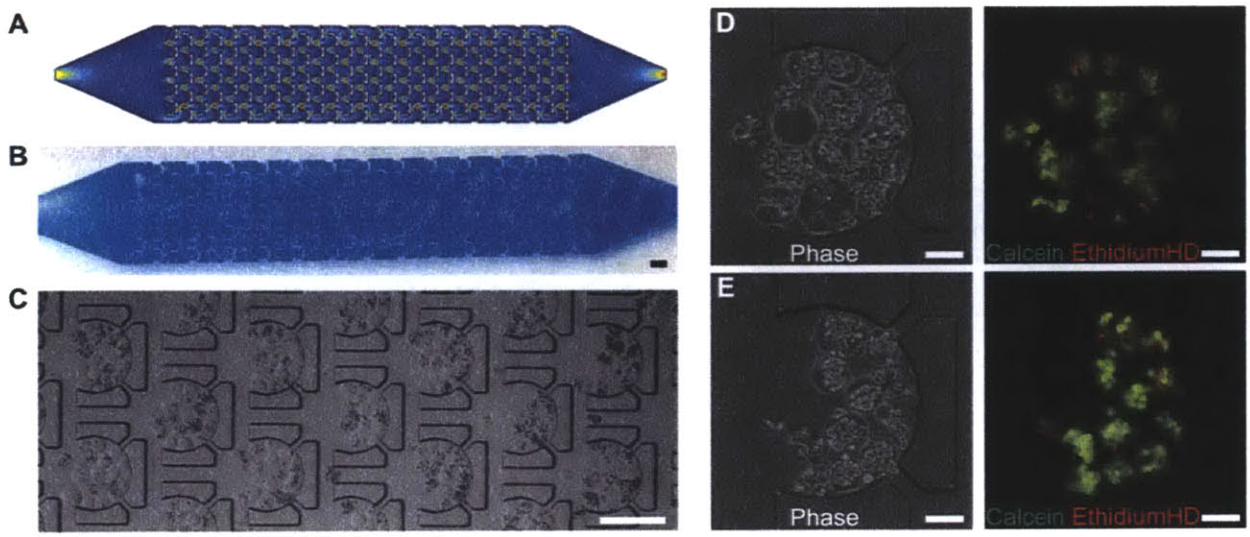

Figure 5.9. Microtissue trapping and perfusion device. (A) Schematic of the device illustrating fluid flow (red – high velocity, dark blue – low velocity) between semicircular traps. (B) Photograph of device filled with colored solution. (C) Phase microscope image of microtissues loaded into traps. (B-C) Scale bar = 500 μm. (D-E) Phase and live/dead fluorescent images of Huh7.5 microtissues in individual traps after 72 hours of perfusion (19 μl/hr).

by morphology (**Fig. 5.10d, e**). While device oxygenation is considered to be a major role of fluid perfusion,[318] microtissues were viable even in un-perfused devices, showing that sufficient amounts of oxygen are able to diffuse through the gas-permeable PDMS device[319], and that the small 15 μl volume of medium in the chamber provides sufficient nutrients for 24 hours. The output medium from perfused and un-perfused devices was monitored for albumin secreted by Huh7.5 cells (**Fig. 5.10**); the successful detection of albumin confirms the ability for small molecules and proteins to transport between the convective flow areas of the device, and microtissue-encapsulated cells in the traps. Optimal albumin production from devices was observed between 19-62 μl/hr. A flow rate of 24 μl/hr (576 μl/day) was selected for further experiments, and produces a estimated flow velocity of 25 μm/s that is comparable to other perfused hepatocyte systems[305]. Flow rates higher than 121 μl/hr were visibly detrimental to

Huh7.5 proliferation and morphology over several days. Accordingly, the albumin output from devices at high flow rates was much lower than at lower flow rates (Figure 9). While high flow rate can be detrimental to cell function due to shear-induced damage[289], cells within microtissues should be protected from shear stress by the hydrogel coating[262] as well as flow profiles around the traps. We have postulated that the higher flower rates are instead diluting out secreted cell-cell interaction molecules.[320, 321]

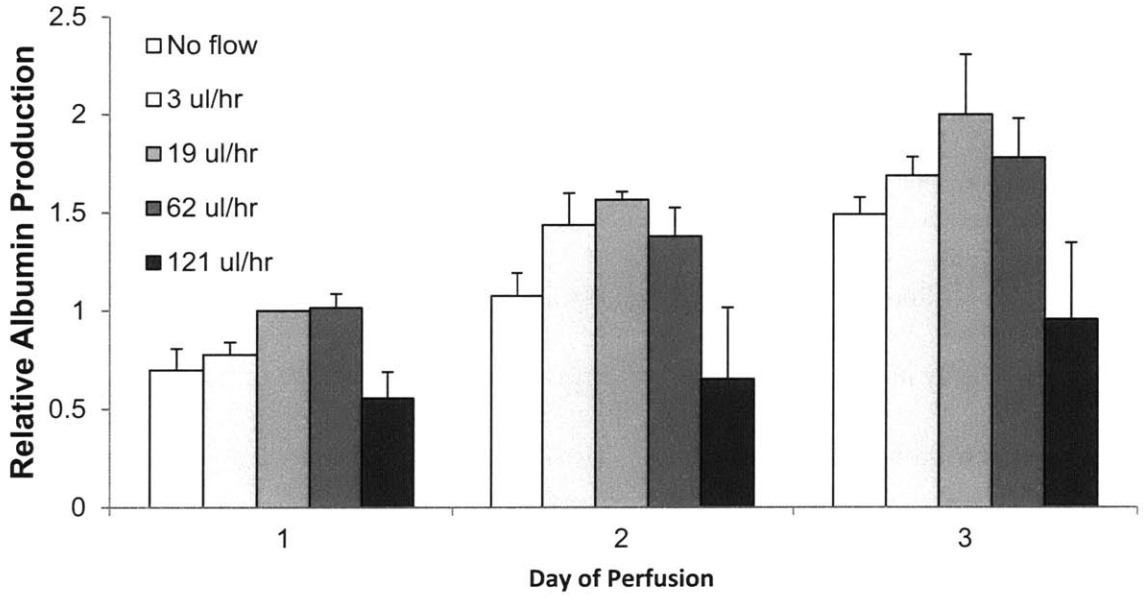

Figure 5.10. Albumin detected in perfusate of Huh7.5 microtissue-loaded devices. Albumin concentrations were normalized to those from 19 μl/hr devices.

Having established that the device architecture and operating procedures were cytocompatible, we next loaded microtissues containing primary human hepatocytes into chamber devices and perfused them with hepatocyte medium at a volumetric flow rate of 24 μl/hr. The output media from each device was collected and analyzed for secreted albumin over

time (**Fig. 5.11a**). Albumin production was in the range of 100-300 ng/day/device, corresponding to about 10-20 μg/10^6 hepatocytes/day and persisting for over 21 days. This three-week longevity will be important for the study of any effects that occur only after temporal sequences of drug combinations, or chronic exposure to liver metabolites. In one such scenario, a pro-drug may be converted in the liver compartment to a metabolite whose exposure slowly induces toxicity on a downstream organ model over time. To demonstrate the metabolism of drug passing through the microtissue liver device, we perfused devices with coumarin and detected rates of metabolite formation comparable to that of microtissues off-chip (**Fig. 5.11d**). Omeprazole induction of CYP1A1 substrate metabolism (**Fig. 5.11b**) and rifampin induction of Cyp2C9 substrate metabolism (**Fig 5.11c**) were also intact and comparable to fold-inductions off-chip (**Fig 5.4c, d**). Collectively, these findings signify that liver-specific functions are maintained on this easily assembled device, and underscore the suitability of human hepatic microtissues for organ-on-a-chip systems.

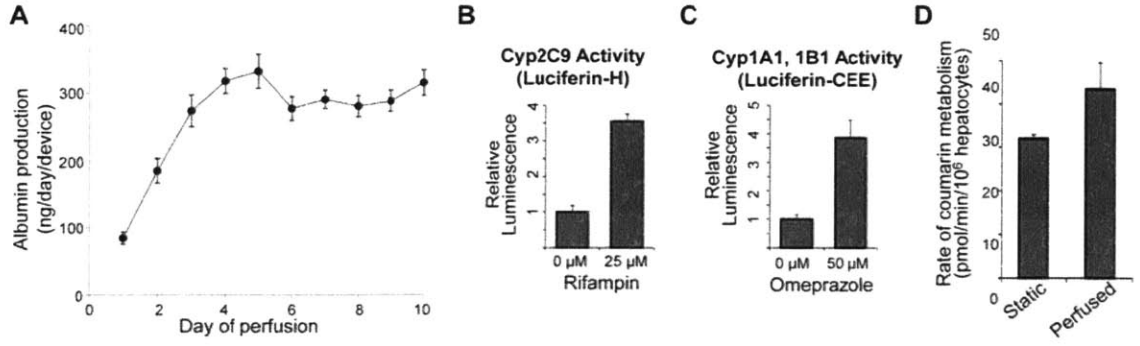

Figure 5.11. Characterization of hepatocyte functions in microtissue perfusion device. (A) Amount of albumin secreted by microtissues into perfusate over time. (B) Induction of Cyp2C9 activity (Day 14) by 72 hours of exposure to rifampin in the perfusate. (C) Induction of Cyp1A1 activity (Day 5) by 72 hours of exposure to omeprazole in the perfusate. (D) Rate of coumarin 7-hydroxylation by microtissues cultured off-chip (static) compared to metabolism rate in one pass through microtissues on-chip (perfused).

5.4 Conclusion

We have developed a method to produce *human* hepatocyte-laden microtissues, containing hepatocyte-fibroblast aggregates in a miniaturized hydrogel scaffold, for modular seeding of *in vitro* liver-on-a-chip devices. The microtissues exhibited species-specific cytochrome P450 induction and inhibition profiles in response to known drugs, as well as reactive metabolite-induced hepatotoxicity, attesting to the stabilization of liver-specific phenotype in the microtissues. We were also able to detect donor-specific differences in Cyp2D6 and Cyp2C19 activity, which would not have been possible using existing hepatic cell lines. For further individualized models of drug metabolism, future efforts will focus on encapsulating induced pluripotent stem cell-derived hepatocytes into microtissues. We have also designed and tested a trap-based microfluidic compartment that efficiently captures and retains microtissues for perfusion culture over 3 weeks, and permits interrogation with soluble drugs. Future work will integrate microtissues into devices with more complex flow geometries, for example those incorporating branching endothelial-lined channels or with built-in oxygenation gradients. We envision that such liver-on-a-chip systems, especially in conjunction with multi-organ models, have the potential to accelerate pre-clinical drug development and dramatically reduce clinical trial attrition.

5.5 Acknowledgements

Dr. Robert Schwartz, Dr. Arnout Schepers, and Brian Alejandro were co-authors on this work. We thank the MIT Microsystems Technology Laboratories for fabrication assistance. Dr. Howard Green (Harvard) provided the fibroblast cell line, and Dr. Peter Zandstra (Toronto) provided microwell plates. This project was funded by the National Institutes of Health (NIH), as well as individual fellowship support from the National Science Foundation Graduate Research Fellowship Award (C.Y.L.) and the American Gastroenterological Association Research Scholar Fellowship (R.E.S.). S.N.B. is an HHMI investigator.

Chapter 6: Perspectives and Future Direction

6.1 Microfluidic Fabrication of 3D Microtissues

In this thesis, we explored the construction of defined cellular microenvironments through the paradigm of individually stabilized, 3D microtissue units. We first designed a microfluidic device in *Chapter 2* that uses flow-focusing to encapsulate cells into droplets of pre-polymer in oil, which were photopolymerized on-chip to produce 100 μm-diameter spherical PEG microtissues. Throughout *Chapters 3-5*, we encapsulated a range of mammalian cells including primary liver, tumor, and stromal cells, validating the first continuous process to quickly manufacture uniform microtissues while preserving the long-term (~weeks) survival, function, and proliferation of encapsulated mammalian cells. Several groups in parallel have since described similar microfluidic droplet-based encapsulation strategies using alginate,[141] agarose,[139] or self-assembling peptide gels,[322] though these alternative materials have inherent cell-interactive properties and thus do not offer the combination of blank background and ease of modification that PEG hydrogels do.

Although we have shown here that a single flow-focusing junction can generate 10^5 microtissues/hour, in the future we will be pursuing even higher production rates to facilitate larger-scale drug screening or bottom-up microtissue assembly. New device designs with many parallel microtissue encapsulation junctions are being tested. These will require uniform UV-illumination over a wide area of polymerization channels, and must avoid the scattering of light to other regions of the device[323] to avoid premature polymerization. To address any concerns

about the use of UV light, future prepolymers can incorporate novel photoinitiators that absorb in the visible-light range.[120]

6.2 Systematic Control of Microenvironmental Stimuli

Leveraging various microfabrication and bioconjugation techniques, we have demonstrated methods to control the interactions of cells in microtissues with other co-cultured cells, extracellular matrix, and soluble stimuli. These platforms open the door to numerous investigations surrounding the influence of specific microenvironmental stimuli on cell fate and function, especially when such cues are interpreted by cells cultured in a 3D setting. For example, ongoing studies are testing whether the co-encapsulation of particular stromal cell lines can confer chemoresistance to tumor cells from a range of tissue origins, similar to screens that have been previously performed on 2D cultures.[219] As seen in the different opposing responses of mouse lung adenocarcinoma cells to TGF-β and to a TGFβR1/TGFβR2 inhibitor (LY2157299) when cultured in a 2D plate compared to in 3D microtissues (*Chapter 3*), the thorough study of tumor biology and response to therapy is be contingent on having an appropriate *in vitro* model. Future work is required to confirm whether 3D tumor models are indeed more predictive of human *in vivo* response to chemotherapeutics: a follow-up study to our work here could be to compare results from individual patients in clinical trials of LY2157299, with the effect of the drug on microtissues containing biopsied tumor cells.

6.3 High-Throughput 3D Phenotypic Screening

Towards high-throughput microtissue-based drug screening, we have developed a platform based on large populations ($n > 1000$) of 3D microtissues to measure cancer cell proliferation in response to chemotherapeutic candidates, or liver tissue injury in the presence of potential hepatotoxins. By using a flow cytometry-like readout for these screens, we were able to quickly measure fluorescent labels of cell density or cell viability for each individual microtissue in a treatment group, providing information on both population average and spread.

In order to investigate hepatotoxicity using an ideally relevant model cell type, we examined factors to maintain primary human hepatocyte function in microtissues for the first time (*Chapters 4-5*), validated by the preservation of important drug metabolizing cytochrome P450 enzymes and sensitivity to known hepatotoxins and drug combinations. It is particularly interesting that depending on the donor lot of cryopreserved hepatocytes used, resulting microtissues metabolized test substrates for CYP2D6 and CYP2C19 at different rates. Up to 10% of Caucasians are poor CYP2D6 metabolizers and up to 5% are poor CYP2C19 metabolizers.[13] That microtissues reflect individual liver phenotypes could be useful in pre-clinical studies to detect idiosyncratic toxicity due to donor-specific enzyme polymorphisms, or to identify target patient populations for clinical trials.[316]

In these studies we have performed toxicity assays on uniform hepatic microtissues, but a future area of investigation could be to mix and match the types of microtissues cultured together. Hepatic microtissues could be mixed in a single well with microtissues containing cardiomyocytes, for example, to assess if liver metabolites of a drug candidate caused

cardiotoxocity. Similarly, some pro-drugs might require activation by liver microtissues before they are effective on nearby tumor microtissues. The modularity of microtissue culture allows the two cell types to be co-cultured and exchange soluble signals, but then later be decoded[149] and analyzed separately to decouple any hepatotoxicity from potential anti-tumor activity. Looking forward, while this thesis uses the live-dead stains calcein AM and ethidium homodimer as a proof of concept for toxicity screening, a wide array of fluorescent stains or genetic labeling is available to probe more subtle measures of hepatocyte damage, such as mitochondrial abnormalities, lipid accumulation, oxidative stress, and intracellular glutathione depletion.[283]

Successful long-term culture of human microtissues could also have important future applications *in vivo* as injectable implants for disease therapy or to "humanize" mouse livers,[75] obviating the need for invasive surgical procedures. An optimized microtissue scaffold could protect and provide stabilizing signals for hepatocytes, potentially improving engraftment efficiencies in various locations. Further exploration of scaffold modifications, especially towards cell-degradable PEG materials,[121, 125, 131, 324] will be of benefit for vascularization and permanent integration of implanted microtissues.

6.4 Towards Modular Organ-on-a-Chip Devices

In *Chapter 5*, we encapsulated primary *human* hepatocytes in microtissues with the ultimate objective of being able to modularly seed hepatocytes into a range of liver-on-a-chip device designs. Using a proof-of-concept microfluidic chamber containing an array of

microtissue-retaining traps, we demonstrated that at optimal flow rates (20-60 μl/hr) hepatic microtissues remained viable and continued to secrete albumin during over 3 weeks of perfusion. We also detected drug metabolism of perfused substrates and induction by rifampin and omeprazole on-chip. Together, these results verified transport of proteins and small molecules to and from encapsulated cells via convective fluid transport and then diffusion through the microtissue hydrogel scaffold, and suggest the utility of such devices as metabolite-generating liver compartments for integration with multi-organ models. In order for on-chip results to be clinically relevant, further experiments will be necessary to correlate rates of metabolite production and area under the curve (AUC) data on-chip with clearance rates *in vivo*.

Future directions will leverage microtissue modularity to populate increasingly complex devices with these pre-stabilized hepatocyte units, for example to incorporate vascular-like branching, endothelial lined channels, or chemical and oxygen gradients. Hepatocytes have been shown to have CYP450 profiles that depending on position along an oxygen gradient,[291] representing centrilobular vs. periportal phenotypes.[237, 238] Spatial differences in sensitivity to systemic hepatotoxins can also arise due to higher concentrations of metabolites accumulating downstream i.e. in the centrilobular zone.[325] Perfusion systems that encompass such additional facets of tissue physiology could further improve the modeling of the human body on-chip. Finally, to address the lack of appropriate hepatic cell lines and when primary cells are not practical options, induced pluripotent stem (iPS) cells may provide an alternative solution to cell sourcing and produce individual-specific iPS-derived hepatocyte-like cells (iHLCs) with unique genetic backgrounds.[326] Future undertakings will endeavor to encapsulate and maintain

iHLCs in microtissues while directing their differentiation past the current fetal hepatic phenotype into mature hepatocytes.

Bibliography

1. J. A. DiMasi, R. W. Hansen and H. G. Grabowski, *The price of innovation: new estimates of drug development costs.* Journal of health economics, 2003. **22**(2): p. 151-185.
2. I. Kola and J. Landis, *Can the pharmaceutical industry reduce attrition rates?* Nature Reviews Drug Discovery, 2004. **3**: p. 711-715.
3. J. A. Dimasi, *Risks in new drug development: approval success rates for investigational drugs.* Clinical pharmacology and therapeutics, 2001. **69**(5): p. 297-307.
4. A. Marusyk, V. Almendro and K. Polyak, *Intra-tumour heterogeneity: a looking glass for cancer?* Nat Rev Cancer, 2012. **12**(5): p. 323-334.
5. G. H. Heppner, *Tumor heterogeneity.* Cancer research, 1984. **44**(6): p. 2259-2265.
6. A. Kamb, *What's wrong with our cancer models?* Nature Reviews Drug Discovery, 2005. **4**(2): p. 161-165.
7. N. A. Bhowmick and H. L. Moses, *Tumor-stroma interactions.* Curr Opin Genet Dev, 2005. **15**(1): p. 97-101.
8. L. Yang and D. P. Carbone, *Tumor-host immune interactions and dendritic cell dysfunction.* Advances in cancer research, 2004. **92**: p. 13-27.
9. R. A. Wilke, D. W. Lin, D. M. Roden, P. B. Watkins, D. Flockhart, I. Zineh, K. M. Giacomini and R. M. Krauss, *Identifying genetic risk factors for serious adverse drug reactions: current progress and challenges.* Nature Reviews Drug Discovery, 2007. **6**(11): p. 904-916.
10. P. B. Watkins, *Idiosyncratic liver injury: Challenges and approaches.* Toxicol Pathol, 2005. **33**(1): p. 1-5.
11. N. Kaplowitz, *Idiosyncratic drug hepatotoxicity.* Nature Reviews Drug Discovery, 2005. **4**(6): p. 489-499.
12. C. Gunaratna, *Drug Metabolism and Pharmacokinetics in Drug Discovery: A Primer for Bioanalytical Chemists, Part I.* Current separations, 2000. **19**(1): p. 17-23.
13. D. J. Belle and H. Singh, *Genetic factors in drug metabolism.* Am Fam Physician, 2008. **77**(11): p. 1553-1560.
14. N. E. Sharpless and R. A. Depinho, *The mighty mouse: genetically engineered mouse models in cancer drug development.* Nat Rev Drug Discov, 2006. **5**(9): p. 741-754.
15. M. Singh and L. Johnson, *Using genetically engineered mouse models of cancer to aid drug development: An industry perspective.* Clin Cancer Res, 2006. **12**(18): p. 5312-5328.
16. M. M. Winslow, T. L. Dayton, R. G. W. Verhaak, C. Kim-Kiselak, E. L. Snyder, D. M. Feldser, D. D. Hubbard, M. J. DuPage, C. A. Whittaker, S. Hoersch, S. Yoon, D. Crowley, R. T. Bronson, D. Y. Chiang, M. Meyerson and T. Jacks, *Suppression of lung adenocarcinoma progression by Nkx2-1.* Nature, 2011. **473**(7345): p. 101-104.
17. C. Lu and A. P. Li, *Species comparison in P450 induction: effects of dexamethasone, omeprazole, and rifampin on P450 isoforms 1A and 3A in primary cultured hepatocytes from man, Sprague-Dawley rat, minipig, and beagle dog.* Chemico-biological interactions, 2001. **134**(3): p. 271-281.

18. M. Martignoni, G. M. M. Groothuis and R. de Kanter, *Species differences between mouse, rat, dog, monkey and human CYP-mediated drug metabolism, inhibition and induction.* Expert Opin Drug Met, 2006. **2**(6): p. 875-894.
19. H. Shih, G. V. Pickwell, D. K. Guenette, B. Bilir and L. C. Quattrochi, *Species differences in hepatocyte induction of CYP1A1 and CYP1A2 by omeprazole.* Human & experimental toxicology, 1999. **18**(2): p. 95-105.
20. A. McQueen, *In Vitro Toxicology: Model Systems and Methods*, CRC Press, 1989.
21. H. Azuma, N. Paulk, A. Ranade, C. Dorrell, M. Al-Dhalimy, E. Ellis, S. Strom, M. A. Kay, M. Finegold and M. Grompe, *Robust expansion of human hepatocytes in Fah(-/-)/Rag2(-/-)/Il2rg(-/-) mice.* Nature biotechnology, 2007. **25**(8): p. 903-910.
22. C. Tateno, Y. Yoshizane, N. Saito, M. Kataoka, R. Utoh, C. Yamasaki, A. Tachibana, Y. Soeno, K. Asahina, H. Hino, T. Asahara, T. Yokoi, T. Furukawa and K. Yoshizato, *Near completely humanized liver in mice shows human-type metabolic responses to drugs.* The American journal of pathology, 2004. **165**(3): p. 901-912.
23. S. A. Wrighton, M. Vandenbranden, J. C. Stevens, L. A. Shipley, B. J. Ring, A. E. Rettie and J. R. Cashman, *In vitro methods for assessing human hepatic drug metabolism: their use in drug development.* Drug metabolism reviews, 1993. **25**(4): p. 453-484.
24. E. L. LeCluyse, *Human hepatocyte culture systems for the in vitro evaluation of cytochrome P450 expression and regulation.* European journal of pharmaceutical sciences : official journal of the European Federation for Pharmaceutical Sciences, 2001. **13**(4): p. 343-368.
25. S. Wilkening, F. Stahl and A. Bader, *Comparison of primary human hepatocytes and hepatoma cell line Hepg2 with regard to their biotransformation properties.* Drug Metab Dispos, 2003. **31**(8): p. 1035-1042.
26. N. J. Hewitt, M. J. Lechon, J. B. Houston, D. Hallifax, H. S. Brown, P. Maurel, J. G. Kenna, L. Gustavsson, C. Lohmann, C. Skonberg, A. Guillouzo, G. Tuschl, A. P. Li, E. LeCluyse, G. M. Groothuis and J. G. Hengstler, *Primary hepatocytes: current understanding of the regulation of metabolic enzymes and transporter proteins, and pharmaceutical practice for the use of hepatocytes in metabolism, enzyme induction, transporter, clearance, and hepatotoxicity studies.* Drug metabolism reviews, 2007. **39**(1): p. 159-234.
27. D. Binda, D. Lasserre-Bigot, A. Bonet, M. Thomassin, M. P. Come, C. Guinchard, R. Bars, A. Jacqueson and L. Richert, *Time course of cytochromes P450 decline during rat hepatocyte isolation and culture: effect of L-NAME.* Toxicology in Vitro, 2003. **17**(1): p. 59-67.
28. J. Beigel, K. Fella, P. J. Kramer, M. Kroeger and P. Hewitt, *Genomics and proteomics analysis of cultured primary rat hepatocytes.* Toxicology in vitro : an international journal published in association with BIBRA, 2008. **22**(1): p. 171-181.
29. J. V. Castell, R. Jover, C. P. Martinez-Jimenez and M. J. Gomez-Lechon, *Hepatocyte cell lines: their use, scope and limitations in drug metabolism studies.* Expert Opin Drug Met, 2006. **2**(2): p. 183-212.
30. W. M. A. Westerink and W. G. E. J. Schoonen, *Cytochrome P450 enzyme levels in HepG2 cells and cryopreserved primary human hepatocytes and their induction in HepG2 cells.* Toxicology in Vitro, 2007. **21**(8): p. 1581-1591.

31. A. Phillips, S. R. Hood, G. G. Gibson and N. J. Plant, *Impact of transcription factor profile and chromatin conformation on human hepatocyte CYP3A gene expression.* Drug Metab Dispos, 2005. **33**(2): p. 233-242.
32. H. H. Gerets, K. Tilmant, B. Gerin, H. Chanteux, B. O. Depelchin, S. Dhalluin and F. A. Atienzar, *Characterization of primary human hepatocytes, HepG2 cells, and HepaRG cells at the mRNA level and CYP activity in response to inducers and their predictivity for the detection of human hepatotoxins.* Cell biology and toxicology, 2012. **28**(2): p. 69-87.
33. J. Fraczek, J. Bolleyn, T. Vanhaecke, V. Rogiers and M. Vinken, *Primary hepatocyte cultures for pharmaco-toxicological studies: at the busy crossroad of various anti-dedifferentiation strategies.* Archives of toxicology, 2013. **87**(4): p. 577-610.
34. K. Bhadriraju and C. S. Chen, *Engineering cellular microenvironments to improve cell-based drug testing.* Drug discovery today, 2002. **7**(11): p. 612-620.
35. Y. Sun, C. S. Chen and J. Fu, *Forcing stem cells to behave: a biophysical perspective of the cellular microenvironment.* Annual review of biophysics, 2012. **41**: p. 519-542.
36. D. E. Discher, D. J. Mooney and P. W. Zandstra, *Growth factors, matrices, and forces combine and control stem cells.* Science, 2009. **324**(5935): p. 1673-1677.
37. B. Farrow, D. Albo and D. H. Berger, *The role of the tumor microenvironment in the progression of pancreatic cancer.* The Journal of surgical research, 2008. **149**(2): p. 319-328.
38. J. A. Joyce and J. W. Pollard, *Microenvironmental regulation of metastasis.* Nat Rev Cancer, 2009. **9**(4): p. 239-252.
39. T. D. Tlsty and L. M. Coussens, *Tumor stroma and regulation of cancer development.* Annual Review of Pathology: Mechanisms of Disease, 2006. **1**(1): p. 119-150.
40. B. Psaila and D. Lyden, *The metastatic niche: adapting the foreign soil.* Nat Rev Cancer, 2009. **9**(4): p. 285-293.
41. P. Friedl and S. Alexander, *Cancer invasion and the microenvironment: plasticity and reciprocity.* Cell, 2011. **147**(5): p. 992-1009.
42. G. J. Tortora and B. Derrickson, *Principles of anatomy & physiology*, Wiley, Hoboken, NJ, 2012.
43. J. S. Sidhu, F. Liu and C. J. Omiecinski, *Phenobarbital responsiveness as a uniquely sensitive indicator of hepatocyte differentiation status: requirement of dexamethasone and extracellular matrix in establishing the functional integrity of cultured primary rat hepatocytes.* Exp Cell Res, 2004. **292**(2): p. 252-264.
44. J. M. Pascussi, L. Drocourt, J. M. Fabre, P. Maurel and M. J. Vilarem, *Dexamethasone induces pregnane X receptor and retinoid X receptor-alpha expression in human hepatocytes: synergistic increase of CYP3A4 induction by pregnane X receptor activators.* Molecular pharmacology, 2000. **58**(2): p. 361-372.
45. E. L. LeCluyse, P. L. Bullock and A. Parkinson, *Strategies for restoration and maintenance of normal hepatic structure and function in long-term cultures of rat hepatocytes.* Adv Drug Deliver Rev, 1996. **22**(1-2): p. 133-186.
46. A. Benzeev, G. S. Robinson, N. L. R. Bucher and S. R. Farmer, *Cell Cell and Cell Matrix Interactions Differentially Regulate the Expression of Hepatic and Cytoskeletal Genes in Primary Cultures of Rat Hepatocytes.* Proceedings of the National Academy of Sciences of the United States of America, 1988. **85**(7): p. 2161-2165.

47. J. S. Sidhu, F. M. Farin and C. J. Omiecinski, *Influence of extracellular matrix overlay on phenobarbital-mediated induction of CYP2B1, 2B2, and 3A1 genes in primary adult rat hepatocyte culture.* Archives of biochemistry and biophysics, 1993. **301**(1): p. 103-113.
48. P. Lin, W. C. W. Chan, S. F. Badylak and S. N. Bhatia, *Assessing porcine liver-derived biomatrix for hepatic tissue engineering.* Tissue engineering, 2004. **10**(7-8): p. 1046-1053.
49. J. C. Dunn, R. G. Tompkins and M. L. Yarmush, *Long-term in vitro function of adult hepatocytes in a collagen sandwich configuration.* Biotechnol Prog, 1991. **7**(3): p. 237-245.
50. L. Richert, D. Binda, G. Hamilton, C. Viollon-Abadie, E. Alexandre, D. Bigot-Lasserre, R. Bars, P. Coassolo and E. LeCluyse, *Evaluation of the effect of culture configuration on morphology, survival time, antioxidant status and metabolic capacities of cultured rat hepatocytes.* Toxicology in vitro : an international journal published in association with BIBRA, 2002. **16**(1): p. 89-99.
51. P. V. Moghe, R. N. Coger, M. Toner and M. L. Yarmush, *Cell-cell interactions are essential for maintenance of hepatocyte function in collagen gel but not on matrigel.* Biotechnol Bioeng, 1997. **56**(6): p. 706-711.
52. E. Genove, S. Schmitmeier, A. Sala, S. Borros, A. Bader, L. G. Griffith and C. E. Semino, *Functionalized self-assembling peptide hydrogel enhance maintenance of hepatocyte activity in vitro.* Journal of cellular and molecular medicine, 2009. **13**(9B): p. 3387-3397.
53. A. Lazar, H. J. Mann, R. P. Remmel, R. A. Shatford, F. B. Cerra and W. S. Hu, *Extended liver-specific functions of porcine hepatocyte spheroids entrapped in collagen gel.* In vitro cellular & developmental biology. Animal, 1995. **31**(5): p. 340-346.
54. H. G. Koebe, S. Pahernik, P. Eyer and F. W. Schildberg, *Collagen Gel Immobilization - a Useful Cell-Culture Technique for Long-Term Metabolic Studies on Human Hepatocytes.* Xenobiotica, 1994. **24**(2): p. 95-107.
55. Y. Nishikawa, Y. Tokusashi, T. Kadohama, H. Nishimori and K. Ogawa, *Hepatocytic cells form bile duct-like structures within a three-dimensional collagen gel matrix.* Exp Cell Res, 1996. **223**(2): p. 357-371.
56. S. N. Bhatia, U. J. Balis, M. L. Yarmush and M. Toner, *Probing heterotypic cell interactions: hepatocyte function in microfabricated co-cultures.* Journal of biomaterials science. Polymer edition, 1998. **9**(11): p. 1137-1160.
57. F. Goulet, C. Normand and O. Morin, *Cellular interactions promote tissue-specific function, biomatrix deposition and junctional communication of primary cultured hepatocytes.* Hepatology, 1988. **8**(5): p. 1010-1018.
58. H. F. Lu, K. N. Chua, P. C. Zhang, W. S. Lim, S. Ramakrishna, K. W. Leong and H. Q. Mao, *Three-dimensional co-culture of rat hepatocyte spheroids and NIH/3T3 fibroblasts enhances hepatocyte functional maintenance.* Acta biomaterialia, 2005. **1**(4): p. 399-410.
59. S. R. Khetani and S. N. Bhatia, *Microscale culture of human liver cells for drug development.* Nature biotechnology, 2008. **26**(1): p. 120-126.
60. O. Morin and C. Normand, *Long-term maintenance of hepatocyte functional activity in co-culture: requirements for sinusoidal endothelial cells and dexamethasone.* Journal of cellular physiology, 1986. **129**(1): p. 103-110.

61. S. N. Bhatia, U. J. Balis, M. L. Yarmush and M. Toner, *Effect of cell-cell interactions in preservation of cellular phenotype: cocultivation of hepatocytes and nonparenchymal cells.* FASEB J, 1999. **13**(14): p. 1883-1900.
62. D. H. Lee, H. H. Yoon, J. H. Lee, K. W. Lee, S. K. Lee, S. K. Kim, J. E. Choi, Y. J. Kim and J. K. Park, *Enhanced liver-specific functions of endothelial cell-covered hepatocyte hetero-spheroids.* Biochem Eng J, 2004. **20**(2-3): p. 181-187.
63. S. R. Khetani, G. Szulgit, J. A. Del Rio, C. Barlow and S. N. Bhatia, *Exploring interactions between rat hepatocytes and nonparenchymal cells using gene expression profiling.* Hepatology, 2004. **40**(3): p. 545-554.
64. M. T. Donato, M. J. Gomez-Lechon and J. V. Castell, *Drug metabolizing enzymes in rat hepatocytes co-cultured with cell lines.* In vitro cellular & developmental biology : journal of the Tissue Culture Association, 1990. **26**(11): p. 1057-1062.
65. M. T. Donato, J. V. Castell and M. J. Gomez-Lechon, *Cytochrome P450 activities in pure and co-cultured rat hepatocytes. Effects of model inducers.* In vitro cellular & developmental biology. Animal, 1994. **30A**(12): p. 825-832.
66. M. K. Auth, M. Okamoto, Y. Ishida, A. Keogh, S. H. Auth, J. Gerlach, A. Encke, P. McMaster and A. J. Strain, *Maintained function of primary human hepatocytes by cellular interactions in coculture: implications for liver support systems.* Transpl Int, 1998. **11 Suppl 1**: p. S439-443.
67. J. M. Begue, C. Guguen-Guillouzo, N. Pasdeloup and A. Guillouzo, *Prolonged maintenance of active cytochrome P-450 in adult rat hepatocytes co-cultured with another liver cell type.* Hepatology, 1984. **4**(5): p. 839-842.
68. J. P. Miranda, S. B. Leite, U. Muller-Vieira, A. Rodrigues, M. J. T. Carrondo and P. M. Alves, *Towards an Extended Functional Hepatocyte In Vitro Culture.* Tissue Eng Part C-Me, 2009. **15**(2): p. 157-167.
69. C. M. Brophy, J. L. Luebke-Wheeler, B. P. Amiot, H. Khan, R. P. Remmel, P. Rinaldo and S. L. Nyberg, *Rat hepatocyte spheroids formed by rocked technique maintain differentiated hepatocyte gene expression and function.* Hepatology, 2009. **49**(2): p. 578-586.
70. F. J. Wu, J. R. Friend, C. C. Hsiao, M. J. Zilliox, W. J. Ko, F. B. Cerra and W. S. Hu, *Efficient assembly of rat hepatocyte spheroids for tissue engineering applications.* Biotechnol Bioeng, 1996. **50**(4): p. 404-415.
71. R. Glicklis, L. Shapiro, R. Agbaria, J. C. Merchuk and S. Cohen, *Hepatocyte behavior within three-dimensional porous alginate scaffolds.* Biotechnol Bioeng, 2000. **67**(3): p. 344-353.
72. J. Bierwolf, M. Lutgehetmann, S. Deichmann, J. Erbes, T. Volz, M. Dandri, S. Cohen, B. Nashan and J. M. Pollok, *Primary Human Hepatocytes from Metabolic-Disordered Children Recreate Highly Differentiated Liver-Tissue-Like Spheroids on Alginate Scaffolds.* Tissue Eng Pt A, 2012. **18**(13-14): p. 1443-1453.
73. P. M. Kaufmann, S. Heimrath, B. S. Kim and D. J. Mooney, *Highly porous polymer matrices as a three-dimensional culture system for hepatocytes.* Cell Transplantation, 1997. **6**(5): p. 463-468.
74. R. Kostadinova, F. Boess, D. Applegate, L. Suter, T. Weiser, T. Singer, B. Naughton and A. Roth, *A long-term three dimensional liver co-culture system for improved prediction of*

clinically relevant drug-induced hepatotoxicity. Toxicology and applied pharmacology, 2013. **268**(1): p. 1-16.

75. A. A. Chen, D. K. Thomas, L. L. Ong, R. E. Schwartz, T. R. Golub and S. N. Bhatia, *Humanized mice with ectopic artificial liver tissues.* Proceedings of the National Academy of Sciences of the United States of America, 2011. **108**(29): p. 11842-11847.
76. H. Tanaka, C. L. Murphy, C. Murphy, M. Kimura, S. Kawai and J. M. Polak, *Chondrogenic differentiation of murine embryonic stem cells: Effects of culture conditions and dexamethasone.* J Cell Biochem, 2004. **93**(3): p. 454-462.
77. S. Levenberg, N. F. Huang, E. Lavik, A. B. Rogers, J. Itskovitz-Eldor and R. Langer, *Differentiation of human embryonic stem cells on three-dimensional polymer scaffolds.* Proceedings of the National Academy of Sciences of the United States of America, 2003. **100**(22): p. 12741-12746.
78. W. J. Wang, K. Itaka, S. Ohba, N. Nishiyama, U. I. Chung, Y. Yamasaki and K. Kataoka, *3D spheroid culture system on micropatterned substrates for improved differentiation efficiency of multipotent mesenchymal stem cells.* Biomaterials, 2009. **30**(14): p. 2705-2715.
79. H. Liu and K. Roy, *Biomimetic three-dimensional cultures significantly increase hematopoietic differentiation efficacy of embryonic stem cells.* Tissue engineering, 2005. **11**(1-2): p. 319-330.
80. H. Baharvand, S. M. Hashemi, S. K. Ashtian and A. Farrokhi, *Differentiation of human embryonic stem cells into hepatocytes in 2D and 3D culture systems in vitro.* Int J Dev Biol, 2006. **50**(7): p. 645-652.
81. C. M. Nelson and M. J. Bissell, *Modeling dynamic reciprocity: engineering three-dimensional culture models of breast architecture, function, and neoplastic transformation.* Seminars in cancer biology, 2005. **15**(5): p. 342-352.
82. C. Fischbach, R. Chen, T. Matsumoto, T. Schmelzle, J. S. Brugge, P. J. Polverini and D. J. Mooney, *Engineering tumors with 3D scaffolds.* Nat Methods, 2007. **4**(10): p. 855-860.
83. C. Fischbach, H. J. Kong, S. X. Hsiong, M. B. Evangelista, W. Yuen and D. J. Mooney, *Cancer cell angiogenic capability is regulated by 3D culture and integrin engagement.* Proceedings of the National Academy of Sciences of the United States of America, 2009. **106**(2): p. 399-404.
84. K. L. Schmeichel and M. J. Bissell, *Modeling tissue-specific signaling and organ function in three dimensions.* J Cell Sci, 2003. **116**(12): p. 2377-2388.
85. Y. Torisawa, H. Shiku, T. Yasukawa, M. Nishizawa and T. Matsue, *Multi-channel 3-D cell culture device integrated on a silicon chip for anticancer drug sensitivity test.* Biomaterials, 2005. **26**(14): p. 2165-2172.
86. M. Faute, L. Laurent, D. Ploton, M.-F. Poupon, J.-C. Jardillier and H. l. n. Bobichon, *Distinctive alterations of invasiveness, drug resistance and cell-cell organization in 3D-cultures of MCF-7, a human breast cancer cell line, and its multidrug resistant variant.* Clinical and Experimental Metastasis, 2002. **19**(2): p. 161-167.
87. B. Desoize and J. Jardillier, *Multicellular resistance: a paradigm for clinical resistance?* Critical reviews in oncology/hematology, 2000. **36**(2-3): p. 193-207.
88. X. Xiang, Y. Phung, M. Feng, K. Nagashima, J. Zhang, V. C. Broaddus, R. Hassan, D. Fitzgerald and M. Ho, *The development and characterization of a human mesothelioma in vitro 3D model to investigate immunotoxin therapy.* PloS one, 2011. **6**(1): p. e14640.

89. P. L. Olive and R. E. Durand, *Drug and radiation resistance in spheroids: cell contact and kinetics.* Cancer Metastasis Rev, 1994. **13**(2): p. 121-138.
90. E. Cukierman, R. Pankov, D. R. Stevens and K. M. Yamada, *Taking cell-matrix adhesions to the third dimension.* Science, 2001. **294**(5547): p. 1708-1712.
91. M. A. Schwartz and M. H. Ginsberg, *Networks and crosstalk: integrin signalling spreads.* Nat Cell Biol, 2002. **4**(4): p. E65-E68.
92. F. Wang, V. M. Weaver, O. W. Petersen, C. A. Larabell, S. Dedhar, P. Briand, R. Lupu and M. J. Bissell, *Reciprocal interactions between beta1-integrin and epidermal growth factor receptor in three-dimensional basement membrane breast cultures: a different perspective in epithelial biology.* Proceedings of the National Academy of Sciences of the United States of America, 1998. **95**(25): p. 14821-14826.
93. D. J. Irvine, K. A. Hue, A. M. Mayes and L. G. Griffith, *Simulations of cell-surface integrin binding to nanoscale-clustered adhesion ligands.* Biophys J, 2002. **82**(1): p. 120-132.
94. L. G. Griffith and M. A. Swartz, *Capturing complex 3D tissue physiology in vitro.* Nat Rev Mol Cell Biol, 2006. **7**(3): p. 211-224.
95. D. E. Discher, P. Janmey and Y. L. Wang, *Tissue cells feel and respond to the stiffness of their substrate.* Science, 2005. **310**(5751): p. 1139-1143.
96. E. Cukierman, R. Pankov and K. M. Yamada, *Cell interactions with three-dimensional matrices.* Current Opinion in Cell Biology, 2002. **14**(5): p. 633-639.
97. F. Grinnell, *Fibroblast biology in three-dimensional collagen matrices.* Trends in Cell Biology, 2003. **13**(5): p. 264-269.
98. M. H. Zaman, L. M. Trapani, A. Siemeski, D. MacKellar, H. Gong, R. D. Kamm, A. Wells, D. A. Lauffenburger and P. Matsudaira, *Migration of tumor cells in 3D matrices is governed by matrix stiffness along with cell-matrix adhesion and proteolysis (vol 103, pg 10889, 2006).* Proceedings of the National Academy of Sciences of the United States of America, 2006. **103**(37): p. 13897-13897.
99. C. S. Chen, M. Mrksich, S. Huang, G. M. Whitesides and D. E. Ingber, *Geometric control of cell life and death.* Science, 1997. **276**(5317): p. 1425-1428.
100. P. Friedl and E. B. Brocker, *The biology of cell locomotion within three-dimensional extracellular matrix.* Cell Mol Life Sci, 2000. **57**(1): p. 41-64.
101. G. Hamilton, *Multicellular spheroids as an in vitro tumor model.* Cancer Letters, 1998. **131**(1): p. 29-34.
102. Y. Ling, J. Rubin, Y. Deng, C. Huang, U. Demirci, J. M. Karp and A. Khademhosseini, *A cell-laden microfluidic hydrogel.* Lab on a chip, 2007. 7(6): p. 756-762.
103. M. Yamada, R. Utoh, K. Ohashi, K. Tatsumi, M. Yamato, T. Okano and M. Seki, *Controlled formation of heterotypic hepatic micro-organoids in anisotropic hydrogel microfibers for long-term preservation of liver-specific functions.* Biomaterials, 2012. **33**(33): p. 8304-8315.
104. P. M. van Midwoud, M. T. Merema, N. Verweij, G. M. M. Groothuis and E. Verpoorte, *Hydrogel Embedding of Precision-Cut Liver Slices in a Microfluidic Device Improves Drug Metabolic Activity.* Biotechnol Bioeng, 2011. **108**(6): p. 1404-1412.
105. K. R. Stevens, M. D. Ungrin, R. E. Schwartz, B. Carvalho, K. S. Christine, R. Chaturvedi, C. Y. Li, P. W. Zandstra, C. S. Chen and S. N. Bhatia, *InVERT molding for scalable control of tissue microarchitecture.* Nature Communications, 2013.

106. H. Bruns, U. Kneser, S. Holzhuter, B. Roth, J. Kluth, P. M. Kaufmann, D. Kluth and H. C. Fiegel, *Injectable liver: A novel approach using fibrin gel as a matrix for culture and intrahepatic transplantation of hepatocytes.* Tissue engineering, 2005. **11**(11-12): p. 1718-1726.
107. G. S. Schultz and A. Wysocki, *Interactions between extracellular matrix and growth factors in wound healing.* Wound Repair Regen, 2009. **17**(2): p. 153-162.
108. M. P. Lutolf and J. A. Hubbell, *Synthetic biomaterials as instructive extracellular microenvironments for morphogenesis in tissue engineering.* Nature biotechnology, 2005. **23**(1): p. 47-55.
109. M. P. Lutolf, *Integration column: Artificial ECM: expanding the cell biology toolbox in 3D.* Integr Biol-Uk, 2009. **1**(3): p. 235-241.
110. A. S. Hoffman, *Hydrogels for biomedical applications.* Adv Drug Deliv Rev, 2002. **54**(1): p. 3-12.
111. G. Maheshwari, G. Brown, D. A. Lauffenburger, A. Wells and L. G. Griffith, *Cell adhesion and motility depend on nanoscale RGD clustering.* J Cell Sci, 2000. **113**(10): p. 1677-1686.
112. G. Mehta, C. M. Williams, L. Alvarez, M. Lesniewski, R. D. Kamm and L. G. Griffith, *Synergistic effects of tethered growth factors and adhesion ligands on DNA synthesis and function of primary hepatocytes cultured on soft synthetic hydrogels.* Biomaterials, 2010. **31**(17): p. 4657-4671.
113. V. Liu Tsang, A. A. Chen, L. M. Cho, K. D. Jadin, R. L. Sah, S. DeLong, J. L. West and S. N. Bhatia, *Fabrication of 3D hepatic tissues by additive photopatterning of cellular hydrogels.* FASEB J, 2007. **21**(3): p. 790-801.
114. G. H. Underhill, A. A. Chen, D. R. Albrecht and S. N. Bhatia, *Assessment of hepatocellular function within PEG hydrogels.* Biomaterials, 2007. **28**(2): p. 256-270.
115. L. J. Itle, W. G. Koh and M. V. Pishko, *Hepatocyte viability and protein expression within hydrogel microstructures.* Biotechnol Progr, 2005. **21**(3): p. 926-932.
116. J. A. Burdick and K. S. Anseth, *Photoencapsulation of osteoblasts in injectable RGD-modified PEG hydrogels for bone tissue engineering.* Biomaterials, 2002. **23**(22): p. 4315-4323.
117. J. A. Burdick, M. N. Mason, A. D. Hinman, K. Thorne and K. S. Anseth, *Delivery of osteoinductive growth factors from degradable PEG hydrogels influences osteoblast differentiation and mineralization.* J Control Release, 2002. **83**(1): p. 53-63.
118. S. J. Bryant, J. A. Arthur and K. S. Anseth, *Incorporation of tissue-specific molecules alters chondrocyte metabolism and gene expression in photocrosslinked hydrogels.* Acta biomaterialia, 2005. **1**(2): p. 243-252.
119. S. J. Bryant and K. S. Anseth, *Hydrogel properties influence ECM production by chondrocytes photoencapsulated in poly(ethylene glycol) hydrogels.* Journal of biomedical materials research, 2002. **59**(1): p. 63-72.
120. B. D. Fairbanks, M. P. Schwartz, C. N. Bowman and K. S. Anseth, *Photoinitiated polymerization of PEG-diacrylate with lithium phenyl-2,4,6-trimethylbenzoylphosphinate: polymerization rate and cytocompatibility.* Biomaterials, 2009. **30**(35): p. 6702-6707.
121. M. P. Lutolf, J. L. Lauer-Fields, H. G. Schmoekel, A. T. Metters, F. E. Weber, G. B. Fields and J. A. Hubbell, *Synthetic matrix metalloproteinase-sensitive hydrogels for the conduction of tissue regeneration: engineering cell-invasion characteristics.* Proceedings of the National Academy of Sciences of the United States of America, 2003. **100**(9): p. 5413-5418.

122. K. Bott, Z. Upton, K. Schrobback, M. Ehrbar, J. A. Hubbell, M. P. Lutolf and S. C. Rizzi, *The effect of matrix characteristics on fibroblast proliferation in 3D gels.* Biomaterials, 2010. **31**(32): p. 8454-8464.
123. J. J. Moon, M. S. Hahn, I. Kim, B. A. Nsiah and J. L. West, *Micropatterning of Poly(Ethylene Glycol) Diacrylate Hydrogels with Biomolecules to Regulate and Guide Endothelial Morphogenesis.* Tissue Eng Pt A, 2009. **15**(3): p. 579-585.
124. !!! INVALID CITATION !!!
125. S. B. Anderson, C. C. Lin, D. V. Kuntzler and K. S. Anseth, *The performance of human mesenchymal stem cells encapsulated in cell-degradable polymer-peptide hydrogels.* Biomaterials, 2011. **32**(14): p. 3564-3574.
126. N. S. Hwang, S. Varghese, H. Li and J. Elisseeff, *Regulation of osteogenic and chondrogenic differentiation of mesenchymal stem cells in PEG-ECM hydrogels.* Cell and tissue research, 2011. **344**(3): p. 499-509.
127. C. G. Williams, T. K. Kim, A. Taboas, A. Malik, P. Manson and J. Elisseeff, *In vitro chondrogenesis of bone marrow-derived mesenchymal stem cells in a photopolymerizing hydrogel.* Tissue engineering, 2003. **9**(4): p. 679-688.
128. C. R. Nuttelman, M. C. Tripodi and K. S. Anseth, *In vitro osteogenic differentiation of human mesenchymal stem cells photoencapsulated in PEG hydrogels.* Journal of Biomedical Materials Research Part A, 2004. **68A**(4): p. 773-782.
129. C. C. Lin, A. Raza and H. Shih, *PEG hydrogels formed by thiol-ene photo-click chemistry and their effect on the formation and recovery of insulin-secreting cell spheroids.* Biomaterials, 2011. **32**(36): p. 9685-9695.
130. A. A. Aimetti, A. J. Machen and K. S. Anseth, *Poly(ethylene glycol) hydrogels formed by thiol-ene photopolymerization for enzyme-responsive protein delivery.* Biomaterials, 2009. **30**(30): p. 6048-6054.
131. E. Jabbari, *Bioconjugation of hydrogels for tissue engineering.* Curr Opin Biotechnol, 2011.
132. C. C. Lin and K. S. Anseth, *Cell-cell communication mimicry with poly(ethylene glycol) hydrogels for enhancing beta-cell function.* Proceedings of the National Academy of Sciences of the United States of America, 2011. **108**(16): p. 6380-6385.
133. S. A. DeLong, J. J. Moon and J. L. West, *Covalently immobilized gradients of bFGF on hydrogel scaffolds for directed cell migration.* Biomaterials, 2005. **26**(16): p. 3227-3234.
134. S. A. DeLong, B. K. Mann and J. L. West, *Scaffolds modified with tethered growth factors to influence smooth muscle cell behavior.* Faseb Journal, 2002. **16**(4): p. A36-A36.
135. C. C. Lin, A. T. Metters and K. S. Anseth, *Functional PEG-peptide hydrogels to modulate local inflammation induced by the pro-inflammatory cytokine TNFalpha.* Biomaterials, 2009. **30**(28): p. 4907-4914.
136. P. S. Hume and K. S. Anseth, *Polymerizable superoxide dismutase mimetic protects cells encapsulated in poly(ethylene glycol) hydrogels from reactive oxygen species-mediated damage.* Journal of Biomedical Materials Research Part A, 2011. **99A**(1): p. 29-37.
137. F. Pampaloni, E. G. Reynaud and E. H. K. Stelzer, *The third dimension bridges the gap between cell culture and live tissue.* Nat Rev Mol Cell Bio, 2007. **8**(10): p. 839-845.

138. Y. J. Lin, C. N. Yen, Y. C. Hu, Y. C. Wu, C. J. Liao and I. M. Chu, *Chondrocytes culture in three-dimensional porous alginate scaffolds enhanced cell proliferation, matrix synthesis and gene expression.* Journal of biomedical materials research. Part A, 2009. **88**(1): p. 23-33.
139. E. Tumarkin, L. Tzadu, E. Csaszar, M. Seo, H. Zhang, A. Lee, R. Peerani, K. Purpura, P. W. Zandstra and E. Kumacheva, *High-throughput combinatorial cell co-culture using microfluidics.* Integr Biol (Camb), 2011. **3**(6): p. 653-662.
140. L. M. Weber, C. G. Lopez and K. S. Anseth, *Effects of PEG hydrogel crosslinking density on protein diffusion and encapsulated islet survival and function.* Journal of Biomedical Materials Research Part A, 2009. **90A**(3): p. 720-729.
141. L. F. Yu, M. C. W. Chen and K. C. Cheung, *Droplet-based microfluidic system for multicellular tumor spheroid formation and anticancer drug testing.* Lab on a chip, 2010. **10**(18): p. 2424-2432.
142. R. James, L. Jenkins, S. E. Ellis and K. J. L. Burg, *Histological processing of hydrogel scaffolds for tissue-engineering applications.* J Histotechnol, 2004. **27**(2): p. 133-139.
143. J. P. Fisher, A. G. Mikos, J. D. Bronzino and D. R. Peterson, *Tissue Engineering: Principles and Practices,* CRC Press, 2012.
144. W. K. Hong and American Association for Cancer Research., *Holland Frei cancer medicine 8,* People's Medical Pub. House, Shelton, Conn., 2010.
145. A. Krogh, *The number and distribution of capillaries in muscles with calculations of the oxygen pressure head necessary for supplying the tissue.* J Physiol-London, 1919. **52**(6): p. 409-415.
146. E. E. Hui and S. N. Bhatia, *Micromechanical control of cell-cell interactions.* Proceedings of the National Academy of Sciences of the United States of America, 2007. **104**(14): p. 5722-5726.
147. J. W. Nichol and A. Khademhosseini, *Modular tissue engineering: engineering biological tissues from the bottom up.* Soft Matter, 2009. **5**(7): p. 1312-1319.
148. O. F. Khan and M. V. Sefton, *Perfusion and characterization of an endothelial cell-seeded modular tissue engineered construct formed in a microfluidic remodeling chamber.* Biomaterials, 2010. **31**(32): p. 8254-8261.
149. A. A. Chen, G. H. Underhill and S. N. Bhatia, *Multiplexed, high-throughput analysis of 3D microtissue suspensions.* Integr Biol-Uk, 2010. **2**(10): p. 517-527.
150. J. P. Rolland, B. W. Maynor, L. E. Euliss, A. E. Exner, G. M. Denison and J. M. DeSimone, *Direct fabrication and harvesting of monodisperse, shape-specific nanobiomaterials.* J Am Chem Soc, 2005. **127**(28): p. 10096-10100.
151. A. Garcia, P. Mack, S. Williams, C. Fromen, T. Shen, J. Tully, J. Pillai, P. Kuehl, M. Napier, J. M. Desimone and B. W. Maynor, *Microfabricated engineered particle systems for respiratory drug delivery and other pharmaceutical applications.* Journal of drug delivery, 2012. **2012**: p. 941243.
152. J. Yeh, Y. Ling, J. M. Karp, J. Gantz, A. Chandawarkar, G. Eng, J. Blumling, 3rd, R. Langer and A. Khademhosseini, *Micromolding of shape-controlled, harvestable cell-laden hydrogels.* Biomaterials, 2006. **27**(31): p. 5391-5398.
153. D. R. Albrecht, V. L. Tsang, R. L. Sah and S. N. Bhatia, *Photo- and electropatterning of hydrogel-encapsulated living cell arrays.* Lab on a chip, 2005. **5**(1): p. 111-118.

154. B. Zamanian, M. Masaeli, J. W. Nichol, M. Khabiry, M. J. Hancock, H. Bae and A. Khademhosseini, *Interface-directed self-assembly of cell-laden microgels.* Small, 2010. **6**(8): p. 937-944.
155. D. Dendukuri, S. S. Gu, D. C. Pregibon, T. A. Hatton and P. S. Doyle, *Stop-flow lithography in a microfluidic device.* Lab on a chip, 2007. **7**(7): p. 818-828.
156. P. Panda, S. Ali, E. Lo, B. G. Chung, T. A. Hatton, A. Khademhosseini and P. S. Doyle, *Stop-flow lithography to generate cell-laden microgel particles.* Lab on a chip, 2008. **8**(7): p. 1056-1061.
157. C. L. Franco, J. Price and J. L. West, *Development and optimization of a dual-photoinitiator, emulsion-based technique for rapid generation of cell-laden hydrogel microspheres.* Acta biomaterialia, 2011. **7**(9): p. 3267-3276.
158. N. R. Beer, B. J. Hindson, E. K. Wheeler, S. B. Hall, K. A. Rose, I. M. Kennedy and B. W. Colston, *On-chip, real-time, single-copy polymerase chain reaction in picoliter droplets.* Anal Chem, 2007. **79**(22): p. 8471-8475.
159. W. Shi, J. Qin, N. Ye and B. Lin, *Droplet-based microfluidic system for individual Caenorhabditis elegans assay.* Lab on a chip, 2008. **8**(9): p. 1432-1435.
160. D. K. Hwang, D. Dendukuri and P. S. Doyle, *Microfluidic-based synthesis of non-spherical magnetic hydrogel microparticles.* Lab on a chip, 2008. **8**(10): p. 1640-1647.
161. D. Dendukuri and P. S. Doyle, *The Synthesis and Assembly of Polymeric Microparticles Using Microfluidics.* Adv Mater, 2009. **21**(41): p. 4071-4086.
162. K. Liu, H. J. Ding, J. Liu, Y. Chen and X. Z. Zhao, *Shape-controlled production of biodegradable calcium alginate gel microparticles using a novel microfluidic device.* Langmuir : the ACS journal of surfaces and colloids, 2006. **22**(22): p. 9453-9457.
163. J. J. Agresti, E. Antipov, A. R. Abate, K. Ahn, A. C. Rowat, J. C. Baret, M. Marquez, A. M. Klibanov, A. D. Griffiths and D. A. Weitz, *Ultrahigh-throughput screening in drop-based microfluidics for directed evolution.* Proceedings of the National Academy of Sciences of the United States of America, 2010. **107**(9): p. 4004-4009.
164. A. C. Hatch, J. S. Fisher, A. R. Tovar, A. T. Hsieh, R. Lin, S. L. Pentoney, D. L. Yang and A. P. Lee, *1-Million droplet array with wide-field fluorescence imaging for digital PCR.* Lab on a chip, 2011. **11**(22): p. 3838-3845.
165. C. Holtze, A. C. Rowat, J. J. Agresti, J. B. Hutchison, F. E. Angile, C. H. Schmitz, S. Koster, H. Duan, K. J. Humphry, R. A. Scanga, J. S. Johnson, D. Pisignano and D. A. Weitz, *Biocompatible surfactants for water-in-fluorocarbon emulsions.* Lab on a chip, 2008. **8**(10): p. 1632-1639.
166. J. Clausell-Tormos, D. Lieber, J. C. Baret, A. El-Harrak, O. J. Miller, L. Frenz, J. Blouwolff, K. J. Humphry, S. Koster, H. Duan, C. Holtze, D. A. Weitz, A. D. Griffiths and C. A. Merten, *Droplet-based microfluidic platforms for the encapsulation and screening of Mammalian cells and multicellular organisms.* Chemistry & biology, 2008. **15**(5): p. 427-437.
167. D. Dendukuri, K. Tsoi, T. A. Hatton and P. S. Doyle, *Controlled synthesis of nonspherical microparticles using microfluidics.* Langmuir : the ACS journal of surfaces and colloids, 2005. **21**(6): p. 2113-2116.
168. S. Q. Xu, Z. H. Nie, M. Seo, P. Lewis, E. Kumacheva, H. A. Stone, P. Garstecki, D. B. Weibel, I. Gitlin and G. M. Whitesides, *Generation of monodisperse particles by using*

microfluidics: Control over size, shape, and composition. Angew Chem Int Edit, 2005. **44**(5): p. 724-728.

169. Z. H. Nie, S. Q. Xu, M. Seo, P. C. Lewis and E. Kumacheva, *Polymer particles with various shapes and morphologies produced in continuous microfluidic reactors.* Journal of the American Chemical Society, 2005. **127**(22): p. 8058-8063.
170. S. Sugiura, T. Oda, Y. Aoyagi, R. Matsuo, T. Enomoto, K. Matsumoto, T. Nakamura, M. Satake, A. Ochiai, N. Ohkohchi and M. Nakajima, *Microfabricated airflow nozzle for microencapsulation of living cells into 150 micrometer microcapsules.* Biomedical microdevices, 2007. **9**(1): p. 91-99.
171. W. H. Tan and S. Takeuchi, *Monodisperse alginate hydrogel microbeads for cell encapsulation.* Adv Mater, 2007. **19**(18): p. 2696-+.
172. F. Yanagawa, H. Kaji, Y. H. Jang, H. Bae, D. Yanan, J. Fukuda, H. Qi and A. Khademhosseini, *Directed assembly of cell-laden microgels for building porous three-dimensional tissue constructs.* Journal of biomedical materials research. Part A, 2011.
173. A. P. McGuigan, B. Leung and M. V. Sefton, *Fabrication of cells containing gel modules to assemble modular tissue-engineered constructs.* Nat Protoc, 2006. **1**(6): p. 2963-2969.
174. J. Hong, A. J. deMello and S. N. Jayasinghe, *Bio-electrospraying and droplet-based microfluidics: control of cell numbers within living residues.* Biomed Mater, 2010. **5**(2).
175. S. Stolberg and K. E. McCloskey, *Can Shear Stress Direct Stem Cell Fate?* Biotechnol Progr, 2009. **25**(1): p. 10-19.
176. N. E. Fedorovich, M. H. Oudshoorn, D. van Geemen, W. E. Hennink, J. Alblas and W. J. Dhert, *The effect of photopolymerization on stem cells embedded in hydrogels.* Biomaterials, 2009. **30**(3): p. 344-353.
177. W. K. Kaufmann and R. S. Paules, *DNA damage and cell cycle checkpoints.* FASEB J, 1996. **10**(2): p. 238-247.
178. C. G. Williams, A. N. Malik, T. K. Kim, P. N. Manson and J. H. Elisseeff, *Variable cytocompatibility of six cell lines with photoinitiators used for polymerizing hydrogels and cell encapsulation.* Biomaterials, 2005. **26**(11): p. 1211-1218.
179. S. K. Hamilton, H. Lu and J. S. Temenoff, *Micropatterned Hydrogels for Stem Cell Culture.* Stud Mechanobiol Tis, 2010. **2**: p. 119-152.
180. A. Khademhosseini, R. Langer, J. Borenstein and J. P. Vacanti, *Microscale technologies for tissue engineering and biology.* Proceedings of the National Academy of Sciences of the United States of America, 2006. **103**(8): p. 2480-2487.
181. J. Jung, M. Zheng, M. Goldfarb and K. S. Zaret, *Initiation of mammalian liver development from endoderm by fibroblast growth factors.* Science, 1999. **284**(5422): p. 1998-2003.
182. O. Cleaver and D. A. Melton, *Endothelial signaling during development.* Nat Med, 2003. **9**(6): p. 661-668.
183. S. J. Morrison and A. C. Spradling, *Stem cells and niches: Mechanisms that promote stem cell maintenance throughout life.* Cell, 2008. **132**(4): p. 598-611.
184. N. A. Bhowmick, E. G. Neilson and H. L. Moses, *Stromal fibroblasts in cancer initiation and progression.* Nature, 2004. **432**(7015): p. 332-337.
185. S. L. Friedman, *Molecular regulation of hepatic fibrosis, an integrated cellular response to tissue injury.* J Biol Chem, 2000. **275**(4): p. 2247-2250.

186. D. Hanahan and R. A. Weinberg, *Hallmarks of Cancer: The Next Generation.* Cell, 2011. **144**(5): p. 646-674.
187. S. March, E. E. Hui, G. H. Underhill, S. Khetani and S. N. Bhatia, *Microenvironmental regulation of the sinusoidal endothelial cell phenotype in vitro.* Hepatology, 2009. **50**(3): p. 920-928.
188. D. Huh, B. D. Matthews, A. Mammoto, M. Montoya-Zavala, H. Y. Hsin and D. E. Ingber, *Reconstituting organ-level lung functions on a chip.* Science, 2010. **328**(5986): p. 1662-1668.
189. M. A. LaBarge, C. M. Nelson, R. Villadsen, A. Fridriksdottir, J. R. Ruth, M. R. Stampfer, O. W. Petersen and M. J. Bissell, *Human mammary progenitor cell fate decisions are products of interactions with combinatorial microenvironments.* Integr Biol-Uk, 2009. **1**(1): p. 70-79.
190. K. R. Stevens, K. L. Kreutziger, S. K. Dupras, F. S. Korte, M. Regnier, V. Muskheli, M. B. Nourse, K. Bendixen, H. Reinecke and C. E. Murry, *Physiological function and transplantation of scaffold-free and vascularized human cardiac muscle tissue.* Proceedings of the National Academy of Sciences of the United States of America, 2009. **106**(39): p. 16568-16573.
191. D. R. Albrecht, G. H. Underhill, T. B. Wassermann, R. L. Sah and S. N. Bhatia, *Probing the role of multicellular organization in three-dimensional microenvironments.* Nat Methods, 2006. **3**(5): p. 369-375.
192. V. Chan, P. Zorlutuna, J. H. Jeong, H. Kong and R. Bashir, *Three-dimensional photopatterning of hydrogels using stereolithography for long-term cell encapsulation.* Lab on a chip, 2010. **10**(16): p. 2062-2070.
193. W. Tan and T. A. Desai, *Layer-by-layer microfluidics for biomimetic three-dimensional structures.* Biomaterials, 2004. **25**(7-8): p. 1355-1364.
194. A. P. McGuigan and M. V. Sefton, *Vascularized organoid engineered by modular assembly enables blood perfusion.* Proceedings of the National Academy of Sciences of the United States of America, 2006. **103**(31): p. 11461-11466.
195. Z. J. Gartner and C. R. Bertozzi, *Programmed assembly of 3-dimensional microtissues with defined cellular connectivity.* Proceedings of the National Academy of Sciences of the United States of America, 2009. **106**(12): p. 4606-4610.
196. Y. Du, E. Lo, S. Ali and A. Khademhosseini, *Directed assembly of cell-laden microgels for fabrication of 3D tissue constructs.* Proceedings of the National Academy of Sciences of the United States of America, 2008. **105**(28): p. 9522-9527.
197. B. Guillotin and F. Guillemot, *Cell patterning technologies for organotypic tissue fabrication.* Trends Biotechnol, 2011.
198. G. M. Whitesides and B. Grzybowski, *Self-assembly at all scales.* Science, 2002. **295**(5564): p. 2418-2421.
199. D. A. Bruzewicz, A. P. McGuigan and G. M. Whitesides, *Fabrication of a modular tissue construct in a microfluidic chip.* Lab on a chip, 2008. **8**(5): p. 663-671.
200. Y. Du, M. Ghodousi, E. Lo, M. K. Vidula, O. Emiroglu and A. Khademhosseini, *Surface-directed assembly of cell-laden microgels.* Biotechnol Bioeng, 2009.
201. A. Khademhosseini and R. Langer, *Microengineered hydrogels for tissue engineering.* Biomaterials, 2007. **28**(34): p. 5087-5092.

202. S. Y. Teh, R. Lin, L. H. Hung and A. P. Lee, *Droplet microfluidics.* Lab on a chip, 2008. **8**(2): p. 198-220.
203. A. Liau, R. Karnik, A. Majumdar and J. H. Cate, *Mixing crowded biological solutions in milliseconds.* Anal Chem, 2005. **77**(23): p. 7618-7625.
204. G. M. Cruise, D. S. Scharp and J. A. Hubbell, *Characterization of permeability and network structure of interfacially photopolymerized poly(ethylene glycol) diacrylate hydrogels.* Biomaterials, 1998. **19**(14): p. 1287-1294.
205. R. Novak, Y. Zeng, J. Shuga, G. Venugopalan, D. A. Fletcher, M. T. Smith and R. A. Mathies, *Single-Cell Multiplex Gene Detection and Sequencing with Microfluidically Generated Agarose Emulsions.* Angew Chem Int Edit, 2011. **50**(2): p. 390-395.
206. D. J. Quick and K. S. Anseth, *DNA delivery from photocrosslinked PEG hydrogels: encapsulation efficiency, release profiles, and DNA quality.* J Control Release, 2004. **96**(2): p. 341-351.
207. D. C. Pregibon, M. Toner and P. S. Doyle, *Multifunctional encoded particles for high-throughput biomolecule analysis.* Science, 2007. **315**(5817): p. 1393-1396.
208. G. T. Hermanson, *Bioconjugate techniques*, Academic Press, San Diego, 1996.
209. Z. J. Gartner and D. R. Liu, *The generality of DNA-templated synthesis as a basis for evolving non-natural small molecules.* J Am Chem Soc, 2001. **123**(28): p. 6961-6963.
210. C. A. Mirkin, R. L. Letsinger, R. C. Mucic and J. J. Storhoff, *A DNA-based method for rationally assembling nanoparticles into macroscopic materials.* Nature, 1996. **382**(6592): p. 607-609.
211. G. A. Kwong, C. G. Radu, K. Hwang, C. J. Shu, C. Ma, R. C. Koya, B. Comin-Anduix, S. R. Hadrup, R. C. Bailey, O. N. Witte, T. N. Schumacher, A. Ribas and J. R. Heath, *Modular nucleic acid assembled p/MHC microarrays for multiplexed sorting of antigen-specific T cells.* J Am Chem Soc, 2009. **131**(28): p. 9695-9703.
212. E. S. Douglas, R. A. Chandra, C. R. Bertozzi, R. A. Mathies and M. B. Francis, *Self-assembled cellular microarrays patterned using DNA barcodes.* Lab on a chip, 2007. **7**(11): p. 1442-1448.
213. M. P. Valignat, O. Theodoly, J. C. Crocker, W. B. Russel and P. M. Chaikin, *Reversible self-assembly and directed assembly of DNA-linked micrometer-sized colloids.* Proceedings of the National Academy of Sciences of the United States of America, 2005. **102**(12): p. 4225-4229.
214. D. Nykypanchuk, M. M. Maye, D. van der Lelie and O. Gang, *DNA-guided crystallization of colloidal nanoparticles.* Nature, 2008. **451**(7178): p. 549-552.
215. G. M. Whitesides and M. Boncheva, *Beyond molecules: self-assembly of mesoscopic and macroscopic components.* Proceedings of the National Academy of Sciences of the United States of America, 2002. **99**(8): p. 4769-4774.
216. D. Dendukuri, P. Panda, R. Haghgooie, J. M. Kim, T. A. Hatton and P. S. Doyle, *Modeling of Oxygen-Inhibited Free Radical Photopolymerization in a PDMS Microfluidic Device.* Macromolecules, 2008. **41**(22): p. 8547-8556.
217. R. C. Fry, J. P. Svensson, C. Valiathan, E. Wang, B. J. Hogan, S. Bhattacharya, J. M. Bugni, C. A. Whittaker and L. D. Samson, *Genomic predictors of interindividual differences in response to DNA damaging agents.* Gene Dev, 2008. **22**(19): p. 2621-2626.

218. S. J. Bryant, C. R. Nuttelman and K. S. Anseth, *Cytocompatibility of UV and visible light photoinitiating systems on cultured NIH/3T3 fibroblasts in vitro.* J Biomat Sci-Polym E, 2000. **11**(5): p. 439-457.
219. R. Straussman, T. Morikawa, K. Shee, M. Barzily-Rokni, Z. R. Qian, J. Y. Du, A. Davis, M. M. Mongare, J. Gould, D. T. Frederick, Z. A. Cooper, P. B. Chapman, D. B. Solit, A. Ribas, R. S. Lo, K. T. Flaherty, S. Ogino, J. A. Wargo and T. R. Golub, *Tumour micro-environment elicits innate resistance to RAF inhibitors through HGF secretion.* Nature, 2012. **487**(7408): p. 500-U118.
220. R.-Z. Lin and H.-Y. Chang, *Recent advances in three-dimensional multicellular spheroid culture for biomedical research.* Biotechnology Journal, 2008. **3**(9-10): p. 1172-1184.
221. K. B. Hotary, E. D. Allen, P. C. Brooks, N. S. Datta, M. W. Long and S. J. Weiss, *Membrane type I matrix metalloproteinase usurps tumor growth control imposed by the three-dimensional extracellular matrix.* Cell, 2003. **114**(1): p. 33-45.
222. E. Rosines, R. V. Sampogna, K. Johkura, D. A. Vaughn, Y. Choi, H. Sakurai, M. M. Shah and S. K. Nigam, *Staged in vitro reconstitution and implantation of engineered rat kidney tissue.* Proceedings of the National Academy of Sciences of the United States of America, 2007. **104**(52): p. 20938-20943.
223. C. D. Roskelley, P. Y. Desprez and M. J. Bissell, *Extracellular matrix-dependent tissue-specific gene expression in mammary epithelial cells requires both physical and biochemical signal transduction.* Proceedings of the National Academy of Sciences of the United States of America, 1994. **91**(26): p. 12378-12382.
224. V. L. Tsang and S. N. Bhatia, *Three-dimensional tissue fabrication.* Adv Drug Deliv Rev, 2004. **56**(11): p. 1635-1647.
225. C. Y. Li, D. K. Wood, C. M. Hsu and S. N. Bhatia, *DNA-templated assembly of droplet-derived PEG microtissues.* Lab on a chip, 2011. **11**(17): p. 2967-2975.
226. V. Trivedi, E. S. Ereifej, A. Doshi, P. Sehgal, P. J. VandeVord and A. S. Basu, *Microfluidic encapsulation of cells in alginate capsules for high throughput screening.* Proc. Annual Int. Conf. of the IEEE Engineering in Medicine and Biology Society EMBC 2009, 2009: p. 7037-7040.
227. S. Hong, H. J. Hsu, R. Kaunas and J. Kameoka, *Collagen microsphere production on a chip.* Lab on a chip, 2012. **12**(18): p. 3277-3280.
228. C. K. Choi, M. T. Breckenridge and C. S. Chen, *Engineered materials and the cellular microenvironment: a strengthening interface between cell biology and bioengineering.* Trends Cell Biol, 2010. **20**(12): p. 705-714.
229. C. Y. Cheung, S. J. McCartney and K. S. Anseth, *Synthesis of Polymerizable Superoxide Dismutase Mimetics to Reduce Reactive Oxygen Species Damage in Transplanted Biomedical Devices.* Advanced Functional Materials, 2008. **18**(20): p. 3119-3126.
230. J. F. Edd, Di Carlo, Dino, K. J. Humphry, S. Köster, D. Irimia, D. A. Weitz and M. Toner, *Controlled encapsulation of single-cells into monodisperse picolitre drops.* Lab on a chip, 2008. **8**(8): p. 1262-1264.
231. A. R. Abate, C.-H. Chen, J. J. Agresti and D. A. Weitz, *Beating Poisson encapsulation statistics using close-packed ordering.* Lab on a chip, 2009. **9**(18): p. 2628-2631.

232. N. E. Reticker-Flynn, D. F. Malta, M. M. Winslow, J. M. Lamar, M. J. Xu, G. H. Underhill, R. O. Hynes, T. E. Jacks and S. N. Bhatia, *A combinatorial extracellular matrix platform identifies cell-extracellular matrix interactions that correlate with metastasis.* Nat Commun, 2012. **3**: p. 1122.
233. S. Valastyan and R. A. Weinberg, *Tumor metastasis: molecular insights and evolving paradigms.* Cell, 2011. **147**(2): p. 275-292.
234. R. A. Weinberg, *The Biology of Cancer*, Garland Science, 2007.
235. J. Condeelis and J. W. Pollard, *Macrophages: obligate partners for tumor cell migration, invasion, and metastasis.* Cell, 2006. **124**(2): p. 263-266.
236. G. M. Cruise, O. D. Hegre, F. V. Lamberti, S. R. Hager, R. Hill, D. S. Scharp and J. A. Hubbell, *In vitro and in vivo performance of porcine islets encapsulated in interfacially photopolymerized poly(ethylene glycol) diacrylate membranes.* Cell Transplant, 1999. **8**(3): p. 293-306.
237. A. A. Chen, S. R. Khetani, S. Lee, S. N. Bhatia and Van Vliet, Krystyn J., *Modulation of hepatocyte phenotype in vitro via chemomechanical tuning of polyelectrolyte multilayers.* Biomaterials, 2009. **30**(6): p. 1113-1120.
238. D. Padua and J. Massagué, *Roles of TGFbeta in metastasis.* Cell Res, 2009. **19**(1): p. 89-102.
239. G. Anumanthan, S. K. Halder, H. Osada, T. Takahashi, P. P. Massion, D. P. Carbone and P. K. Datta, *Restoration of TGF-beta signalling reduces tumorigenicity in human lung cancer cells.* Br J Cancer, 2005. **93**(10): p. 1157-1167.
240. J. E. Meredith, S. Winitz, J. M. Lewis, S. Hess, X. D. Ren, M. W. Renshaw and M. A. Schwartz, *The regulation of growth and intracellular signaling by integrins.* Endocr Rev, 1996. **17**(3): p. 207-220.
241. P. M. Comoglio, C. Boccaccio and L. Trusolino, *Interactions between growth factor receptors and adhesion molecules: breaking the rules.* Curr Opin Cell Biol, 2003. **15**(5): p. 565-571.
242. S. K. Akiyama, K. Olden and K. M. Yamada, *Fibronectin and integrins in invasion and metastasis.* Cancer Metastasis Rev, 1995. **14**(3): p. 173-189.
243. J. Y. Han, H. S. Kim, S. H. Lee, W. S. Park, J. Y. Lee and N. J. Yoo, *Immunohistochemical expression of integrins and extracellular matrix proteins in non-small cell lung cancer: correlation with lymph node metastasis.* Lung Cancer, 2003. **41**.
244. Y. Shintani, M. Maeda, N. Chaika, K. R. Johnson and M. J. Wheelock, *Collagen I promotes epithelial-to-mesenchymal transition in lung cancer cells via transforming growth factor-beta signaling.* Am J Respir Cell Mol Biol, 2008. **38**(1): p. 95-104.
245. E. Lilly, A study combining LY2157299 with temozolomide-based radiochemotherapy in patients with newly diagnosed malignant glioma, http://clinicaltrials.gov/ct2/show/NCT01220271, 2012.
246. E. Calvo-Aller, J. Baselga, S. Glatt, A. Cleverly, M. Lahn, C. L. Arteaga, M. L. Rothenberg and M. A. Carducci, *First human dose escalation study in patients with metastatic malignancies to determine safety and pharmacokinetics of LY2157299, a small molecule inhibitor of the transforming growth factor-beta receptor I kinase.* Journal of Clinical Oncology, 2008. **26**(15S): p. 14554.
247. E. Lilly, A study of LY2157299 in Patients with Hepatocellular Carcinoma, http://clinicaltrials.gove/ct2/show/NCT01246986, 2012.

248. SelleckChem, LY2157299 Biological Activity, http://www.selleckchem.com/products/ly2157299, 2012.
249. B. Bierie and H. L. Moses, *Tumour microenvironment: TGFbeta: the molecular Jekyll and Hyde of cancer.* Nat Rev Cancer, 2006. **6**(7): p. 506-520.
250. R. H. Chen, R. Ebner and R. Derynck, *Inactivation of the type II receptor reveals two receptor pathways for the diverse TGF-beta activities.* Science, 1993. **260**(5112): p. 1335-1338.
251. R. Derynck and X. H. Feng, *TGF-beta receptor signaling.* Biochim Biophys Acta, 1997. **1333**(2): p. F105-F150.
252. M. Centrella, S. Casinghino, J. Kim, T. Pham, V. Rosen, J. Wozney and T. L. McCarthy, *Independent changes in type I and type II receptors for transforming growth factor beta induced by bone morphogenetic protein 2 parallel expression of the osteoblast phenotype.* Mol Cell Biol, 1995. **15**(6): p. 3273-3281.
253. J. M. Yingling, K. L. Blanchard and J. S. Sawyer, *Development of TGF-beta signalling inhibitors for cancer therapy.* Nat Rev Drug Discov, 2004. **3**(12): p. 1011-1022.
254. R. Lang, M. M. Stern, L. Smith, Y. Liu, S. Bharadwaj, G. Liu, P. M. Baptista, C. R. Bergman, S. Soker, J. J. Yoo, A. Atala and Y. Zhang, *Three-dimensional culture of hepatocytes on porcine liver tissue-derived extracellular matrix.* Biomaterials, 2011. **32**(29): p. 7042-7052.
255. R. M. Tostoes, S. B. Leite, M. Serra, J. Jensen, P. Bjorquist, M. J. T. Carrondo, C. Brito and P. M. Alves, *Human liver cell spheroids in extended perfusion bioreactor culture for repeated-dose drug testing.* Hepatology, 2012. **55**(4): p. 1227-1236.
256. J. Z. Tong, O. Bernard and F. Alvarez, *Long-Term Culture of Rat-Liver Cell Spheroids in Hormonally Defined Media.* Exp Cell Res, 1990. **189**(1): p. 87-92.
257. J. Z. Tong, P. Delagausie, V. Furlan, T. Cresteil, O. Bernard and F. Alvarez, *Long-Term Culture of Adult-Rat Hepatocyte Spheroids.* Exp Cell Res, 1992. **200**(2): p. 326-332.
258. G. Hamilton, C. Westmoreland and E. George, *Effects of medium composition on the morphology and function of rat hepatocytes cultured as spheroids and monolayers.* In Vitro Cell Dev-An, 2001. **37**(10): p. 656-667.
259. M. Dvir-Ginzberg, T. Elkayam, E. D. Aflalo, R. Agbaria and S. Cohen, *Ultrastructural and functional investigations of adult hepatocyte spheroids during in vitro cultivation.* Tissue engineering, 2004. **10**(11-12): p. 1806-1817.
260. R. Glicklis, J. C. Merchuk and S. Cohen, *Modeling mass transfer in hepatocyte spheroids via cell viability, spheroid size, and hepatocellular functions.* Biotechnol Bioeng, 2004. **86**(6): p. 672-680.
261. S. Surapaneni, T. Pryor, M. D. Klein and H. W. T. Matthew, *Rapid hepatocyte spheroid formation: Optimization and long term function in perfused microcapsules.* Asaio J, 1997. **43**(5): p. M848-M853.
262. R. M. Tostoes, S. B. Leite, J. P. Miranda, M. Sousa, D. I. Wang, M. J. Carrondo and P. M. Alves, *Perfusion of 3D encapsulated hepatocytes--a synergistic effect enhancing long-term functionality in bioreactors.* Biotechnol Bioeng, 2011. **108**(1): p. 41-49.
263. E. Curcio, S. Salerno, G. Barbieri, L. De Bartolo, E. Drioli and A. Bader, *Mass transfer and metabolic reactions in hepatocyte spheroids cultured in rotating wall gas-permeable membrane system.* Biomaterials, 2007. **28**(36): p. 5487-5497.

264. C. Y. Li, D. K. Wood, J. H. Huang and S. N. Bhatia, *Flow-based pipeline for systematic modulation and analysis of 3D tumor microenvironments.* Lab on a chip, 2013: p. DOI: 10.1039/C1033LC41300D
265. P. O. Seglen, *Preparation of isolated rat liver cells.* Methods in cell biology, 1976. **13**: p. 29-83.
266. J. E. Leslie-Barbick, J. J. Moon and J. L. West, *Covalently-immobilized vascular endothelial growth factor promotes endothelial cell tubulogenesis in poly(ethylene glycol) diacrylate hydrogels.* Journal of biomaterials science. Polymer edition, 2009. **20**(12): p. 1763-1779.
267. G. Lemaire, C. Delescluse, M. Pralavorio, N. Ledirac, P. Lesca and R. Rahmani, *The role of protein tyrosine kinases in CYP1A1 induction by omeprazole and thiabendazole in rat hepatocytes.* Life sciences, 2004. **74**(18): p. 2265-2278.
268. Y. P. Chen, S. S. Ferguson, M. Negishi and J. A. Goldstein, *Induction of human CYP2C9 by rifampicin, hyperforin, and phenobarbital is mediated by the pregnane X receptor.* J Pharmacol Exp Ther, 2004. **308**(2): p. 495-501.
269. C. J. Patten, P. E. Thomas, R. L. Guy, M. Lee, F. J. Gonzalez, F. P. Guengerich and C. S. Yang, *Cytochrome P450 enzymes involved in acetaminophen activation by rat and human liver microsomes and their kinetics.* Chemical research in toxicology, 1993. **6**(4): p. 511-518.
270. M. Schutte, B. Fox, M. O. Baradez, A. Devonshire, J. Minguez, M. Bokhari, S. Przyborski and D. Marshall, *Rat Primary Hepatocytes Show Enhanced Performance and Sensitivity to Acetaminophen During Three-Dimensional Culture on a Polystyrene Scaffold Designed for Routine Use.* Assay Drug Dev Techn, 2011. **9**(5): p. 475-486.
271. L. P. James, P. R. Mayeux and J. A. Hinson, *Acetaminophen-induced hepatotoxicity.* Drug Metab Dispos, 2003. **31**(12): p. 1499-1506.
272. K. Domansky, W. Inman, J. Serdy, A. Dash, M. H. M. Lim and L. G. Griffith, *Perfused multiwell plate for 3D liver tissue engineering.* Lab on a chip, 2010. **10**(1): p. 51-58.
273. Y. Sakai, K. Naruse, I. Nagashima, T. Muto and M. Suzuki, *Large-scale preparation and function of porcine hepatocyte spheroids.* The International journal of artificial organs, 1996. **19**(5): p. 294-301.
274. J. Landry, D. Bernier, C. Ouellet, R. Goyette and N. Marceau, *Spheroidal aggregate culture of rat liver cells: histotypic reorganization, biomatrix deposition, and maintenance of functional activities.* The Journal of cell biology, 1985. **101**(3): p. 914-923.
275. M. Drewitz, M. Helbling, N. Fried, M. Bieri, W. Moritz, J. Lichtenberg and J. M. Kelm, *Towards automated production and drug sensitivity testing using scaffold-free spherical tumor microtissues.* Biotechnology Journal, 2011. **6**(12): p. 1488-1496.
276. M. D. Ungrin, C. Joshi, A. Nica, C. Bauwens and P. W. Zandstra, *Reproducible, ultra high-throughput formation of multicellular organization from single cell suspension-derived human embryonic stem cell aggregates.* PloS one, 2008. **3**(2): p. e1565.
277. A. Ichihara, *Mechanisms Controlling Growth of Hepatocytes in Primary Culture.* Digest Dis Sci, 1991. **36**(4): p. 489-493.
278. G. G. M. Pinkse, R. Jiawan-Lalai, J. A. Bruijn and E. de Heer, *RGD peptides confer survival to hepatocytes via the beta 1-integrin-ILK-pAkt pathway.* J Hepatol, 2005. **42**(1): p. 87-93.

279. G. G. M. Pinkse, M. P. Voorhoeve, M. Noteborn, O. T. Terpstra, J. A. Bruijn and E. de Heer, *Hepatocyte survival depends on beta 1-integrin-mediated attachment of hepatocytes to hepatic extracellular matrix.* Liver Int, 2004. **24**(3): p. 218-226.
280. J. P. Miranda, A. Rodrigues, R. M. Tostoes, S. Leite, H. Zimmerman, M. J. Carrondo and P. M. Alves, *Extending hepatocyte functionality for drug-testing applications using high-viscosity alginate-encapsulated three-dimensional cultures in bioreactors.* Tissue engineering. Part C, Methods, 2010. **16**(6): p. 1223-1232.
281. A. W. Tilles, F. Berthiaume, M. L. Yarmush, R. G. Tompkins and M. Toner, *Bioengineering of liver assist devices.* Journal of hepato-biliary-pancreatic surgery, 2002. **9**(6): p. 686-696.
282. E. Torok, J. M. Pollok, P. X. Ma, P. M. Kaufmann, M. Dandri, J. Petersen, M. R. Burda, D. Kluth, F. Perner and X. Rogiers, *Optimization of hepatocyte spheroid formation for hepatic tissue engineering on three-dimensional biodegradable polymer within a flow bioreactor prior to implantation.* Cells, tissues, organs, 2001. **169**(1): p. 34-41.
283. J. J. Xu, P. V. Henstock, M. C. Dunn, A. R. Smith, J. R. Chabot and D. de Graaf, *Cellular imaging predictions of clinical drug-induced liver injury.* Toxicological sciences : an official journal of the Society of Toxicology, 2008. **105**(1): p. 97-105.
284. N. Katsura, I. Ikai, T. Mitaka, T. Shiotani, S. Yamanokuchi, S. Sugimoto, A. Kanazawa, H. Terajima, Y. Mochizuki and Y. Yamaoka, *Long-term culture of primary human hepatocytes with preservation of proliferative capacity and differentiated functions.* The Journal of surgical research, 2002. **106**(1): p. 115-123.
285. S. B. Leite, A. P. Teixeira, J. P. Miranda, R. M. Tostoes, J. J. Clemente, M. F. Sousa, M. J. Carrondo and P. M. Alves, *Merging bioreactor technology with 3D hepatocyte-fibroblast culturing approaches: Improved in vitro models for toxicological applications.* Toxicology in vitro : an international journal published in association with BIBRA, 2011. **25**(4): p. 825-832.
286. A. Kern, A. Bader, R. Pichlmayr and K. F. Sewing, *Drug metabolism in hepatocyte sandwich cultures of rats and humans.* Biochemical pharmacology, 1997. **54**(7): p. 761-772.
287. J. Z. Tong, S. Sarrazin, D. Cassio, F. Gauthier and F. Alvarez, *Application of Spheroid Culture to Human Hepatocytes and Maintenance of Their Differentiation.* Biol Cell, 1994. **81**(1): p. 77-81.
288. E. Eschbach, S. S. Chatterjee, M. Noldner, E. Gottwald, H. Dertinger, K. F. Weibezahn and G. Knedlitschek, *Microstructured scaffolds for liver tissue cultures of high cell density: Morphological and biochemical characterization of tissue aggregates.* J Cell Biochem, 2005. **95**(2): p. 243-255.
289. V. N. Goral and P. K. Yuen, *Microfluidic platforms for hepatocyte cell culture: new technologies and applications.* Annals of biomedical engineering, 2012. **40**(6): p. 1244-1254.
290. M. J. Powers, D. M. Janigian, K. E. Wack, C. S. Baker, D. Beer Stolz and L. G. Griffith, *Functional behavior of primary rat liver cells in a three-dimensional perfused microarray bioreactor.* Tissue engineering, 2002. **8**(3): p. 499-513.
291. J. W. Allen and S. N. Bhatia, *Formation of steady-state oxygen gradients in vitro - Application to liver zonation.* Biotechnol Bioeng, 2003. **82**(3): p. 253-262.

292. L. De Bartolo, S. Salerno, S. Morelli, L. Giorno, M. Rende, B. Memoli, A. Procino, V. E. Andreucci, A. Bader and E. Drioli, *Long-term maintenance of human hepatocytes in oxygen-permeable membrane bioreactor.* Biomaterials, 2006. **27**(27): p. 4794-4803.
293. A. Sivaraman, J. K. Leach, S. Townsend, T. Iida, B. J. Hogan, D. B. Stolz, R. Fry, L. D. Samson, S. R. Tannenbaum and L. G. Griffith, *A microscale in vitro physiological model of the liver: Predictive screens for drug metabolism and enzyme induction.* Curr Drug Metab, 2005. **6**(6): p. 569-591.
294. K. Zeilinger, T. Schreiter, M. Darnell, T. Soderdahl, M. Lubberstedt, B. Dillner, D. Knobeloch, A. K. Nussler, J. C. Gerlach and T. B. Andersson, *Scaling Down of a Clinical Three-Dimensional Perfusion Multicompartment Hollow Fiber Liver Bioreactor Developed for Extracorporeal Liver Support to an Analytical Scale Device Useful for Hepatic Pharmacological In Vitro Studies.* Tissue Eng Part C-Me, 2011. **17**(5): p. 549-556.
295. B. Vinci, C. Duret, S. Klieber, S. Gerbal-Chaloin, A. Sa-Cunha, S. Laporte, B. Suc, P. Maurel, A. Ahluwalia and M. Daujat-Chavanieu, *Modular bioreactor for primary human hepatocyte culture: Medium flow stimulates expression and activity of detoxification genes.* Biotechnology Journal, 2011. **6**(5): p. 554-564.
296. M. H. Wu, S. B. Huang and G. B. Lee, *Microfluidic cell culture systems for drug research.* Lab on a chip, 2010. **10**(8): p. 939-956.
297. J. M. Prot, O. Videau, C. Brochot, C. Legallais, H. Benech and E. Leclerc, *A cocktail of metabolic probes demonstrates the relevance of primary human hepatocyte cultures in a microfluidic biochip for pharmaceutical drug screening.* International journal of pharmaceutics, 2011. **408**(1-2): p. 67-75.
298. J. H. Sung, C. Kam and M. L. Shuler, *A microfluidic device for a pharmacokinetic-pharmacodynamic (PK-PD) model on a chip.* Lab on a chip, 2010. **10**(4): p. 446-455.
299. C. Zhang, Z. Zhao, N. A. Abdul Rahim, D. van Noort and H. Yu, *Towards a human-on-chip: culturing multiple cell types on a chip with compartmentalized microenvironments.* Lab on a chip, 2009. **9**(22): p. 3185-3192.
300. P. Chao, T. Maguire, E. Novik, K. C. Cheng and M. L. Yarmush, *Evaluation of a microfluidic based cell culture platform with primary human hepatocytes for the prediction of hepatic clearance in human.* Biochemical pharmacology, 2009. **78**(6): p. 625-632.
301. B. J. Kane, M. J. Zinner, M. L. Yarmush and M. Toner, *Liver-specific functional studies in a microfluidic array of primary mammalian hepatocytes.* Analytical Chemistry, 2006. **78**(13): p. 4291-4298.
302. A. W. Tilles, H. Baskaran, P. Roy, M. L. Yarmush and M. Toner, *Effects of oxygenation and flow on the viability and function of rat hepatocytes cocultured in a microchannel flat-plate bioreactor.* Biotechnol Bioeng, 2001. **73**(5): p. 379-389.
303. M. S. Kim, J. H. Yeon and J. K. Park, *A microfluidic platform for 3-dimensional cell culture and cell-based assays.* Biomedical microdevices, 2007. **9**(1): p. 25-34.
304. Y. C. Toh, T. C. Lim, D. Tai, G. Xiao, D. van Noort and H. Yu, *A microfluidic 3D hepatocyte chip for drug toxicity testing.* Lab on a chip, 2009. **9**(14): p. 2026-2035.
305. P. J. Lee, P. J. Hung and L. P. Lee, *An artificial liver sinusoid with a microfluidic endothelial-like barrier for primary hepatocyte culture.* Biotechnol Bioeng, 2007. **97**(5): p. 1340-1346.

306. V. N. Goral, Y. C. Hsieh, O. N. Petzold, J. S. Clark, P. K. Yuen and R. A. Faris, *Perfusion-based microfluidic device for three-dimensional dynamic primary human hepatocyte cell culture in the absence of biological or synthetic matrices or coagulants.* Lab on a chip, 2010. **10**(24): p. 3380-3386.
307. Y. Nakao, H. Kimura, Y. Sakai and T. Fujii, *Bile canaliculi formation by aligning rat primary hepatocytes in a microfluidic device.* Biomicrofluidics, 2011. **5**(2): p. 22212.
308. C. Y. Li, K. R. Stevens, R. E. Schwartz, B. S. Alejandro, J. H. Huang and S. N. Bhatia, *Micropatterned cell-cell interactions enable high-throughput encapsulation of primary hepatocytes in PEG microtissues for 3D functional studies.* submitted, 2013.
309. U. S. FDA, Drug Development and Drug Interactions: Table of Substrates, Inhibitors and Inducers, http://www.fda.gov/drugs/developmentapprovalprocess/developmentresources/druginteractionslabeling/ucm093664.htm, Accessed April 20, 2013.
310. M. T. Donato, P. Viitala, C. Rodriguez-Antona, A. Lindfors, J. V. Castell, H. Raunio, M. J. Gomez-Lechon and O. Pelkonen, *CYP2A5/CYP2A6 expression in mouse and human hepatocytes treated with various in vivo inducers.* Drug Metab Dispos, 2000. **28**(11): p. 1321-1326.
311. J. W. Ko, N. Sukhova, D. Thacker, P. Chen and D. A. Flockhart, *Evaluation of omeprazole and lansoprazole as inhibitors of cytochrome P450 isoforms.* Drug Metab Dispos, 1997. **25**(7): p. 853-862.
312. T. Jaakkola, J. Laitila, P. J. Neuvonen and J. T. Backman, *Pioglitazone is metabolised by CYP2C8 and CYP3A4 in vitro: Potential for interactions with CYP2C8 inhibitors.* Basic Clin Pharmacol, 2006. **99**(1): p. 44-51.
313. O. Pelkonen, A. Rautio, H. Raunio and M. Pasanen, *CYP2A6: a human coumarin 7-hydroxylase.* Toxicology, 2000. **144**(1-3): p. 139-147.
314. M. Bourrie, V. Meunier, Y. Berger and G. Fabre, *Cytochrome P450 isoform inhibitors as a tool for the investigation of metabolic reactions catalyzed by human liver microsomes.* J Pharmacol Exp Ther, 1996. **277**(1): p. 321-332.
315. G. M. Giancarlo, K. Venkatakrishnan, B. W. Granda, L. L. von Moltke and D. J. Greenblatt, *Relative contributions of CYP2C9 and 2C19 to phenytoin 4-hydroxylation in vitro: inhibition by sulfaphenazole, omeprazole, and ticlopidine.* Eur J Clin Pharmacol, 2001. **57**(1): p. 31-36.
316. T. Lynch and A. Price, *The effect of cytochrome P450 metabolism on drug response, interactions, and adverse effects.* Am Fam Physician, 2007. **76**(3): p. 391-396.
317. M. K. Ma, M. H. Woo and H. L. McLeod, *Genetic basis of drug metabolism.* American journal of health-system pharmacy : AJHP : official journal of the American Society of Health-System Pharmacists, 2002. **59**(21): p. 2061-2069.
318. S. S. Kim, C. A. Sundback, S. Kaihara, M. S. Benvenuto, B. S. Kim, D. J. Mooney and J. P. Vacanti, *Dynamic seeding and in vitro culture of hepatocytes in a flow perfusion system.* Tissue engineering, 2000. **6**(1): p. 39-44.
319. H. Shiku, T. Saito, C. C. Wu, T. Yasukawa, M. Yokoo, H. Abe, T. Matsue and H. Yamada, *Oxygen permeability of surface-modified poly(dimethylsiloxane) characterized by scanning electrochemical microscopy.* Chem Lett, 2006. **35**(2): p. 234-235.

320. K. Saeki, A. Yuo, M. Kato, K. Miyazono, Y. Yazaki and F. Takaku, *Cell density-dependent apoptosis in HL-60 cells, which is mediated by an unknown soluble factor, is inhibited by transforming growth factor beta 1 and overexpression of bcl-24.* Journal of Biological Chemistry, 1997. **272**(32): p. 20003-20010.
321. M. P. Lynch, S. Nawaz and L. E. Gerschenson, *Evidence for Soluble Factors Regulating Cell-Death and Cell-Proliferation in Primary Cultures of Rabbit Endometrial Cells Grown on Collagen.* Proceedings of the National Academy of Sciences of the United States of America, 1986. **83**(13): p. 4784-4788.
322. Y. Tsuda, Y. Morimoto and S. Takeuchi, *Monodisperse cell-encapsulating peptide microgel beads for 3D cell culture.* Langmuir : the ACS journal of surfaces and colloids, 2010. **26**(4): p. 2645-2649.
323. S. Seiffert, J. Dubbert, W. Richtering and D. A. Weitz, *Reduced UV light scattering in PDMS microfluidic devices.* Lab on a chip, 2011. **11**(5): p. 966-968.
324. J. S. Miller, C. J. Shen, W. R. Legant, J. D. Baranski, B. L. Blakely and C. S. Chen, *Bioactive hydrogels made from step-growth derived PEG-peptide macromers.* Biomaterials, 2010. **31**(13): p. 3736-3743.
325. R. Ramachandran and S. Kakar, *Histological patterns in drug-induced liver disease.* Journal of clinical pathology, 2009. **62**(6): p. 481-492.
326. R. E. Schwartz, K. Trehan, L. Andrus, T. P. Sheahan, A. Ploss, S. A. Duncan, C. M. Rice and S. N. Bhatia, *Modeling hepatitis C virus infection using human induced pluripotent stem cells.* Proceedings of the National Academy of Sciences of the United States of America, 2012. **109**(7): p. 2544-2548.